Politecnico di Torino

Politecnico di Torino

Corso di Laurea Magistrale in Ingegneria Biomedica
A.a. 2023/2024
Sessione di Laurea Marzo 2024

Design and fabrication of electroconductive photocurable hydrogels for bioelectronic interfacing

Relatori:

Professor Danilo Demarchi

Professoressa Francesca Santoro

Dottoressa Valeria Criscuolo

Candidato:

Marco Buzio

Acknowledgments

To my family, my parents Cristina and Mauro, that always believed in me: you should be proud of your self because whatever good I have been able to do until now is mostly thanks to you.

I owe immense gratitude to my esteemed professors, Francesca and Valeria, for their invaluable guidance, expertise, and steadfast support throughout this journey. Your advice and encouragement have significantly shaped the evolution of my thesis and my academic growth.

To my Friends, for the laughter and light-hearted moments that provided much-needed breaks from my studies, thank you. Your support has been a vital component of my success.

Abstract

Bioelectronic devices interact with cells and tissues, sense electrical activity and modulate cellular behavior through electrical fields. Typically, *in vitro* devices are based on flat, rigid metal electrodes that are designed for 2D cell models. 3D electrodes, providing physical and biological stimuli, enhance cell-chip coupling creating a more bio-mimetic environment. Topography and aspect ratio of nano and micro structured surfaces can modulate the interaction with cell membrane affecting also intracellular signaling. Substrate mimicking mechanical properties of the native extracellular matrix (ECM) enhances cell interaction. Here, natural and synthetic materials such as gelatin and polyethylene glycol diacrylate (PEGDA) can be used to obtain 3D patterned structures at microscale and resemble the typical architectures of the ECM with also major challenges is additionally providing dynamic electrical and morphological stimuli. The integration of such materials into more complex circuitry requires patterning resolution, flexibility, and control over the geometry to be achieved. To this aim, this thesis presents an innovative approach for the fabrication of conductive 3D structures for cell sensing and stimulation. A conductive hydrogel comprising modified gelatin and the PEDOT:PSS conductive polymer has been engineered. Gelatin, modified with methacrylate groups, serves as photocurable material with bioactive features, while PEDOT:PSS acts as the electro conductive element. The obtained blend has been 3D photo-patterned exploiting multiple techniques from drop casting and subsequent UV-photopolymerization to two-photon-polymerization (2PP) lithography. The degree of methacrylation (DOM) was assessed by proton nuclear magnetic resonance (^{1}H-NMR). The resulting 3D structures has been characterized by optical microscopy and electrochemical measurements. Finally, biocompatibility assays were carried out with neuronal cells. In this work, GelMA with different DOMs, and GelMA\PEDOT:PSS blends with PEDOT:PSS concentration up to 5%wt were obtained. The presence of PEDOT:PSS reduces the impedance of blends. The obtained blends can be exploited to develop photo cured hydrogels at macro- , meso- and micro-scale. HT-22 cells cultured on GelMA and GelMA\PEDOT:PSS hydrogels showed high viability. The proposed approach offers a promising pathway for creating fully organic and bioactive 3D electrodes with controlled morphology for sensing and stimulating cells and tissues. Such electrodes could find applications in biomedical devices such as implants, probes, and epidermal devices where flexible, soft, and conductive materials are essential requirements.

Contents

1 Introduction

The use of cell-based in vitro models has seen a significant increase across various applications, including tissue engineering, drug discovery, toxicology, and bioelectronics [1]. This surge is partly due to the evolving field of bioelectronics, which integrates principles from electrical engineering, biology, medicine, chemistry, and materials science. The goal is to create a synergy between electronic devices and living systems, facilitating the sensing and stimulation of cells, tissues, and organs. [2]. The journey of bioelectronics commenced in the 1960s with the advent of implantable electronic devices designed to interact with and stimulate organs, marking the beginning of new trends in the field [3]. In recent years, bioelectronics has emerged as a highly promising research area, particularly noted for its contributions to regenerative medicine. By harnessing electricity, this field aims at restoring lost or damaged physiological functions, ultimately enhancing the quality of life for individuals [4]. A significant portion of research in bioelectronics has focused on developing *in vitro* platforms that allow for the direct cultivation of cells on electronic devices. Among these, multi-electrode arrays (MEAs) have gained prominence. These devices, comprising tens to thousands of micro- or nano-scale metal electrodes, are adept at recording and stimulating the extracellular electrical activity of single cells, cell networks, and entire tissues at multiple sites. Bioelectronics has shown great promise for its dual ability to continuously monitor biological systems without labels and to precisely control biological activity, expanding its applications to *in vitro* environments.[5]. This expansion is supported by the rise of microfluidics and significant improvements in the reliability and complexity of in vitro models, which hold the potential to greatly reduce or even replace animal studies in drug discovery and toxicology testing [5]. Concurrently, the fields of tissue engineering and regenerative medicine (TERM) have acknowledged the beneficial effects of bioelectricity on excitable tissues, such as enhancing cell proliferation, differentiation, and migration, as well as improving tissue functions.[6]. In this context, biomaterials are indispensable, providing essential mechanical, structural and functional support for cells [7], [8], [9]. The use of traditional electronic materials like gold, platinum, and silicon, leveraged from the integrated circuit industry, has proven effective for *in vitro* bio interfacing across various scenarios [5]. However conventional electronic materials sometimes fail to establish intimate cell−electrode coupling that is necessary to accurately record a signal, limiting the type and depth of biological information that could be acquired in 3D biological systems [10], [11], [12]. In contrast, organic conductive materials, that can be easily functionalized to impart different properties, have been shown to more seamlessly integrate with biological systems of advanced complexity, providing a better cell−electrode coupling and thus more effective signal transduction of biological events. [10], [13], [14] Significant research and development have been dedicated to creating biomaterials that mimic various microenvironmental signals (e.g., biochemical, mechanical, electrical, and structural cues). Among these, electrical cues, including electrical signals and conductive networks within tissues, are particularly critical for stem cell differentiation and the development of organs [15]. This is especially

true for tissues that are electrically excitable, such as those involved in neural activities within the nervous system, the contraction of the heart muscle and skeletal muscles, and the generation of piezoelectric effects in bones [16], [17], [18], [19](Figure 1.1).

To bio mimic the conductive networks in these excitable tissues, nonconductive components, mainly including some natural and synthetic polymers lacking electron transport ability, are often combined with conductive components (e.g., conductive polymers, carbon-based nanomaterials, metals) to facilitate the fabrication of conductive biomaterials [6]. The enhanced conductivity of these biomaterials has been proven to: 1) improve transmission of the electrical activities generated from spontaneously excitable cells (e.g., neural and cardiac cells), and thus promoting their electrical communication, growth and functional maturation *in vitro* [20], [21]; 2) enhance the effect of stimulation on the growth and functionalities of cells by transmission of biomimicking electrical stimulation to regenerated tissues efficiently *in vitro* and *in vivo* [22], [23]; 3) electrically bridge implanted cells with host tissues, or cells inside and outside dysfunctional areas, to provide a seamless integration *in vivo* [24], [25]; 4) transmit electrical stimulation to realize some advanced electrical functionalities, such as electrically-controlled releasing bioactive agents (e.g., growth factors, drugs, DNA vectors), and electrically manipulating and sensing cell behaviours [26], [27]. Cell culture models interfacing with bioelectronics include tissue-engineered structures such as hydrogels, porous scaffolds, and fiber meshes, as well as more complex 3D cell models such as spheroids and organoids. Three-dimensional bioelectronic models, in addition to providing a 3D structure for cell support, are also used to electrically monitor cell growth and tissue formation [5].

Various strategies for the design and fabrication of conductive biomaterials have been explored to match different tissue requirements: the structure (e.g., hydrogels, porous materials, fibrous materials, and films) and spatial distribution of each component (e.g., homogeneous or layered distribution) [6] (Figure 1.1).

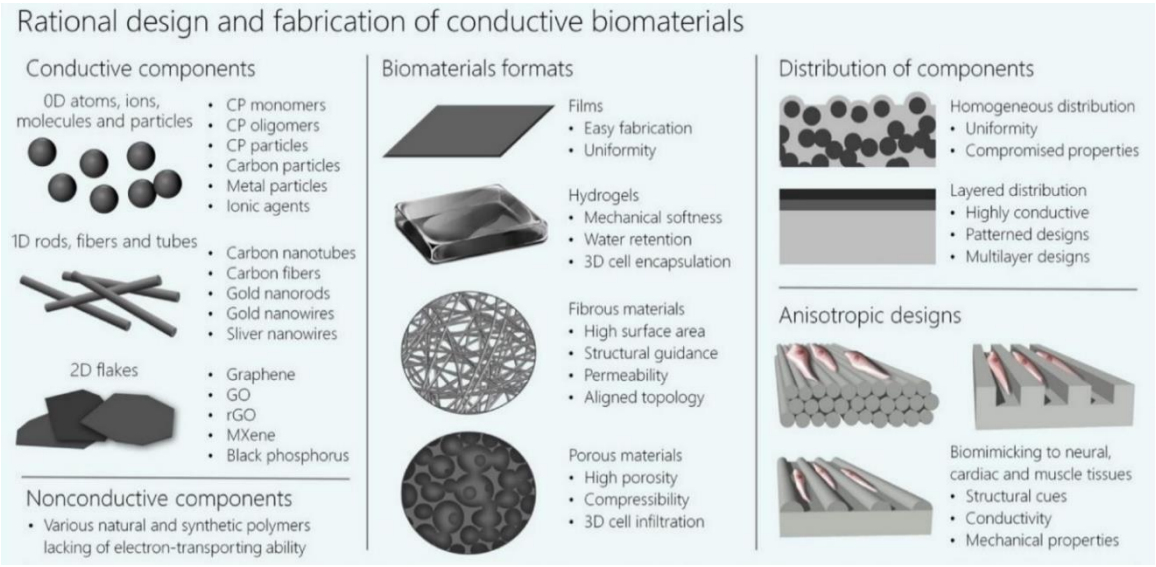

Figure 1.1 Schematics of design and fabrication strategies of conductive biomaterials. Adapted from [3].

1.1 Neural tissue applications

1.1.1 Tissue engineering and regenerative medicine

The role of bioelectricity in living systems has been highlighted by numerous researchers throughout time [5]. The first to bring this aspect to the attention of the wider community was Luigi Galvani [28]. In this section, the strategies of employing conductive biomaterials for the regeneration and manipulation of neural tissues are briefly presented.

Bioelectricity can be produced at different levels in the human body [16], [29]. On a molecular and cellular level, a polarization potential across the cell membrane is created by the action of sodium/potassium ion pumps found in all living cells[30]. These aggregates are capable of coordinating the movement of ions over large areas to collectively generate higher electrical potentials in structures such as epitheliums, vascular walls, and bones [31], [32], [33], or to conduct action potentials in a directional and stable manner, as seen in the nervous system, heart muscle, and skeletal muscles [34], [35], [36]. The movement of ions and the resulting bioelectricity play a crucial role in regulating various biological processes, including cell migration, proliferation, and differentiation, as well as the functionality of tissues and organs, muscle activity, and consciousness [6].

However, damaged nerves, particularly those in the central nervous system, struggle to repair themselves because of the limited ability of nerve cells to regenerate. This results in interrupted nerves, disrupted electrical signal transmission, and consequently, impairments within the nervous system. Various conductive biomaterials functionalized by poly-pyrrole (PPy) [37], [38], poly (3,4-ethylenedioxythiophene) (PEDOT) [39], [40], [41], [42], poly/oligo-aniline (PANi/OANi) [43], [44], carbon nanotubes (CNTs) [45], [46], graphene nanomaterials (GNMs) [47], [48] and gold [49], [50] have been developed to investigate their effects on the regeneration of nerve tissues in vitro and the repair of nerves *in vivo*. Nerve cells within nervous system possess directional axons, especially for those in spinal cord and peripheral nerves, Therefore, the use of conductive biomaterials that provide aligned structural guidance can enhance the directional growth of neurites from nerve cells, both in *in vitro* and within living organisms [51], [52].

The use of electrical stimulation via conductive biomaterials can serve to regulate the functions of regenerated tissues over long periods or to momentarily induce activities in excitable cells (such as the synchronized beating of heart cells or the electrical and secretory activities of nerve cells) as a means to assess their functions [6]. Conductive biomaterials can amplify the beneficial impact of electrical stimulation, enhancing the migration, differentiation, and neurite outgrowth of nerve cells *in vitro* as well as nerve repair *in vivo*. Thus, many conductive biomaterials have been fabricated into nerve guidance conduits by using rod templates [24], [53], rolling 2D biomaterials [54], [55], 3D printing [56], or cutting into tubes [57]. Nerve cells can also migrate into porous and 3D-printed biomaterials [58],

[59], or be laden within hydrogels [60], [61], for 3D culture. Some conductive biomaterials have been implanted in vivo for neural prosthetics with focus on restoring peripheral nerves [24], [62].

Some other methods can achieve rapid and precise manipulations over some cell behaviours, such as on-demand controlling the cell adhesion, detachment, proliferation and differentiation [25], [63], [64]. Research investigating the neurite outgrowth of PC-12 cells under constant applied voltage or current has consistently demonstrated that electrical stimulation leads to longer neurites from PC-12 cells for PEDOT-based,[65] PPy based,[66], [67] and PANI-based [68] substrates. Some of these studies have also examined the resulting PC-12 cultures for neuronal markers, finding that these markers are upregulated under constant voltage electrical stimulation[69]. These data indicate that electrical stimulation can induce differentiation of PC-12 cells into neuronal cells [5]. Recent reviews have highlighted the potential of the combined use of electrical stimulation protocols and conducting materials and stem cells relevant for tissue engineering applications in both in vitro and in vivo studies.[70], [71] Conductive biomaterials modified with biotin/streptavidin/anti- epithelial cell adhesion molecule (EpCAM) can selectively capture cancer cells [72], [73] , and release them under electrical charging.

Electrogenic cells, known for generating electrical signals, also typically respond to electrical stimulation. Organic devices can be engineered to trigger action potentials in neuronal cells, a capability that is especially intriguing for its potential applications in neural stimulation within living organisms [74]. Stimulation through electrodes still results in neurite outgrowth,[75] even when applied in 3D.[76] Moreover, electrical stimulation can also lead to alterations in ionic concentrations within neuronal cells [77], [78]. MEAs can also be constructed to both stimulate and then record the result of the electrical stimulus,[78], [79], [80] as reported in the work from Aqrawe et al.[81]. Many research efforts have explored the use of electrical stimulation on cardiac cells, often employing electroactive substrates. Several of these studies have administered monophasic pulsed stimuli to cultures of cardiac cells [82], [83], [84]. Application of this type of electrical stimulus to cardiomyocytes appears to affect the frequency of firing behaviour [5].

1.1.2 Neuroelectronics

Besides this basic and biomimetic use of conductive biomaterials as materials to support growth and stimulation of living tissue, some other electrical functionalities, such as cell sensing electrically-controlled molecule releasing, have also been developed basing on conductive biomaterials, making them closer to bioelectronics[6]. Interfacing of biological systems with electronics can be a powerful means of controlling biological systems when used carefully. In terms of models, the degree of complexity of an in vitro model can vary from isolated parts of the cell (i.e., cell membranes) to cell monolayer models to complex 3D (or organotypic) cell cultures [5] (Figure 1.2). In neuroelectronics, the biotic–abiotic interface is undeniably the most important factor for communication between biological systems and electronic components. Biocompatibility of the abiotic material is crucial for maintaining living cells, the formation of a lasting interface, and the accurate expression of biological mimicry [5].

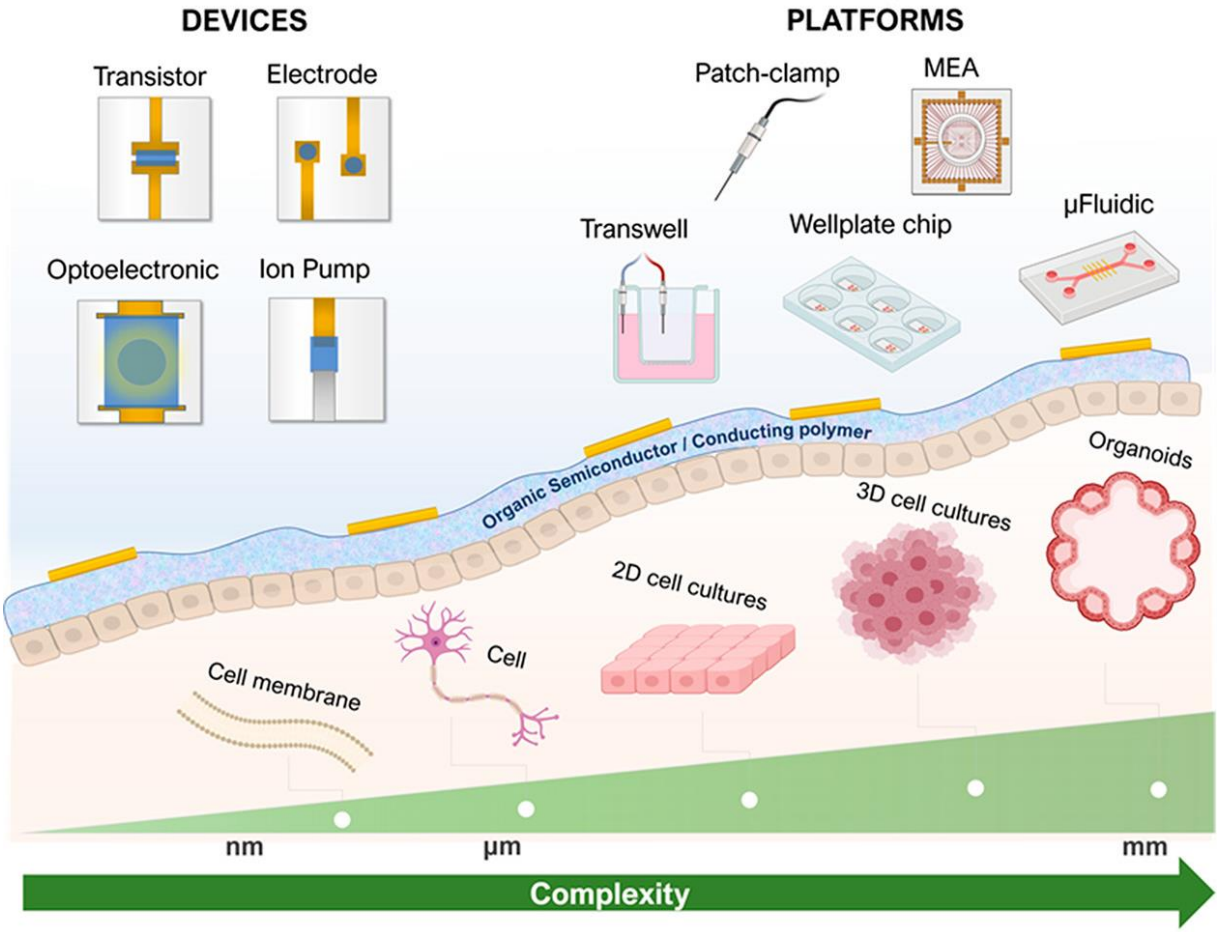

Figure 1.2 Schematic overview of in vitro organic bioelectronics showing the biointerface with state-of-the-art electronic devices and platforms used for monitoring and controlling function and activity of biological systems of increasing complexity.

A wide range of neuroelectronic devices are used to monitor or stimulate cellular activity [5]. For such purpose different devices can be implemented: simple electrodes can be microfabricated in dense arrays (i.e., microelectrode arrays, MEAs), typically used for in vitro recordings and stimulation of electrogenic cells.[85], [86]; cells can be cultured directly on organic thin film transistor, and ionic biological signals are recorded as electronic signal changes due to the modulation of the current flowing in the transistor channel [87]. For non-electroactive cells, electrical measurements can yield insights into cell viability, coverage, growth, and differentiation, in addition to the integrity of the cell layer for cells forming barrier tissues that are not electrically active [1]. For instance, the impedance of cell-cultured conductive biomaterials can be correlated with the changed cell density, and thus can be utilized to monitor the cell adhesion and proliferation [12], [88], [89] Santoro et al. generated a poly(3,4-ethylenedioxythiophene) polystyrene sulfonate (PEDOT:PSS) -based substrate that showed changes in impedance associated with cardiomyocytes cultured on different topographies.[90]; the alteration on I/V curves can be used to monitor the differentiation of neural stem cells (NSCs) [91]. For cells with secreting capability, their secretion activity can be electrochemically sensed by conductive biomaterials. For instance, the secretion of nitric oxide (NO) [89], [92] and hydrogen peroxide (H_2O_2) [93], [94], [95] from normal or cancer cells, transmitters (e.g., dopamine [96], [97], noradrenaline [98]) from neural cells , or catecholamines from chromaffin cells [99], can be electrochemically converted into current signals and monitored by conductive scaffolds. There is a significant demand for sensors capable of precisely identifying biomarkers indicative of a cell's physiological or pathophysiological condition. Such technology is sought after not only to enhance existing in vitro assays but also for early-stage diagnostics, drug screening, and environmental monitoring [100], [101]. For instance, changes in cell activity can lead to variations in the expression of cell surface biomarkers. Therefore, monitoring cellular metabolites under various stimuli or environmental conditions can provide valuable information about the cells' status.[5].

The change of the electrical field within a biomaterial can be used to induce a controlled release of molecules in the environment. Drug delivery systems (DDs) are capable of controlled-releasing drug for treating tissues. Traditional DD methods can regulate drug release through predetermined degradation of vesicles, yet they are susceptible to various environmental factors [6]. In contrast, electrically controlled drug delivery systems (DDSs) present a promising approach for on-demand drug release. This is achieved by applying mild electrical stimulation to drug carriers that respond to electrical or electrothermal stimuli, thereby controlling the drug release [6]. Drugs with molecular sizes smaller than the pores of the biomaterials can slowly diffuse out. The application of an electrical field often accelerates the release rate through the electrophoresis of charged drugs [6]. Conductive polymers exhibiting unique electrical responses have found wide applications in developing electrically-controlled DDSs [102], [103]. PPy is particularly promising for its capability in encapsulating negatively-charged drugs (e.g., dexamethasone (Dex) [104], grow factors [105], clioquinol [106]) during

the electro polymerization of PPy/drug composites, and releasing them when PPy is reduced under electrical stimulation. 3,4-ehtylenedioxythiophene (EDOT) coated biomaterials can electrically control release both positively and negatively charged drugs [107], [108], [109], which is mainly attributed to the electrical actuation of PEDOT coatings and formation of gaps. Integrating conductive biomaterials that display an electrothermal effect with thermally-responsive drug carriers is a viable strategy, as demonstrated in a study where the temperature increase in conductive threads caused a thermally-responsive hydrogel coating to contract. This contraction released cefazolin and vascular endothelial growth factor (VEGF) embedded within it, targeting wound healing applications [110]. Among bioelectronic devices ion pumps can operate as a drugs delivery devices transferring ions from one side of a membrane to the other, in analogy to ion pumps found in cell membranes [5].

1.2 Conductive biomaterials

Biomaterials are substances that have been engineered to interact with biological systems for therapeutic, diagnostic, or research purposes. These materials possess physical, chemical, and biological properties tailored to interface with living tissues or organisms, facilitating desired biological responses while minimizing adverse reactions [111]. Biomaterials encompass a wide range of materials, including synthetic polymers, metals, ceramics, and naturally derived substances, designed to support functions such as tissue regeneration, drug delivery, medical device fabrication, and biological sensing [112]. Their development involves interdisciplinary approaches integrating principles from materials science, biology, engineering, and medicine to address specific clinical needs and challenges [112] [111].

Biomaterials are crafted with the intention of mimicking the structure of the natural extracellular matrix (ECM). This similarity enables cells to undergo directional differentiation, adopt specific morphologies, converge into tissues, and sustain their physiological functionalities over the long term [6]. Electrically conductive biomaterials are employed for the regeneration or connection restoration of excitable tissues where the electrical microenvironment (e.g., bioelectricity and conductive paths) plays great roles in their functionalities [6]

Conductive biomaterials are essentially composed of a conductive component, providing electrical functionalities, and a non-conductive polymeric component, in most cases, yielding the mechanical supports [6]. Typically, the main component of conductive biomaterials is a non-conductive polymeric substrate that determines the mechanical properties, biocompatibility, biodegradability, and environmental resemblance of the overall composite. Different non-conductive components have been explored for fabricating conductive biomaterials, including natural (e.g., collagen, gelatin, chitosan, silk fibroin, alginate, cellulose) and synthetic (e.g., polycaprolactone (PCL), poly (L-lactic acid) (PLLA), poly (lactic-co-glycolic acid) (PLGA), polyurethanes (PU), polyethylene glycole (PEG)) polymers that exhibit some advantages for biomedical applications, such as excellent biocompatibility, easy processability, and controllable biodegradability and mechanical properties. The mechanical properties of conductive biomaterials can be engineered to mimic the mechanical microenvironment of native tissues considering their significant effect on cell differentiation and functionalities [6]. The addition of conductive components can not only impart the conductivity to biomaterials, but can also influence chemical and biological properties, that account for the biocompatibility, biodegradability and bio affinity of biomaterials, mechanical properties. In addition, the concentration and spatial distribution (e.g., blending within or coating on substrates) of conductive components, which are dependent on processing methods, also influence biomaterial properties [1].

The selection of the appropriate components for engineering a conductive biomaterial should follow general requirements [6]: 1) both the conductive and non-conductive components should be biocompatible; 2) the conductive components with higher efficiency in conferring conductivity are ideal

in lowering their concentration; 3) the conductive components should be easily incorporated with nonconductive polymers, or processed into free-standing biomaterials, through non-toxic and mild methods; 4) the conductive components should not affect the biological and mechanical properties of polymeric substrates; 5) the non-conductive polymers should be biodegradable and soft, except for those employed in bone applications; 6) non-conductive polymers should hold excellent bio affinity for promoting cell adhesion and proliferation; 7) non-conductive polymers should be capable of being processed into biomaterials with desirable microstructures and formats for certain tissue applications.

The most common conducive materials employed for conductive biomaterials are: Polypyrrole (PPy), poly/oligo-aniline (PANi and OANi), PEDOT, carbon nanotubes (CNTs), graphene nanomaterials (GNMs), carbon fibers (CFs) gold and silver. on the other hand, collagen, gelatin, gelatin-methacryloyl (GelMA), chitosan, silk fibroin (SF), alginate, cellulose, polycaprolactone (PCL), poly (L-lactic acid) (PLLA), poly (lactic-co-glycolic acid) (PLGA), polyurethane (PU) and polyethylene glycole (PEG) are frequently employed as the non-conductive components [6].

In recent years a very well-stocked and diverse database of 631 high-quality papers on conductive biomaterials for TERM application was collected [6]. A perspective of the work is enclosed in Figure 1.3 and Table 1.

The employing of different conductive components and nonconductive polymers for neural tissue applications is shown in Figure 1.3

Table 1 Overall classification of conductive biomaterials from the aspect of their conductive components. Adapted from [3].also presents all the conductive components used for the fabrication of conductive biomaterials with respect to the fabrication methods, frequently incorporating non-conductive polymers, biomaterial formats, and TERM applications.

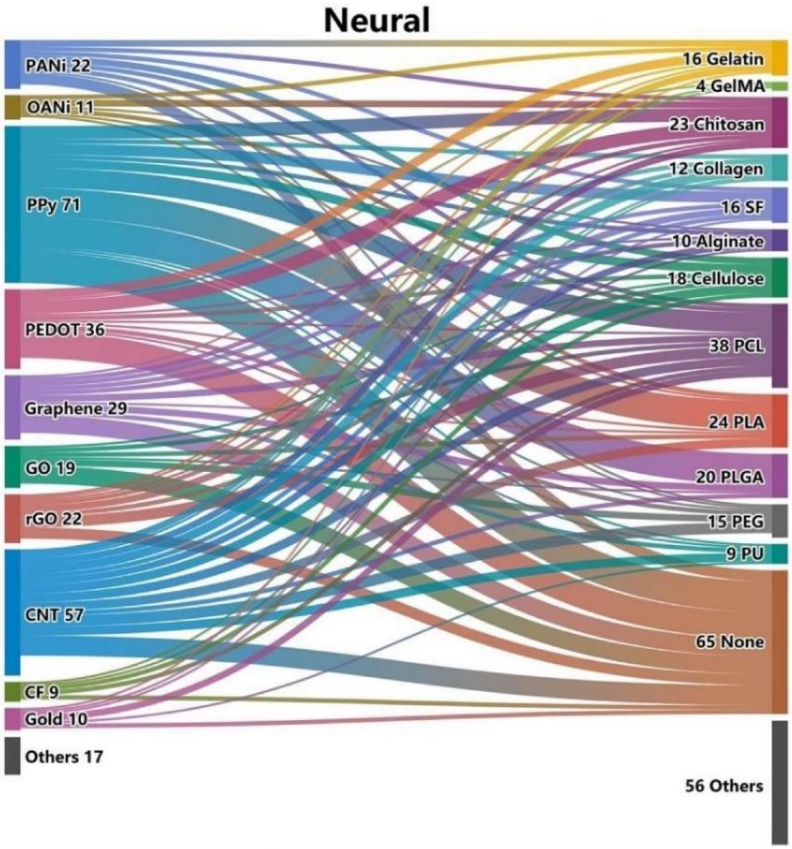

Figure 1.3 Detailed Sankey diagrams classifying and connecting the different conductive components and nonconductive polymers. The reference numbers of each component show the frequency of various conductive and nonconductive components within the range of specific Neural tissues TERM application fields. Sankey flows between conductive and nonconductive components show the frequency of incorporating different conductive components and nonconductive polymers for regenerating certain tissue. Adapted from [3].

Table 1 Overall classification of conductive biomaterials from the aspect of their conductive components. Adapted from [3].

Conductive components	Fabrication methods	Polymeric components	Biomaterial Arrangement	Applications
PANi	Chemical polymerization of aniline: depositing on substrates during polymerization; in-situ polymerization of aniline within biomaterials ; grafting on other polymers during polymerization. Electropolymerization of aniline: depositing on substrates during polymerization. PANi dispersions: blending within substrates; depositing on substrates	PCL , gelatin , chitosan , PLLA, PLCL , silk fibroin , PAN , PU, cellulose , PLGA , heparin, PGS , collagen, PAAm	Films, electrospun fibrous materials, other fibrous materials , porous materials, hydrogels	Neural, cardiac , bone, muscular , skin/wound
OANi	Dimer: grafting on other ,Trimer: block copolymers ; grafting on other polymers Tetramer: grafting on other polymers, Pentamer: block copolymers ; grafting on other polymers Hexamer: grafting on other polymers	PLLA, chitosan , gelatin , PU, PEG, PGS, agarose, hyaluronic acid, alginate, PNIPAAm , PVA , PLGA	Films, electrospun fibrous materials , other fibrous materials , porous materials, hydrogels, uncombined nano/micro materials	Neural, cardiac, bone, muscle, skin/wound
PPy	Chemical polymerization of pyrrole: depositing on substrates during polymerization ; in-situ polymerization of pyrrole within biomaterials ; grafting on other polymers during polymerization; crosslinking pyrrole-functionalized polymers Electropolymerization of pyrrole: depositing on substrates during polymerization Vapor-phase polymerization of pyrrole: depositing on substrates during polymerization PPy dispersions: blending within substrates; depositing on substrates Block copolymers Blending oligopyrrole within substrates	PCL ,PLLA, chitosan PLGA, gelatin, silk fibroin, collagen, alginate, cellulose, PLCL, heparin, hyaluronic acid, PAN, PVA, PCLF, OPF, PAAm, PU, PEG	Films electrospun fibrous materials, other fibrous materials, porous materials, hydrogels.	Neural , cardiac , bone ,muscle, skin/wound

Conductive components	Fabrication methods	Polymeric components	Biomaterial Arrangement	Applications
PEDOT	Electropolymerization of EDOT: depositing on substrates during polymerization; around living cells Chemical polymerization of EDOT: depositing on substrates during polymerization; in-situ polymerization of EDOT within biomaterials PEDOT dispersions: blending within substrates ; depositing on substrates; crosslinked PEDOT materials Vapor-phase polymerization of EDOT: depositing on substrates during polymerization Block copolymers Block copolymers or crosslinked materials from oligoEDOT	Chitosan, gelatin, PDMS, PEG, PCL, cellulose, alginate, silk fibroin, hyaluronic acid, heparin, agarose, PLLA, collagen, PU, PAAm	Films, fibrous materials, porous materials, hydrogels, 3D-printed materials	Neural, cardiac, bone, muscle, skin/wound
CNT	MWCNT: blending within substrates ; depositing on substrates by absorbing, LBL-coating , or printing ; serving as nanofibrous substrates; functionalizing with crosslinkable groups SWCNT: blending within substrates; depositing on substrates by LBL-coating, spraying, filtrating, or printing; serving as nanofibrous substrates Pristine CNTs synthesized by CVD: vertically aligned forests; drawing pristine CNTs into yarns and membranes; wrapping pristine CNTs on substrates	PLLA chitosan collagen PU PCL GelMA gelatin cellulose silk fibroin PEG PLGA OPF alginate PEI PNIPAAm laminin hyaluronic acid matrigel chitin PDMS PAN PVA PLCL agarose PGS PCLF	Films, electrospun fibrous materials other fibrous materials porous materials hydrogels 3D-printed materials	Neural, cardiac, bone, muscle, skin/wound
Graphene	CVD-synthesized graphene: growing on copper foils and then transferring ; growing on nickel foams or other templates and then leaching the templates Mechanically exfoliated or commercially available graphene nanoplatelets: blending within substrates; depositing on substrates	PCL PLGA PEG collagen alginate PCLF PVA chitosan silk fibroin PLLA PU PDMS cellulose	Films, electrospun fibrous materials, other fibrous materials, porous materials, hydrogels, 3D-printed materials	Neural cardiac bone muscle skin/wound
GO	Chemically exfoliated or commercially available GO: depositing on substrates by drop-casting spin-coating spraying adsorbing or electrodepositing ; blending within ; crosslinked GO materials ; blending with cells; GO foams: coating by other components	chitosan PCL cellulose PEG OPF PVA PDMS gelatin GelMA collagen silk fibroin PNIPAAm PAAm MeTro PAN PLLA PVDF PLGA PU alginate PAA	Films,,electrospun fibrous materials, other fibrous materials, porous materials, hydrogels, uncombined nano/micro materials, 3D-printed materials	Neural cardiac bone muscle skin/wound

Conductive components	Fabrication methods	Polymeric components	Biomaterial Arrangement	Applications
rGO	Chemical reduction of GO-based biomaterials into rGO-based biomaterials: depositing GO on substrates by filtrating drop-casting absorbing or LBL-coating ; blending GO within substrates ; substrate-free rGO materials; Chemically reduced or commercially available rGO dispersions: depositing on substrates by drop-casting absorbing electrodepositing filtrating printing or LBL-coating ; blending within substrates; blending with cells	Silk fibroin Chitosan PCL GelMA PAAm gelatin collagen PLCL PDMS PAN PLLA polyimide hyaluronic acid cellulose	Films electrospun fibrous materials other fibrous materials porous materials hydrogels uncombined nano/micro materials D-printed materials Neural cardiac bone muscle skin/wound Carbon fibersCVD synthesized carbon nanofibers: serving as nanofibrous substrates; blending within substrates Carbonized carbon fibers: serving as fibrous substrates ; blending within substrates PLGA PCL alginate chitosan gelatin PVA Fibrous materials porous materials hydrogels	Neural cardiac bone muscle skin/wound
Carbon fibers	CVD synthesized carbon nanofibers: serving as nanofibrous substrates; blending within substrates Carbonized carbon fibers: serving as fibrous substrates; blending within substrates	PLGA, PCL, alginate, chitosan, gelatin, PVA	Fibrous materials, porous materials, hydrogels	Neural cardiac bone muscle
Gold	Chemically synthesized or commercially available AuNPs: blending within substrates ; depositing on substrates; Chemically synthesized or commercially available AuNRs: blending within substrates ; depositing on substrates; Chemically synthesized or commercially available AuNWs: blending within substrates ; depositing on substrates; Electrodeposited Au nanotubes and nanowires; Evaporated or sputtered Au: coating Au layers on plates without or with patterns; depositing AuNPs on substrates	PCL collagen chitosan gelatin GelMA PU alginate silk fibroin PVA albumin PEG PLGA PDMS PLLA BSA	Films electrospun fibrous materials porous materials hydrogels 3D-printed materials	Neural cardiac bone muscle
Others	Other conductive polymers: Polydopamine ; melanin; Other Silver ilver materials: AgNPs ; AgNWs; Other metals: Platinum; titanium ; zinc; Silicon materials: SiNWs ; Si wafers; Metallic compounds: MXene; ITO glass; Black phosphorus; Other carbon materials: carbon black; carbonized materials ; carbon ink; Ionic-conductive agents: salts ; Bio-IL	PCL cellulose GelMA chitosan gelatin PEG PLGA alginate PVA PDMS collagen silk fibroin PU hyaluronic acid agarose PAAm PLCL	Films electrospun fibrous materials other fibrous materials porous materials hydrogels 3D-printed materials uncombined nano/micro materials	Neural cardiac bone muscle skin/wound

1.2.1 Metallic materials

Metallic materials play a significant role in biomedical applications due to their unique combination of mechanical properties, biocompatibility, and corrosion resistance. Gold is known as one of the most universally used noble metals thanks to its excellent electrical conductivity ($4x10^7$ S/m at 20°C) and resistance to oxidation and erosion. Gold nanomaterials, including nanoparticles (AuNPs), nanorods (AuNRs), and nanowires (AuNWs), feature well-defined nanostructures and a vast specific surface area. They also possess the potential to be functionalized with bioactive substances, which can enhance the growth and maturation of excitable cells [113], [114], [115]. Besides gold, some other metals (e.g., silver [116], platinum [45], [117], titanium [118] and zinc [119]) have found applications in fabricating conductive biomaterials. Silver, another commonly utilized noble metal, has been adopted in biomedical fields such as wound treatment and medicine early on, thanks to its antibacterial properties [120]. Silver is often used in forms of nanoparticles (AgNPs) and nanowires (AgNWs) prepared by chemically reducing Ag^+ ions [121], [122]. The incorporation of AgNPs in conductive biomaterials can realize excellent antibacterial activity for wound healing applications [122], [123].

1.2.2 Carbon-based Materials

Carbon-based conductive materials encompass a diverse range of substances primarily composed of carbon atoms, engineered for their electrical conductivity properties.

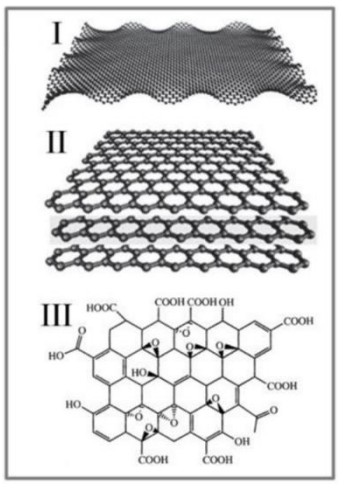

Figure 1.4 Schematics of single-layer graphene (I), few-layers graphene (II), and GO (III).

Graphene is a two-dimensional carbon allotrope composed of a single layer of carbon atoms arranged in a hexagonal lattice. Graphene nanomaterials (GNMs), encompassing graphene, graphene oxides (GO), and reduced graphene oxides (rGO), differentiated by their levels of oxidative groups and defects, have garnered significant interest over the past decade. This attention is due to their outstanding electrical conductivity, strong mechanical properties, and flexible processability [124], [125]. GNMs consist of one to several monolayers of hexagonally arranged carbon atoms (Figure 1.4). Compared to CNTs, the flat shape and more exposed surface of GNMs provide them with better biocompatibility and

biodegradability for TERM applications [126]. GO, the oxidized version of graphene, is produced through the chemical oxidation and exfoliation of graphite. While the extensive oxidative groups and defects in GO significantly reduce its conductivity compared to graphene, often by several orders of magnitude, these characteristics do not notably affect GO's mechanical strength. Additionally, these features offer GO several advantages for tissue engineering and regenerative medicine (TERM) applications, including outstanding hydrophilicity and dispersibility in water, along with high reactivity and bioactivity [127], [128], and capability of loading bioactive agents and nanomaterials [129], [130]. These attributes render GO an ideal choice for the development of biomaterials that prioritize enhanced mechanical properties and superior biological functionality over optimal conductivity [131], [132]. Nevertheless, GO coatings may display limited stability in aqueous environments due to their propensity for redispersion. In addition to using GO-based biomaterials, GO is also appealing for its straightforward conversion into highly conductive reduced graphene oxide (rGO), which is used to produce rGO-based biomaterials. rGO shares many properties with graphene, such as electrical and thermal conductivity, hydrophobicity, dispersibility, and color. Despite these similarities, rGO's effectiveness in enhancing the

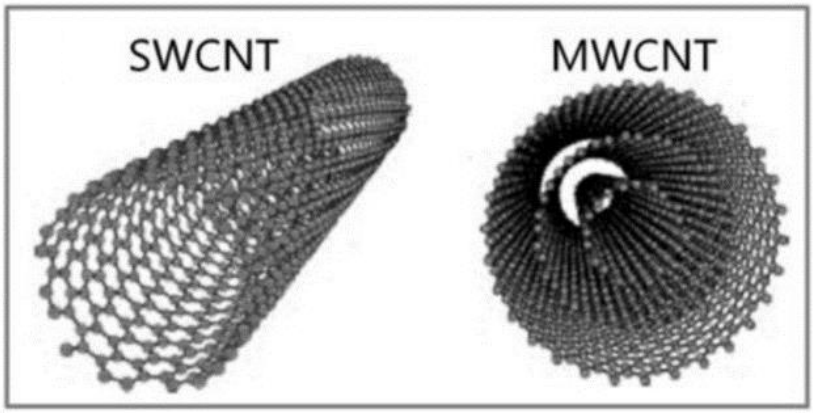

Figure 1.5 Schematics of SWCNT and MWCNT

conductivity of biomaterials remains inferior to that of graphene, as demonstrated by the measurable conductivity of rGO-based biomaterials in both dry and wet states [6].

Carbon nanotubes (CNTs) are constructed from hexagonally arranged carbon atoms that are rolled into cylindrical structures [133], [134], and exhibit excellent electrical conductivity and mechanical strength along their axial direction. CNTs can be classified into single-walled (SW) and multi-walled (MW) CNTs (Figure 1.5). The one-dimensional nanostructure and large aspect ratio of CNTs make them extremely easy and efficient in contacting with each other and forming conductive networks at low concentrations when blended within biomaterials[6]. However, the enhancement on material conductivity by CNTs can inevitably influence other properties, such as mechanical properties[135] and biodegradability [136]. CNTs can be synthesized through chemical vapor deposition (CVD) on inorganic substrates to grow massive CNTs with a vertically aligned nanostructure [6]. CNTs tend to form bundles and aggregations due to strong van der Waals forces. Frequently used strategies for dispersing CNTs include modifying them with functional groups (e.g., carboxyl groups by acid

treatment[137]) or molecules (e.g., polydopamine (PDA) [138], poly (ethyleneimine) (PEI) [139], gelatin methacrylate [140], DNA [141]), and/or using organic solvents [142] or surfactants [143], [144]. Only well-dispersed CNTs can efficiently and controllably form conductive networks within biomaterials [6].

1.2.3 Conductive Polymers

A class of polymers possessing unique properties that is finding great success in bioelectronics is represented by conductive polymers. In fact, they have the benefit of being mechanically flexible, a surface structure that can be easily modified. In contrast to common inorganic conductors and semiconductors which are hard materials, with a Young's modulus of about 100 GPa, conductive polymers are soft solids with a Young's modulus that ranges from 20 kPa to 3 GPa [145]. This softer nature has important consequences since it reduces the strain between the tissue and the electronic platform. Conducting polymers have been widely employed in electrode-tissue interface as they show improvements in terms of both electrical properties and biocompatibility [145]. A conductive polymer (CP) is a polymer (large molecules composed of repeating structural units) that possesses the ability to conduct electricity. Unlike traditional polymers, CPs have conjugated molecular structures that allow for the movement of charge carriers (such as electrons or ions) along their chains. This conductivity can be achieved through doping, where the polymer is chemically modified to introduce charge carriers or through other means like polymerization conditions. CPs comprise a backbone of alternating double and single bonds with overlapping π-orbitals that create a system of delocalized π-electrons [146]. This delocalized system can result in electrical conductivity values several orders of magnitude higher than insulating polymers [146] (i.e., $>10^{-9}$ Scm^{-1}) and strong optical absorption in the visible spectrum of light [147]. Polyaniline (PANI) and polypyrrole (PPy) represent two of the very first CPs reported to exhibit semiconducting properties [1], [2]. Polythiophenes (PTh) and derivatives, including poly(3,4-ethylene dioxythiophene) (PEDOT), have been extensively employed in various applications, including bioelectronics an cell interfacing *in vitro* [5] (Figure 1.6). One of the most important properties of CPs that makes them increasingly popular for bioelectronic applications is their ability to conduct both ionic and electronic currents [150]. When electrically biased in aqueous electrolytes, ions migrate from the electrolyte into the bulk of the polymer to compensate for electronic charges [151]. As such, ionic fluxes originating from biological activity can directly alter the electronic properties of CPs when in contact with cells or tissue [152].

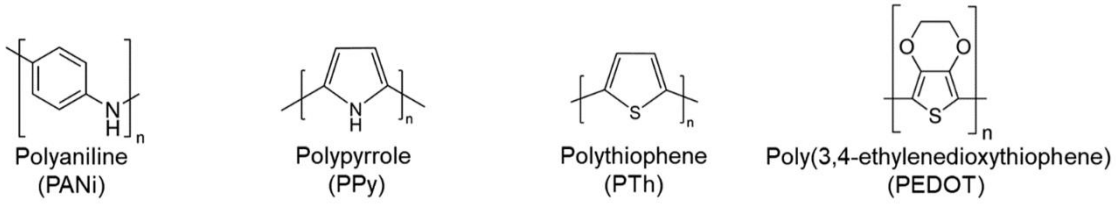

Figure 1.6 Structure of most common conductive polymers.

Polypyrrole

PPy is one of the first developed CPs and has found widespread applications in biomedical fields attributed to its excellent biocompatibility and easy synthesis [102], [153] . Yet, the brittle nature and insolubility of PPy have constrained the processing techniques and functional performance of biomaterials based on PPy [6]. Chemically synthesized or commercially available PPy dispersions can be blended with other components to fabricate hybrid composites in forms of films [154], [155], fibrous materials [60], [156], porous materials [157], [158] or hydrogels [159]. Alternatively, PPy can also be incorporated with other hydrophilic molecules during polymerization (e.g., chitosan [160], [161], [162] dopamine [163], GelMA [164]) and then fabricated into hybrid composites.

Polyaniline

PANi- and OANi-based biomaterials have attracted increasing attention attributed to their excellent biocompatibility and electroactivity [165]. Emeraldine salt is the highest conductive and most commonly used form of PANi and OANi [6]. Biomaterials based on PANi or OANi exhibit responsiveness to both electrical stimuli and pH levels [166] enabling the creation of conductive biomaterials with tunable conductivity and the ability to release substances in a controlled manner. The natural antibacterial properties of PANi and OANi also make them suitable for applications in wound healing [167], [168]. PANi can be formed into pure films [169], or can be applied as coating on substrates to create layered composites during its polymerization process [170], [171]. Additionally, it can be employed to produce conductive biomaterials featuring surfaces with high conductivity. As an alternative, PANi-based hybrid composites can be developed by integrating chemically synthesized amorphous PANi nanomaterials into polymeric substrates. [172], [173]. Electro polymerization is also feasible in fabricating PANi-based biomaterials [174], [175].

Poly 3,4-ethylene dioxythiophene

Recently, PEDOT has been widely investigated and employed thanks to its high conductivity, biocompatibility and versatile fabrication methods [176], [177]. PEDOT is a polythiophene derivative composed of chains of 3,4-ethylenedioxytiophene (EDOT) [177].It has been synthesized for the first time by F. Jonas, G. Heywang and W. Schmidtberg from the Bayer AG research laboratories (Germany) in 1988. It is emerging as the most promising material for its electrical, optical, and mechanical properties. In fact, it is a flexible conductive polymer that can reach a conductivity above 1000 S/cm and has a transmission above 90% in visible spectrum, moreover PEDOT:PSS is also biocompatible and has high chemical and thermal stability. The ionic and electronic conductivity, along with the electrochemical stability of PEDOT, render it especially appropriate for coating bioelectrodes. This suitability makes it ideal for interfacing with living electroactive tissues, allowing for the long-term recording of electrical signals or the application of electrical stimulation [178], [179]. Biomaterials coated with PEDOT have the capability to release drugs in response to electrical stimulation, a process facilitated by the electrical activation of PEDOT [107]. PEDOT can be synthesized by the polymerization of 3,4ethylenedioxythiophene (EDOT) through electro polymerization [40], chemical

oxidation (e.g., Fe^{3+} [180], [181], APS [180], [182]), or vapor-phase polymerization[183]. As many undoped polymers, PEDOT presents poor conductivity in its reduced state, while the oxidated states are conductive. When doped with polystyrene sulfonate (PSS), PEDOT chain is present in its partially oxidized state and shows the aforementioned conductivity, moreover, PEDOT is insoluble in water, while PEDOT:PSS is dispersible in it, allowing versatile fabrication techniques, such as solution casting, spin coating, ink-jet printing, and screen-printing, enabling fabrication on large-area and with cost-effectiveness [184], [185]. Anionic dopants, such as PSS [40], [186], pTS [183], [187] and ClO_4^- [39], [187], are often utilized during polymerization to enhance the structural stability and conductivity of PEDOT. Among them, PSS is the most frequently used dopant given its capability in realizing excellent

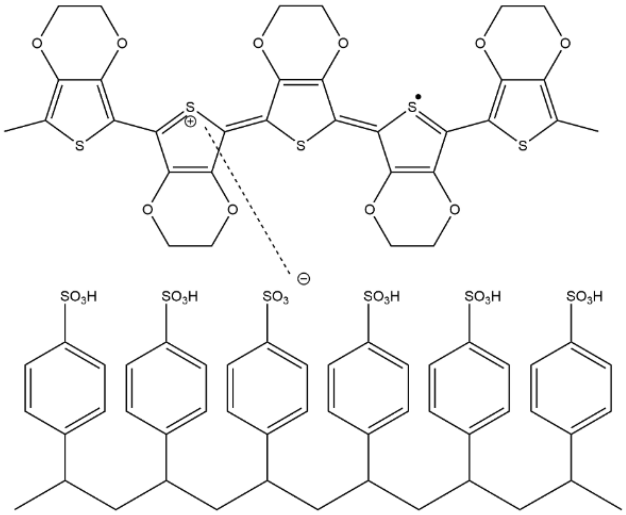

Figure 1.7 PEDOT:PSS structure.

stability and water-dispersibility of PEDOT (Figure 1.7).

The introduction of a hydrophilic PSS also leads to an increase in the ionic conduction of the polymer [188]. However, a high concentration of PSS can lead to less conductive films, due to a decrease in the size of the PEDOT particles in the suspension [189]. Some biomolecules (e.g., alginate [190], [191], peptides [192], heparin [193], laminin [192]) can also be doped with PEDOT to improve its bio affinity. The PEDOT:PSS dispersions can be blended with other components and then fabricated into hybrid biomaterials exhibiting homogeneous properties in forms of films [194], [195], [196], hydrogels [84], [197], [198], [199], [200], fibrous materials [201], [202], [203] and porous materials [204], [205]. PEDOT:PSS dispersions can also be easily coated onto biomaterial substrates through spin-coating [206], [207], [208], printing [41], [209] or absorbing [93], [210], to provide a highly conductive surface.

1.3 Macroscopic arrangement of conductive biomaterials

The components of conductive materials are crucial for their properties (e.g., conductivity, mechanical properties, biocompatibility, and biodegradability). The fabrication method can influence these properties and can lead to different structural features such as macroscopic and microscopic structures spatial distribution of components and anisotropic structural cues [6].

1.3.1 Distribution of conductive components

Based on the spatial arrangement of conductive elements within biomaterials, they can be categorized into two types: those with a homogeneous distribution and those with a layered distribution, each offering unique benefits for manipulating the properties and functions of the materials. Homogeneous biomaterials are typically produced by either mixing conductive elements into the biomaterials or synthesizing them in-situ. In contrast, layered biomaterials are usually created by applying conductive elements onto the surfaces of biomaterial substrates. In instances where conductive oligomers are block-copolymerized or grafted onto nonconductive polymers, biomaterials of significantly higher homogeneity can be achieved compared to other types of homogeneous conductive biomaterials. This superior uniformity is attributed to the low molecular weight of the oligomers. Furthermore, the properties of the materials can be finely tuned by adjusting the content of the oligomers. [211], [212], [213], [214]. Conductive components can lead to an enhanced material conductivity when their concentrations reach a threshold that conductive paths can form within biomaterials [6]. However conductive components at high concentrations may influence the mobility of polymer chains [215], or influence the crosslinking of substrates [216]. Layered composites offer the ability to precisely design which components are exposed to cells while controlling which ones remain completely or partially shielded. The orderly arrangement of neural cells in the spinal and peripheral nerves, as well as muscle cells in the heart and skeletal muscles, contributes to anisotropic electrical and mechanical microenvironments. This includes enhanced conductivity and stronger mechanical properties along the direction of alignment [34], [217]. Therefore, developing biomaterials with anisotropic structural, mechanical, and electrical properties to mimic these native tissue cues holds promise for regenerating neural, cardiac, and muscle tissues with their inherent anisotropic structures and functions [6]. Considerable effort has been devoted to creating conductive biomaterials that feature aligned structural cues. These cues can direct the orientation of cells in culture, thereby enabling the recreation of tissue functionalities that depend on specific alignments. When used in combination with aligned cell growth and directional electrical stimulation — delivered through two electrodes in a laboratory setting or via directional electrical signal propagation in a living organism — the structural cues and anisotropic conductivity of these biomaterials can synergistically mimic the microenvironment found in native neural, cardiac, and muscle tissues [6]. Several studies have shown the beneficial impact of integrating anisotropic biomaterial conductivity, aligned structural guidance, and directional electrical signal propagation on enhancing the regeneration of cardiac and muscle tissues [25], [218], where the

directions of these factors need to be matched with the physiological circumstances. The beneficial impact of conductive biomaterials on tissue regeneration may stem from their ability to enhance the transmission of bioelectric signals or electrical stimulation to cells and tissues. This implies that for conductive biomaterials to effectively direct electrical current preferentially through themselves, rather than through the culture medium or native tissues, they must possess a conductivity higher than that of the culture medium and native tissues, which is in the range of 10^{-3} to 10^{-2} S/cm. [219], [220], [221]. Materials with conductivity that matches or exceeds that of the culture medium or native tissues can effectively facilitate electrical connections between cells and tissues, provided they are sufficiently biocompatible to support cell growth. While conductive nanomaterials with a dispersed distribution might not form continuous conductive pathways or significantly increase the overall conductivity of biomaterials at low concentrations, they still hold the potential to locally connect adjacent cells and improve their electrical communication.

1.3.2 Films

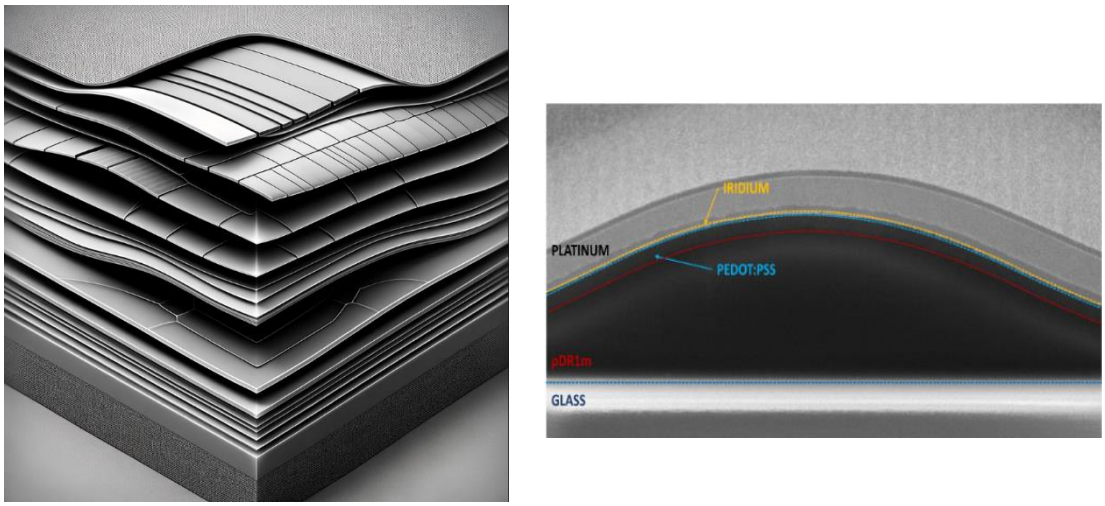

Figure 1.8 Schematics of film conductive biomaterials. Left image generated using DALL·E.

Solid films of conductive and nonconductive components are another kind of widely employed configuration of conductive biomaterials [222], [223]. Conductive films offer several benefits for TERM applications, including the simplicity of mass production and the ability to maintain uniformity across large areas. They also provide flexibility in designing the number of layers and in the patterned distribution of components, making them particularly advantageous for TERM uses (Figure 1.8). The density of films is beneficial for the enhancement of material conductivity attributed to relatively linear conductive paths [6]. However, films typically have a flat surface, a higher Young's modulus compared to soft tissues, and a slower rate of biodegradation compared to biomaterials in other forms. Films can be easily prepared by various methods: solution casting and solvent evaporation [212], [223], [224], spin coating [194], [225], spraying [123], [226], hot-compressing and laser sintering [227], [228], [229], solution molding [216], [230], electro polymerization of CPs on conductive substrates, or chemical polymerization of them on substrates, which can lead to a micro structured surface [37], [129], [231],

physical or electrostatic absorption [232], [233], chemical vapor deposition [234], metal sputtering [222], conductive ink printing. Hybrid films can exhibit compromised conductivity and biological properties, while layered designs of conductive films can bring them with not only highly conductive surface, but also some advanced electrical functionalities by coating conductive layers in a patterned manner and layering multilayer of nonconductive and conductive components [208], [235]. A CP coated on a metal electrode lowers the impedance per unit area by several orders of magnitude[152], due to the high volumetric capacitance of CPs[236], [237].

1.3.3 Fibrous Materials

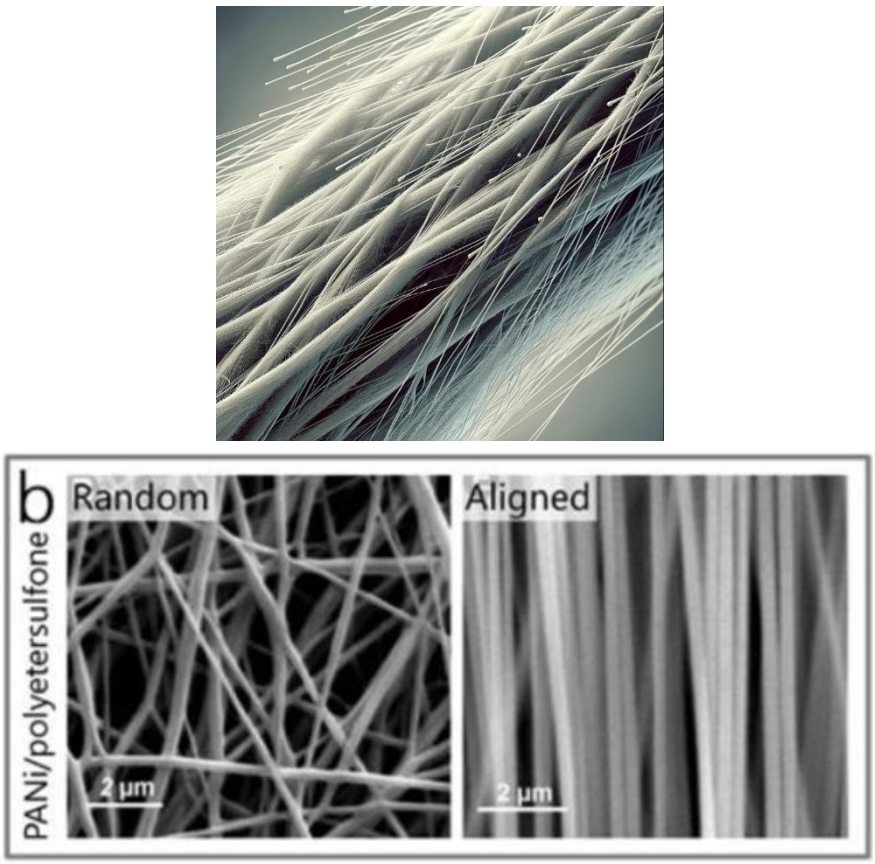

Figure 1.9 Schematics of fibrous conductive biomaterials. Top images generated using DALL·E.

Fibrous conductive biomaterials are made up of fibers whose diameters vary from tens of nanometers to a few millimeters. These materials can be manufactured in various forms, including individual fibers, meshes, membranes, and three-dimensional structures [238]. Conductive fibrous materials display a range of material stiffness that falls between that of porous materials and films, owing to their lower porosity relative to porous materials and the inherent strength of the fibers. However, their electrical conductivity is less than that of porous materials, potentially because the conductive pathways in fibrous materials are more complex [6]. Among the different types of fibrous conductive biomaterials, electrospinning is the most prevalent method used for their production. This established technique allows for the versatile, straightforward, and large-scale creation of fibrous materials, primarily

membranes. It works by electrostatically injecting solutions of polymers that can be electrospun and then elongating the jet flow to form nano- to micro-sized fibers [239], [240]. Electrospinning enables the fabrication of aligned electrospun fibers that can guide the oriented growth of cells [51], [113] (Figure 1.9). Hybrid electrospun conductive biomaterials with compromised conductivity and biological properties can be easily fabricated from the solution blending of all components [172], [241]. Alternatively, applying a coating of conductive elements onto nonconductive electrospun biomaterials is an effective strategy to significantly enhance their conductivity. In this approach, electrospun membranes can be treated with conductive materials, ensuring that the surface of every fiber is uniformly coated, thereby imbuing the fibrous biomaterials with substantially increased electrical conductivity [104], [242]. However, the coated conductive layer may impact the fibrous morphology of electrospun substrates to some extent [243], [244]. Wet-spinning can be conducted by injecting solutions of some polymers or nanomaterials into coagulation baths, where the injected flow can be coagulated into fibers by solvent extraction or chemical reaction [107], [245].The wet-spun fibers used for TERM applications often appear as single fibers with diameters of tens to hundreds of microns. Another frequently used method is 3D-printing based on mechanically [47], [52] or electro hydrodynamically [201] extruding the fluids of polymers or nanomaterials. The 3D-printed fiber can be arranged in highly ordered manners, such as aligned fibers [51], [246], meshes [52], [211], membranes [201] and 3D architectures [49], [247], where intersecting fibers are often bonded at their junctions. Conductive nanofibrous materials fabricated by phase separation have also been employed [43], [248]. Other methods, such as hot drawing [249], mechanical-drawing [250], [251], and molding in tubular templates [72], [96], are also practical in fabricating conductive fibers.

1.3.4 Porous Materials

Porous materials are characterized by their adjustable porosity, pore size, and pore morphology, making them well-suited for cell localization and infiltration. When compared to nonporous materials made from the same substances, porous conductive biomaterials offer several benefits. These include a

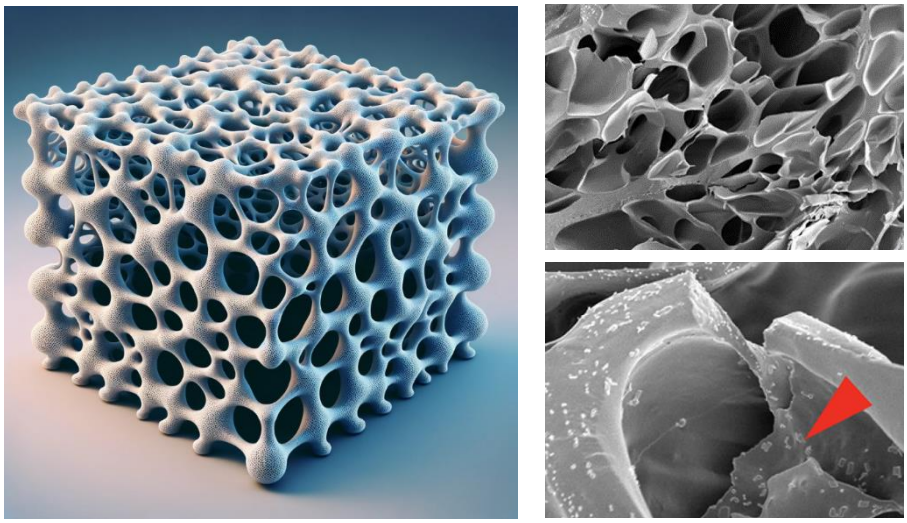

Figure 1.10 Schematics of porous conductive biomaterials. Left image generated using DALL·E.

considerably larger specific surface area, reduced density, greater deformability, a rough surface texture, and enhanced permeability (Figure 1.10). The presence of pores can increase the length of conductive paths, and thickness of materials, thus leading to relatively low conductivity (10^{-7} - 10 S/cm) and modulus (10^{-2} - 102 MPa) of porous materials compared to films [6]. Different strategies can be adopted to obtain porous materials, the most commonly used is freeze-drying induced formation of pores. Ice crystals can spontaneously form within pre-solutions or crosslinked hydrogels to create pores and fix the volume of biomaterials, and then easily removed by lyophilizing [22], [62], [252] or thawing [132], [164], [253]. With this technique it is possible to control pore dimension and alignment by applying controlled temperature gradients thus obtaining anisotropic mechanical properties [254]. Porogen leaching is another technique in which removable pore formers such as sugars [46], [58], salts [255] and polymers [114], can be blended within pre-solutions, and then leached after the formation of biomaterials. Conductive materials based on templates such as foams (e.g., nickel [256] and polymeric [161], [257] foams) and tube arrays [171], can be fabricated by depositing a conductive layer onto their surface, leading to highly controllable porous structures. The templates can be leached, or kept, in using as biomaterials. Additive (i.e., 3D printing [56], [247]) and subtractive (e.g., punching [258], laser-etching [259]) manufacturing methods can be used for preparing biomaterials with highly regular pore. Incorporating conductive elements into the precursor solutions used to create porous materials, or coating the inner surfaces of the pores with conductive components, can endow porous biomaterials with improved electrical conductivity, which is advantageous TERM applications. The rough texture and microscale pores of these conductive porous biomaterials offer an ideal environment for the adhesion and localization of excitable cells. [6].

1.3.5 Hydrogels

Hydrogels are hydrophilic crosslinked polymeric networks with high water content, reversable swelling properties, fast degradation and easy processability. Physical and biochemical properties of hydrogels largely depend on their compositions, methods used for their polymerization, and their crosslinking density [260]. Hydrogels for biomedical applications are designed to resemble the characteristics of native extracellular matrix (ECM) and to provide three-dimensional (3D) supports for cellular growth and tissue formation [260]. Conductive hydrogels are usually constructed via the incorporation of conductive polymers, metal/carbon-based materials, or ionic side groups or salts into elastic 3D hydrogel networks[261]. However, phase separation between the conductive additive and the polymer network usually causes a reduction of mechanical and conductive stability[261]. Therefore, in order to endow conductive hybrid hydrogels with good performance, it is necessary to ensure a stable and strong combination between the polymer network and conductive additive [261]. The conductivity of conductive hydrogels falls within a relatively limited range, typically from 10^{-6} to 10^{-2} S/cm, largely because of water's inherent conductivity and its interference with the formation of conductive pathways by the conductive elements. This range of conductivity closely mimics that of the host tissues [6]. In

addition, the mechanical properties of hydrogels can also be modulated within a biomimetic range (mostly 10^{-4} - 10 MPa of modulus,) comparable to soft tissues by selecting polymeric components and controlling moisture content. Conductive hydrogels for biomedical applications can be crafted from natural-derived polymers (e.g., collagen [60], gelatin [262], [263], GelMA [264], [265], [266], chitosan [267], alginate [41], [84] and bacteria cellulose[54], [268]), synthetic polymers (e.g., PEG [135], [269], [270], PVA [116], [271], PAAm [182], [272] and PNIPAAm [273]), conductive nanomaterials (e.g., CNTs and GNMs [274], [275]) and conductive polymers(e.g., PEDOT:PSS [197], [198], [276]). The enhanced conductivity of hydrogels can be realized by blending conductive components into the pre-gelation solutions (e.g., dispersed CPs and conductive nanomaterials), or in-situ synthesizing CPs within hydrogels [6] (Figure 1.11).

Conductive polymer-based single network hydrogels are obtained by the direct cross-linking of conductive chains to form a 3D network structure by chemical bonding, ionic cross-linking, or physical penetration methods[261]. Hydrogels formed directly from conductive polymers usually exhibit high

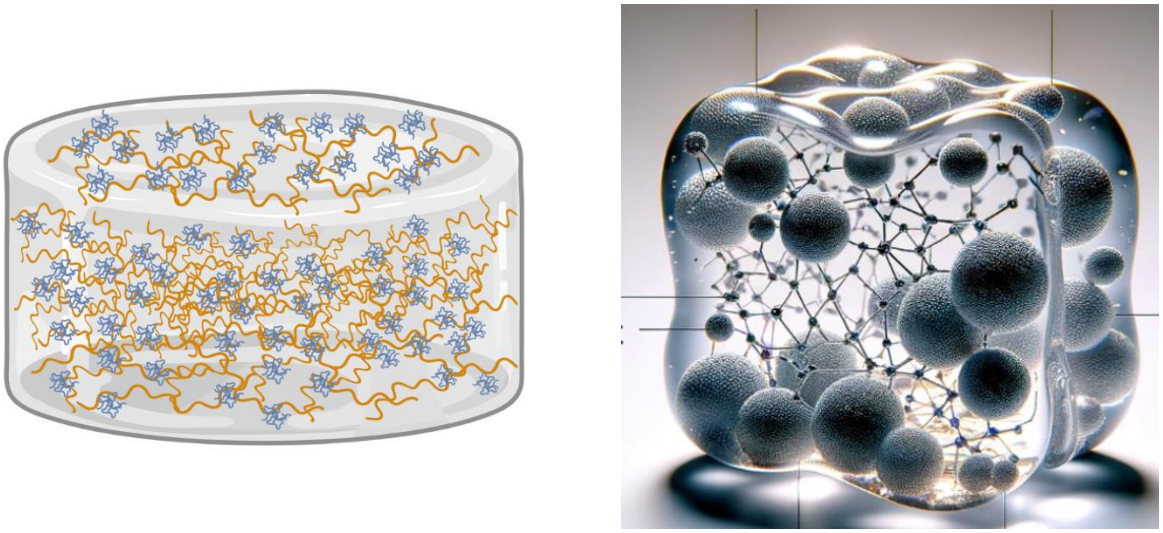

Figure 1.11 Schematics of hydrogel based conductive biomaterials. The image on the right was generated using DALL·E.

conductivity. However, such hydrogels generally exhibit lower stretchability and poor mechanical properties [261]. To improve the mechanical properties, the conductive additive is usually introduced into the polymer network to prepare conductive hydrogels. The hybrid hydrogels simultaneously exhibit superb elasticity, possess a high toughness, and maintain high electrical conductivity [261]. Conductive additives are generally pre-dispersed in the polymer precursors for further cross-linking and polymerization. The conductivity and mechanical properties of the hydrogels can be regulated by adjusting the type and content of the additive [261]. Overall conductive hydrogels represent a promising class of materials for tissue engineering, regenerative medicine and bioelectronic interfacing. Their resemblance to the physiological environment in terms of 3D structure, water content and mechanical properties allows cells and tissue to have a better interfacing reducing risk of inflammation and rejection. The adaptability of conductive hydrogels is further enhanced by their ability to incorporate a wide range

of natural and synthetic polymers, conductive nanomaterials, and functionalization techniques. This adaptability enables the development of application-specific materials. Their easy and mild condition processability is a point of strength, allowing to encapsulate living systems (e.g, cells, organoinds) into final material without compromising viability. Conductive hydrogels emerge as a versatile and promising class of biomaterials representing a significant advancement in the field of biomaterials, offering innovative solutions for complex biomedical challenges.

1.4 Thesis Project

In the previous paragraphs, CP-based hydrogels were introduced as promising neuroelectronic interfaces, to sense and stimulate cellular behaviour, closing the gap in terms of mechanical an electrical mismatch in comparison to metal and silicon-based electrodes. Several challenges are still open in terms of matching biological curvature, size, and interface stiffness. Despite the enormous progress in the organic bioelectronics field, engineering of 3D patterning of the CPs at micro and nanoscale and the combination of biological and physical stimuli and conductivity to better mimic the biological environment remains a challenge.

A common strategy to increase the material/electrode coupling consists in manipulating over different length scales material interface with tissues. In fact, topography, and aspect ratio of nano and micro structured surfaces can modulate the interaction with cell membrane affecting also intracellular signaling [277]. Despite the excellent mechanical features of planar surfaces and their good charge transport properties, the large cleft between the cellular membrane and the surface of the electrode affects the coupling/ adhesion with cells/tissues and consequently the quality of the recorded signals and the stimulation efficiency. Moreover, in *in vitro* applications, 2D cultures fail to fully recapitulate the tissue environment, exhibiting non-optimal structural features due to the planar mechanical constraints which differs greatly from the three-dimensionality and dynamicity of native tissues (Figure 1.12) [277].

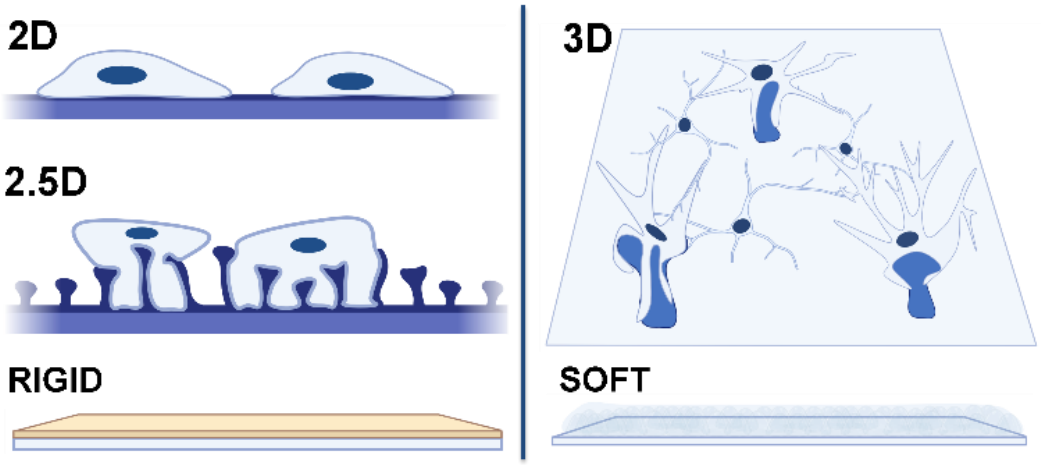

Figure 1.12 Comparison of traditional flat and 2.5D rigid substrates and 3D soft substrates.

Advanced fabrication strategies have been recently proposed to obtain high-resolution patterning and control the 2.5D conductive polymer morphology. For instance, direct photopatterning of PEDOT:PSS was demonstrated by a dry process involving the use of photoacid generators and the synthesis of acid amplifiers to generate PSS autocatalytically [277]. Despite the remarkable coupling improvements brought by patterned 2.5D materials, 3D scaffolds excellent candidates for replicating the complex designs of biological tissues. Indeed, inspired by the extracellular matrix (ECM) architecture, 3D scaffolds can accommodate cells promoting cell-cell and cell-ECM development and interactions. Furthermore, 3D conductive scaffolds ultimately combine the optimal spatial arrangement of cells and

ECM to electrical stimulation and sensing. In fact, 3D conductive scaffolds have been developed for several applications responding to different tissue engineering demands: in brain field, promoting the attachment, proliferation and differentiation of neural stem cell, promising also to trigger cell neurogenesis, while assisting the direction of Schwann cells and increase the proliferation rate in nerve regeneration [277].

In this context, CPs have been engineered to grant three dimensionality to cellular culture along with a high surface area for cell adherence and proliferation as well as electrical conductivity for stimulation or sensing.

Challenges in providing electrical and morphological stimuli via these materials persists. Integration of such materials into more complex circuitry requires patterning resolution, flexibility, and control over the geometry to be achieved (Figure 1.13).

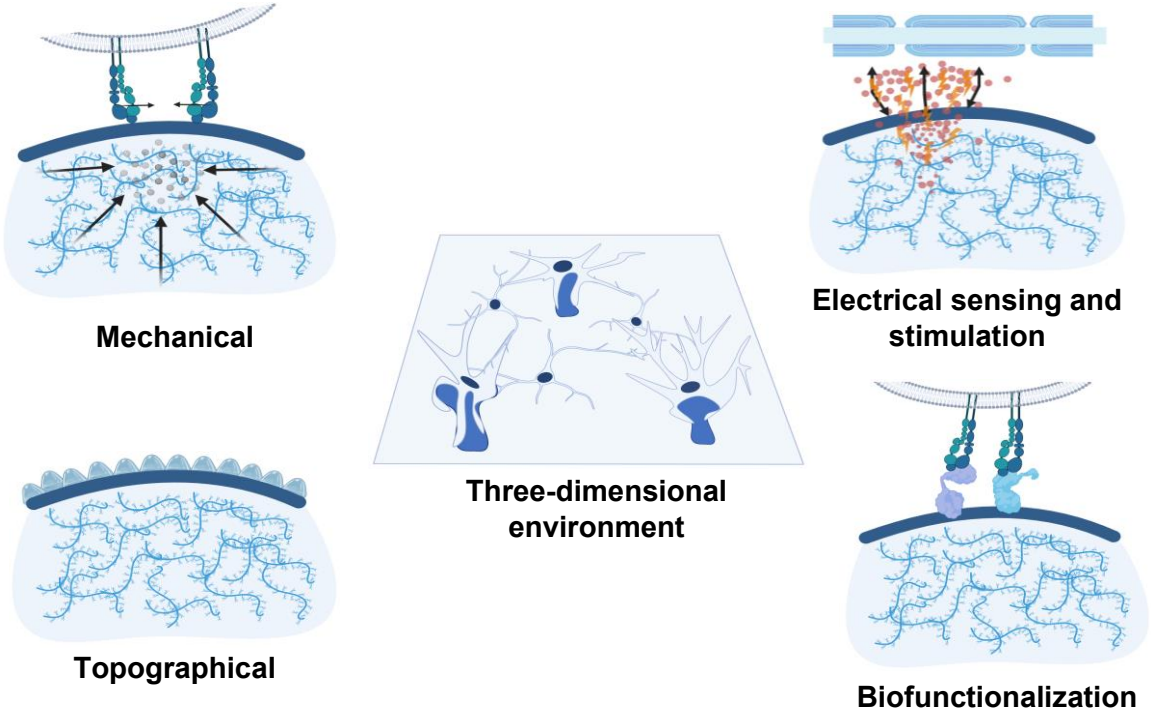

Figure 1.13 Cell-electrode interface requirements.

Photo patterning is a method that enables selective material polymerization under light exposure, facilitating the creation of devices with specific geometries and resolutions. Techniques like UV curing, mask lithography, stereolithography (SLA), direct laser writing (DLW), and two-photon polymerization lithography leverage photopolymerization for this purpose. UV curing is adept at producing large structures (several centimeters) with small features quickly, whereas mask lithography offers somewhat higher resolutions (around 10µm) with fast production times, though it's restricted to 2D patterns. SLA

and DLW are versatile, capable of crafting both small and large 3D structures (ranging from hundreds of micrometers to several centimeters) with decent resolution, albeit at slower printing speeds. Two-photon lithography stands out for creating self-supporting 3D structures from millimeters to hundreds of nanometers with the finest resolution, but it's a slow, hard-to-scale process, requiring costly equipment. Additionally, the materials typically used in this method have drawbacks like poor conductivity and high stiffness. Although recent years have seen a few instances of hydrogel printing using this technology, most applications suffer from slow processing, the use of photo initiators that are neither water-soluble nor readily available commercially [278], [279], [280] .

The objective of this study is to develop and produce an electroconductive hydrogel capable of achieving structures across various length scales that meet the previously mentioned criteria.

To this aim, an electro conductive hydrogel based on gelatin and PEDOT:PSS is presented in this work. Gelatin, modified with methacrylate groups, serves as photo curable material with bioactive features and tuneable mechanical properties, while PEDOT:PSS acts as the electro conductive element. The obtained blend has been 3D photo-patterned exploiting multiple techniques from drop casting and subsequent UV photopolymerization, mask lithography and two-photon-polymerization (2PP) lithography reaching patterning at different scale lengths. The degree of methacrylation (DOM) was assessed by proton nuclear magnetic resonance (^{1}H-NMR). The resulting 3D structures has been characterized by optical microscopy and electrochemical measurements. Finally, biocompatibility assays were carried out with neuronal cells.

2 Materials and methods

In this chapter the materials, the protocols and the characterization techniques used in this thesis are described. All materials, chemicals and instruments used in this work are listed in A | Appendix A.

2.1 Material synthesis and characterization

2.1.1 Synthesis of gelatin methacryloyl

In this work, gelatin methacryloyl (GelMA) (Figure 2.1) with low, medium and high degree of methacryloylation was synthetised accordingly to [281]. Briefly 10g of gelatin were dissolved in 100mL of Dulbecco's modified phosphate buffered saline no calcium, no magnesium (DPBS) at 45°C under slow stirring. Then, methacrylic anhydride (MA) was added drop wise to gelatin solution at 0.06 $mg/g_{gelatin}$, 0.12 $mg/g_{gelatin}$, 0.6 $mg/g_{gelatin}$ and the solution was heated at 50°C while stirring vigorously. After 3 hours, 200 mL of DPBS were added to the solution to stop the reaction. The solution was then centrifugated at 3500g for 4 minutes at RT. After centrifugation a white pellet deposited on the bottom. The clear supernatant was collected and dialyzed against deionized water at 40°C for 5 days changing dialysis medium twice a day. Finally, the solution was freeze dried for two days. GelMA foam was stored at -20°C up to three months.

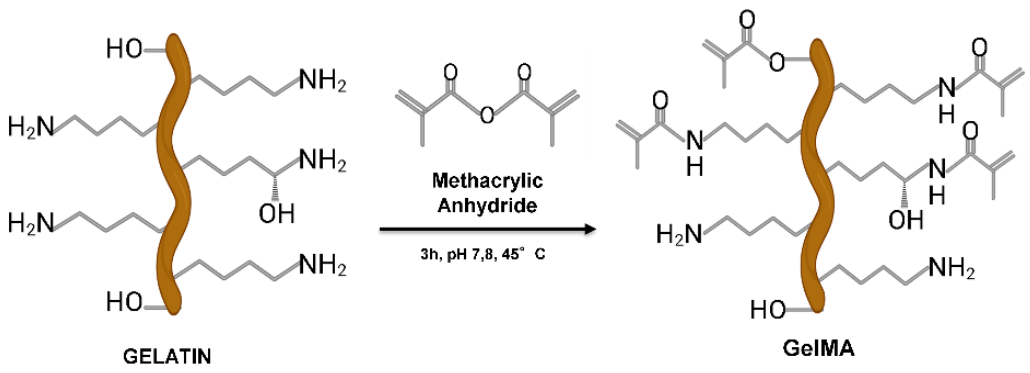

Figure 2.1 Schematics of GelMA synthesis.

2.1.2 Proton nuclear magnetic resonance

Nuclear magnetic resonance (NMR) spectroscopy is one of the most powerful and widely used techniques in chemistry to investigate molecular structures. Such technique exploits an external magnetic field at a certain radiofrequency which interacts with the local magnetic fields around atomic nuclei that have a fractional quantum nuclear spin and generate a magnetic moment (e.g., ^{1}H and ^{13}C).

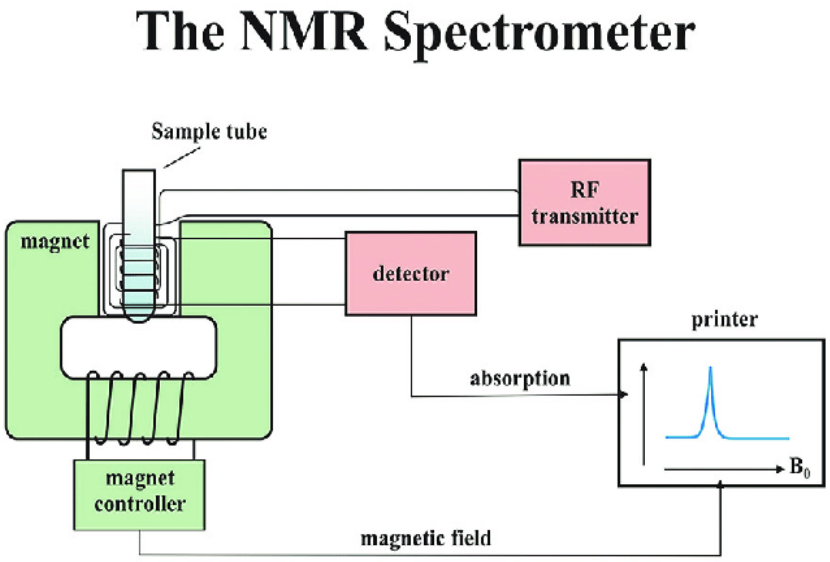

Figure 2.2 Schematics of a typical nuclear magnetic resonance spectrometer.

When the sample is immersed in a magnetic field, the nuclear magnetic moment is aligned to the external field in two directions with different energies. If the sample is irradiated with a pulsed radiofrequency, the low energy nuclei absorb a quantum energy and reach the high energy ones being in resonance with the applied radiation. The decay from the higher energy state produces an induction current, free induction decay (FID), containing all the information of resonance frequencies of the nuclei in the time domain. The application of a Fourier Transformation produces the conventional NMR spectrum in the frequency domain Figure 2.2. The actual resonance frequency of a nucleus also depends on its surrounding atoms, thus producing a shift with respect to the nominal resonance frequency of a given atom. Thanks to this phenomenon, NMR spectroscopy allows to discriminate individuals atoms within a molecule enabling the determination of the overall molecular structure of a compound.

In this work, ^{1}H-NMR experiments were performed with an Avance III 600 MHz (Bruker) spectrometer, operating at 600.0 MHz (^{1}H). The samples were dissolved in 100 mg/ml D_2O at 45°C for 30 minutes. Chemical shifts refer to the residual water peak (H_2O, δ = 4.7 ppm for ^{1}H-NMR). Typical acquisition parameters for ^{1}H spectra were: 45°C, 10 s of recycle delay, 12 scans and the excitation sculpting water suppression was applied to the pulse program. The phenylalanine signal between 7.25 and 7.6 ppm was taken as reference and used to normalize all the spectra, since this peak is proportional to polymer concentration. The amount of lysine methylene signal ($NH_2CH_2CH_2CH_2CH_2$-) at 3 ppm has been

considered to quantify the number of free -NH_2 moieties still present after the reaction with methacrylic anhydride. More in detail, these signals (between 3.0 and 3.25 ppm) were integrated in both gelatin and GelMA spectra to obtain their area and the DoM of GelMA samples was calculated following Equation 2.1:

Equation 2.1

$$DoM = \left(1 - \frac{Lysine\ proton\ of\ GelMA}{Lysine\ proton\ of\ gelatin}\right) * 100$$

2.1.3 GelMA\PEDOT:PSS blend preparation

For all following experiments GelMA with high DOM was selected. GelMA and GelMA\PEDOT:PSS precursors with 0%wt, 1%wt%, 3%wt and 5%wt PEDOT:PSS where prepared as follows. GelMA content was fixed at 10%w/v unless specified. Commercial PEDOT:PSS solution (Clevios PH1000) was sonicated at 4°C for 30 minutes and filtered with 0.22 µm hydrophobic syringe filter. Concentration was verified after freeze-drying and weighing. Filtered solution was allowed to warm up to RT. GelMA\PEDOT:PSS 1%wt was obtained by dissolving 100 mg of GelMA in 0.9 mL of deionized water (DI-H_2O) at 45°C for 10 minutes. 30 mg of the photoinitiator lithium phenyl-2,4,6-trimethylbenzoylphosphinate (LAP) were added to the solution. LAP content was fixed at 3%w/v for all formulations. After 20 minutes, 0.1 mL of filtered PEDOT:PSS were added dropwise to the solution under vigorous stirring at 50°C. After 30 minutes, the solution was centrifuged at 3000g for 2 minutes to remove bubbles. Similarly, GelMA\PEDOT:PSS 3%wt and GelMA\PEDOT:PSS 5%wt were obtained by dissolving GelMA in 0.7mL DI-H_2O adding 0.3 mL PEDOT:PSS, and 0.5 mL DI-H_2O adding 0.5mL PEDOT:PSS, respectively. For bare GelMA hydrogels, GelMA was dissolved in 1 mL of DI-H_2O. During preparation the mixture was maintained in the dark to avoid exposure to light preventing crosslinking. After preparation, the solution was stored into a 4 mL amber vial at 5°C up to two weeks.

2.1.4 Tube inverting test

Tube inverting test is a simple method used to analyse the sol-gel transition of a solution subjected to a gradual temperature change. In this work, “inverse” tube inverting test was carried out to determine how PEDOT:PSS concentration influences characteristic physical gelation. To this aim, GelMA 10% and GelMA\PEDOT:PSS solutions with different PEDOT:PSS concentrations (1%wt, 3%wt and 5%wt) were analysed. Solutions were prepared as described in 2.1.3 and 1 mL of each was transferred into a 4 mL vial. Then the samples were subjected to a controlled temperature change from 37°C, 20°C and 4°C and then from 4°C to 20°C and from 4°C to 37°C. At each step, the samples were observed every 2 minutes and maintained for a total of 20 minutes. The samples were considered as a gel when “no flow” was visible with 30 s of tube inversion.

2.1.5 Photorheology

Rheology is the study of the flow and deformation of materials, primarily liquids and soft solids, under the influence of applied forces or stresses. The physical principles underlying rheology involve the concept of stress and strain. Stress refers to the force applied per unit area, while strain represents the resulting deformation or change in shape of the material. Different materials exhibit diverse rheological behaviours, including Newtonian fluids, non-Newtonian fluids, viscoelastic materials, and solids. Rheological measurements typically involve the application of controlled stresses or strains to a material and the observation of its response. Common rheological techniques include rotational and oscillatory rheometry, capillary rheometry, and extensional rheometry. These techniques allow to characterize various properties of materials, such as viscosity, elasticity, yield stress, and shear modulus, under different conditions. Photorheology is a specialized branch of rheology that involves the use of light to manipulate and study the rheological properties of materials. In photorheology, photoresponsive molecules or materials are incorporated into the sample, allowing for the control of rheological properties upon light exposure. Photoresponsive molecules or materials undergo structural changes, such as isomerization, cis-trans conversion, or photo-crosslinking, upon exposure to specific wavelengths of light. These structural changes can lead to modifications in the rheological behaviour of the material, such as changes in viscosity, elasticity, or flow properties.

In this work, photorheology was performed to investigate photopolymerization kinetics of the UV-cured hydrogels. All experiments were performed on a TA instrumets Discovery Hybrid Rheometer HR30 equipped with a UV curing module in parallel-plate mode (20 mm diameter, 0.2 mm of gap) at 37°C. Linear visco-elastic region was identified with a strain sweep test at an oscillatory frequency of 1 Hz. Photorheological measurements were performed at the same oscillatory frequency and with 1% of strain. The irradiating light (50 mW/cm^2 of intensity) was turned on after 60 seconds to allow the stabilization of the system before the onset of the photopolymerization. The evolution of the storage modulus (G′) during the time was recorded to evaluate the polymerization kinetics. Sol-gel phase transition was further evaluated by recording the cross-over points (i.e. time point where G”/G’ = tan δ = 1).

2.2 Fabrication and characterization

2.2.1 Fabrication of GelMA\PEDOT:PSS hydrogels at macroscale

GelMA and GelMA\PEDOT:PSS hydrogels with 1 cm in diameter and 1 mm thickness were obtained as follows. The precursor solution prepared in 2.1.3 was heated at 50°C into a water bath for 10 minutes until the mixture was fluid. A circular mould in poly-lactic acid (PLA) was placed onto a glass slide covered with a plastic film that facilitated the detachment of hydrogels. 80 µL of solution were casted into the mould and exposed to UV light (Spectroline® UV-Lamp, E-Serie, 365nm, 4W). After 15 minutes, the hydrogels were removed from the mould and developed in DI-H_2O for 45 minutes at 45°C. After development, hydrogels were stored into DI-H_2O up to 2 weeks at RT.

2.2.2 Water uptake

Water uptake ability of hydrogels influences cell behaviour by affecting different hydrogel properties, such as: hydrogel mesh size, which in turn affects hydrogel permeability (gas and nutrient diffusion) [282], hydrogel stiffness [283], and electrical properties of conductive hydrogels [284]. In this work, the water uptake of hydrogels was evaluated by a gravimetric method. Briefly, after their preparation, hydrogels were completely dried overnight at room temperature and weighed (W_{dry}). Afterwards, dried hydrogels were immersed in 5 ml of DPBS solution per hydrogel at 37 °C for 24 h. At each time point (1, 2, 4, 8 and 24 hours), the samples were collected and weighed (W_{wet}) after carefully removing the excess of water. The percentage water uptake was calculated according to Equation 2.2 :

Equation 2.2

$$Water\ Uptake\ (\%) = \frac{W_{wet} - W_{dry}}{W_{dry}} * 100$$

2.2.3 Electrochemical polymerization of PEDOT:PSS inside GelMA hydrogels

Two strategies were explored to obtain electropolymerized PEDOT:PSS inside GelMA hydrogels. Electro polymerization occurs when a potential that exceeds EDOT oxidation potential, which is between 0.8 V and 0.9 V, is applied to an electrolytic solution containing EDOT[186]. The first strategy involved the preparation of a GelMA-based hydrogel as in 2.2.1, air-dried for 24 hours and afterwards immersed for 48 hours in a water solution containing EDOT (10 mM) and NaPSS (100 mM) under moderate stirring. The hydrogels were then placed between two ITO coated glasses and connected to a potentiostat (Biologic VSP-300). Electro polymerization was carried out by applying a potential difference of 1.1 V. The second strategy consisted of preparing a GelMA precursor solution as indicated in 2.1.3 but using as solvent a water solution of EDOT (10 mM) and NaPSS (100 mM) without any pre-polymerized PEDOT:PSS. Then the blend is photo polymerized as explained in 2.2.1. After photo polymerization of GelMA, electro polymerization of PEDOT:PSS was carried out by placing hydrogels between two ITO coated glass and applying a potential difference of 1.1 V.

2.2.4 Oxidative polymerization of PEDOT:PSS inside GelMA hydrogels

Oxidative polymerization was investigated to obtain PEDOT:PSS blends within GelMA hydrogel.

Polystyrene sulfonic acid (PSSH) was stirred in distilled H_2O for 30 minutes before the addition of EDOT. The reaction mixture was vigorously stirred for 30 minutes. Then 1 mL of the solution was used to obtain a precursor solution of 10%w/v GelMA and 3%w/v LAP. The blend was then photo cured as explained in 2.2.1. Development was carried out in a solution of $Na_2S_2O_8$ and $Fe_2(SO_4)_3$ for 48h in order to initiate oxidative polymerization of PEDOT:PSS.

2.2.5 Impedance Spectroscopy

The impedance is the opposition of a component of an electrical circuit to alternating current (AC), it is composed by the combined effect of resistance and reactance in the circuit, and it is analogous to the resistance, which is the opposition of a component to direct current (DC). Quantitatively, the impedance of a two-terminal circuit element is the ratio between the complex representation of the sinusoidal voltage between its terminals, and the complex representation of the current flowing through it. In general, it depends upon the frequency of the applied sinusoidal voltage. Impedance extends the concept of resistance to alternating current (AC) circuits, and is described with both magnitude and phase, unlike resistance, which is described only with the magnitude. Impedance spectroscopy represents a powerful tool to investigate both the rate and the mechanism of charge transfer processes in electrochemical systems. Therefore, it is widely used also for the characterization of conducting polymer films and membranes. Since an AC is applied, the impedance is defined with two parameters: the total impedance Z and the phase shift Φ. Impedance variations are characteristic to the electrical circuit and the material´s impedance response is related to the properties of the working electrode and the ohmic resistance between the working electrode and the reference. In this work, IS data were recorded using two different configurations: a two-electrodes set-up in which two gold coated glass substrate acted as electrodes (Figure 2.3) and a three-electrodes set-up in which an ITO coated glass worked as working electrode

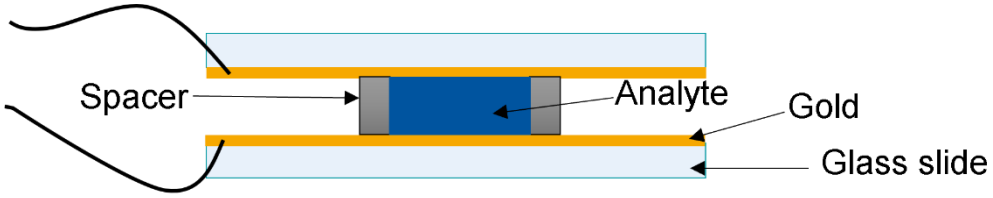

Figure 2.3 Schematic of a two-electrode set-up for IS measurements.

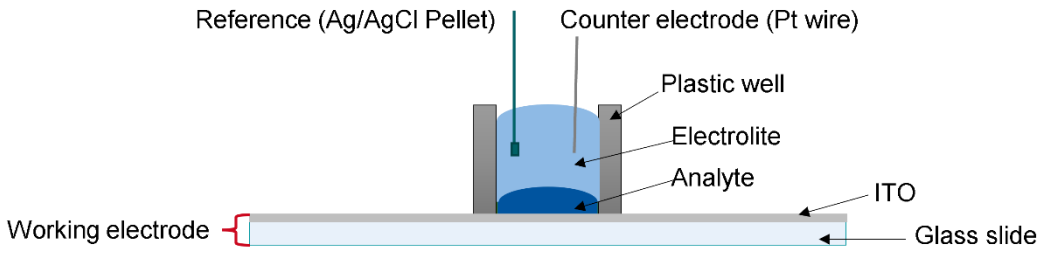

Figure 2.4 Schematic of a three-electrode set-up for IS measurements.

(WE), Ag/AgCl pellet electrode was used as reference electrode (RE) and a platinum wire as counter electrode (CE) (Figure 2.4). For the two-electrodes set-up, the distance between the two electrode was fixed with a 0.9 mm spacer. A potentiostat/galvanostat (Biologic VSP-300) interfaced with a desktop computer, equipped with the EC-Lab software was used to acquire signals. Measurements were performed on 10%w/v GelMA hydrogels containing 0%wt, 1%wt, 3%wt and 5%wt PEDOT:PSS at RT fabricated as in 2.2.1. The sinusoidal input signal was set to 10 mV by scanning a range of frequencies from 0.1 Hz to 100 kHz, this range covers the totality of applications in bioelectronic systems.

2.2.6 Substrate cleaning

Glass coverslips (3 cm, 1 cm and 1.2 cm in diameter and 170 µm in thickness) were soaked into a DI-H_2O solution of Alconox 10g/L and sonicated for 10 minutes at 100% power. The substrates were then soaked into DI-H_2O and sonicated for 10 minutes at 100% power. After this, the substrates were soaked into acetone and sonicated for 10 minutes at 100% power. Finally, the substrated were soaked in 2-propanol (IPA) and sonicated for 10 minutes at 100% power. In conclusion substrates were dried with help of a nitrogen gun.

2.2.7 Silanization of glass substrates

To improve the adhesion of hydrogels to the glass coverslip, the surface was functionalized with the silanization agent 3-(trimethoxysilyl)propyl methacrylate (TMSPMA) accordingly to [285] (Figure 2.5). Briefly, after cleaning as described in 2.2.6, the surface was activated with oxygen plasma (2 min, 100 mW, O_2 20 mL/min). Then substrates were submerged into an ethanol (EtOH) solution of TMSPMA 0.5% v/v and acetic acid (1:10) 3%v/v. After 15 minutes, the substrates were rinsed with IPA and dried with a nitrogen gun. The silanized substrates were stored in the dark at RT up to 1 week.

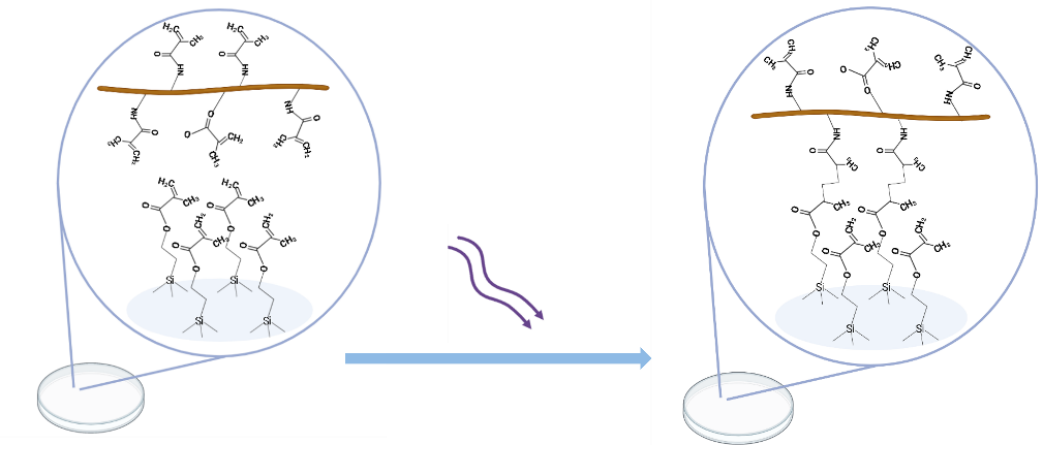

Figure 2.5 Schematics of GelMA binding silanized substrate upon light exposure.

2.2.8 Contact angle

When a drop gets into contact with a solid material, it is possible to define a contact line joining all three phases: solid, liquid and vapor. In this situation it is possible to define an angle between the tangent to the liquid - solid interface and the horizontal plane of the surface, this angle is called contact angle θ_Y. From the physical point of view, it is used to quantify the wettability of a surface because it reflects the behaviour of molecular interactions between the three phases: solid, liquid and vapor (Figure 2.6). The value of the contact angle that water forms when in contact with a surface is a parameter used to classify materials according to their behavior:

- $\theta_Y < 90°$ Hydrophilic behavior: indicates the tendency of some materials to bind with water and consequently to retain it on their surface;

- $\theta_Y > 90°$ Hydrophobic behavior: indicates the tendency of some materials to repel water on their surface;

- $\theta_Y > 150°$ Superhydrophobic behavior;

When the drop reaches its equilibrium position, it is possible to measure its contact angle.

Contact angle measurements of bare glass coverslip, oxygen plasma activated glass coverslip and silanized coverslip were obtained by depositing 2 µL of DI-H_2O onto substrates using a Dataphysics OCA 20 contact angle measurement system.

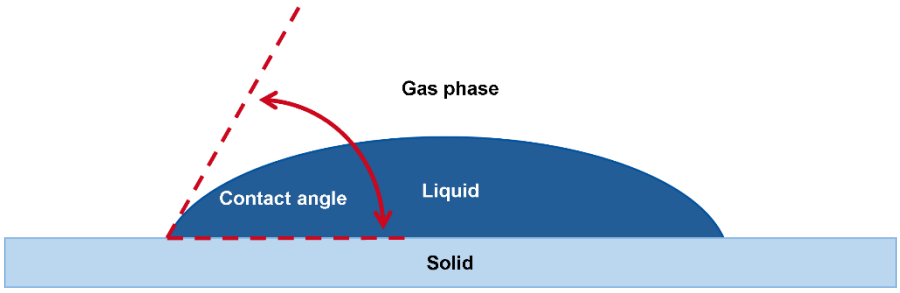

Figure 2.6 Schematics of contact angle.

2.2.9 Fabrication of GelMA\PEDOT:PSS hydrogels at mesoscale

A custom set up for mask lithography was designed using Solidworks and then 3D printed in PLA using an fused deposition 3D printer Anycubic Mega X (Figure 2.7). The mask aligner is composed by a sample holder (Figure 2.7, bottom) with a 25.5 cm × 25.5 cm sample housing equipped with a hole for easy extraction of substrates. The mask is kept in place by a mask holder (Figure 2.7, middle) that precisely align the mask (Figure 2.7, top) to the substrate with the aid of 4 pillars at each corner of the sample holder. The mask was fabricated via micro-milling an aluminum foil (0.5 mm thick) (Figure 2.8). Different circular holes were designed ranging from 500 µm, 200 µm and 100µm in diameter. The

distance between the mask and the sample was set to 0.5 mm. The UV source is directly placed on top of the mask holder since the housing for the mask matches the dimensions of the lamp.

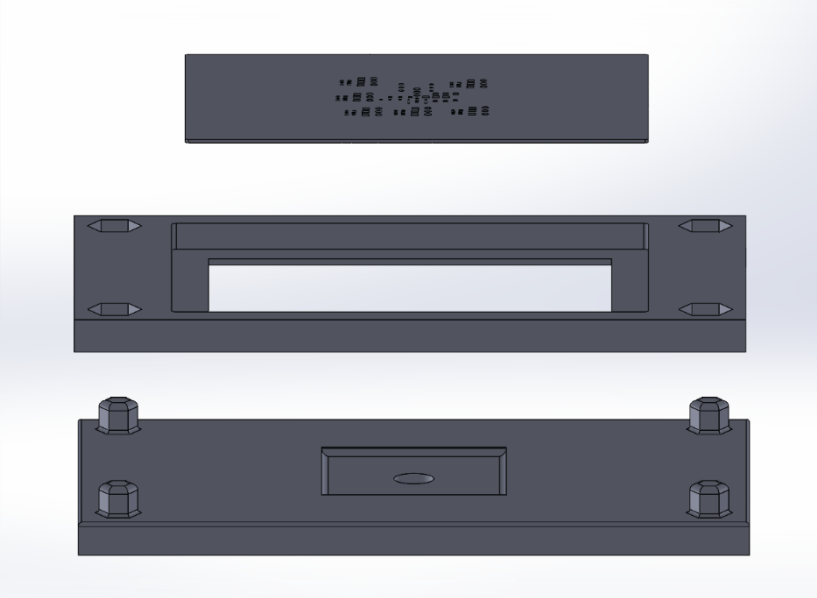

Figure 2.7 Schematic of custom mask aligner.

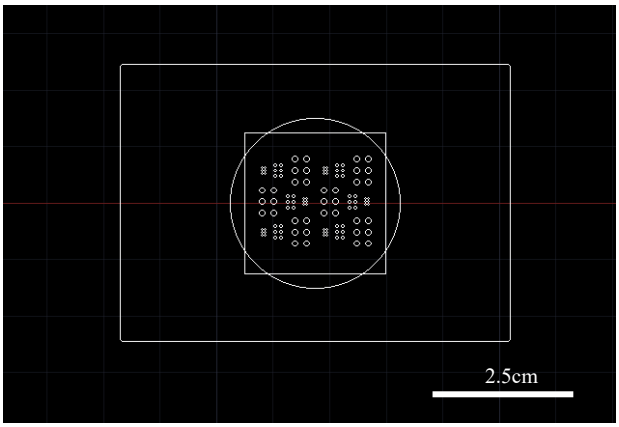

Figure 2.8 Mask design.

The precursor solution (2.1.3) was heated up to 50°C and spin coated (500 rpm, 30s) onto a preheated (70°C) clean (2.2.6) glass slide (25 mm × 25 mm). The substrate was then placed into the custom mask aligner and exposed to UV light for 2 min, 5 min and 10 min (Spectroline® UV-Lamp, E-Serie, 365nm, 4W). After exposure, the substrate was moved to a glass petri dish filled with pre-heated (45°C) DI-H_2O for 45 minutes for development. This process was carried out into a dark room to avoid unwanted exposure of the resist.

2.2.10 Fabrication of GelMA\PEDOT:PSS hydrogels at microscale: Two photon polymerization lithography

Two-photon polymerization (2PP) lithography is a versatile technology for additive manufacturing of 2D and 3Dmicro/nanostructures with sub-wavelength resolved features. Recent advancement in laser technology has enabled the application of 2PP to realize 3D microstructures in several fields such as bio fabrication [278], microelectronics [286], photonics [287], optoelectronics [288], microfluidics [289], and plasmonic devices[290]. However, the lack of two-photon polymerizable resins (TPPRs) induces bottleneck to the growth of 2PP to its true potential, and hence continuous research efforts are focused on developing efficient TPPRs. 2PP relies on two-photon polymerization (2PP) process that involves sensitization of photo-initiator (PI) via two-photon excitation (TPE), and subsequent cross-linking of monomer/oligomer (polymerizable resin or photoresist), using an intense pulsed laser beam. From a materials perspective, the feature size, shape, and resolution of 2PP fabricated microstructures critically depend on the choice of the PI, polymerizable resin or photoresist (PR).

Two photon polymerization (2PP) is enabled by the two-photon absorption (TPA) process in which an atom or a molecule can absorb sequentially or simultaneously two photons. During sequential absorption, the absorbing molecule reaches its excited state passing through a virtual intermediate state with the first photon, the second photon is then absorbed from this state to the excited one; this process has a lifetime from 10^{-9} to 10^{-4} s. In the simultaneous process, the molecule reaches a virtual state, absorbing the first photon, that disappears with the absorption of the second photon to the excited state. The virtual state has an estimated lifetime of 10^{-16} s.

Polymerization can be activated in photon-sensitive materials by TPA, typically in the presence of a photo-initiator capable of absorbing incident light to initiate the radical polymerization process described as follows (Figure 2.9):

$$S \xrightarrow{hv,hv} S^* \xrightarrow{FL} I \longrightarrow I^* \xrightarrow{R} R^*$$
$$R^* + M \longrightarrow RM^* \xrightarrow{M} RMM^* \longrightarrow RM_n^*$$
$$RM_n^* + RM_m^* \longrightarrow RM_{n+m}R$$

Figure 2.9 Reaction mechanism of two photon initiated radical polymerization.

where S is the photosensitizer, I is the photoinitiator, M is the monomer, and R^* is the active radicals. I^* and S^* represent the excited state of photosensitizer and photoinitiator, hυ is the Planck's Equation energy for each adsorbed photon, and FL is the fluorescent light emitted by the excited state photosensitizer, respectively. The laser is focused into the resin and 2PP is triggered only in the focal spot volume (Figure 2.10*a*). The smallest printable 3D volume is termed a voxel, which is analogous to a 2D pixel. Moving the laser focus along a trajectory in all three dimensions enables printing of structures built from multiple voxels and printed lines. Thus, a typical 2PP fabrication system consists of an ultrafast femto-second laser source that emits focused laser beams and a scanning stage that controls the focus of the beam within the photo-sensitive materials (Figure 2.10 *b*).

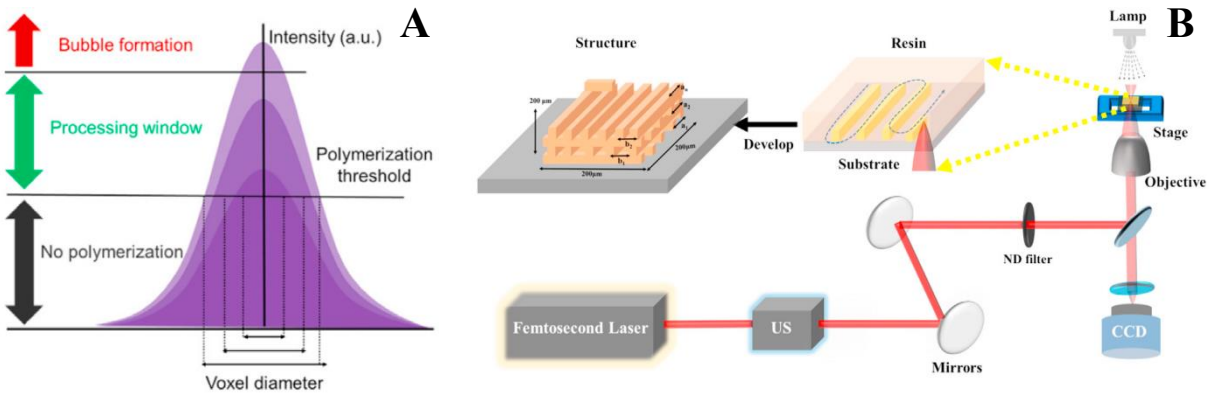

Figure 2.10 (a) threshold and voxel dimension in function of intensity. (b) schematics of TPL set-up.

The printing procedure begins with the realization of a 3D CAD design, that is afterwards converted into a file containing the process parameters and trajectories using the Describe software (Nanoscribe). To set the optimal writing parameters, the first step is the realization of a dose test that consists of an array of repeated structures in which the two main parameters are varied: laser power, which is a percentage of the maximum power of the laser beam, and the scan speed (µm/s); the overall dose can be expressed by Equation 2.3Equation 2.3.

Equation 2.3

$$Dose = \frac{laser\ power^2}{scan\ speed}$$

In this work, 3D photopatterning was performed employing Nanoscribe Photonic Professional GT2 (Nanoscribe). Preliminary dose tests were performed with GelMA 10%w/v and 20%w/v and Irgacure 2959 0.5%w/v as photoinitiator. A cube with dimensions 10 µm × 10 µm × 10 µm was used as test structure. The photoresist was heated up to 50°C for 15min and disposed on a silanized glass coverslip (2.2.7) (3 cm diameter). After 45 minutes at RT (gelation time) the printing process started. Laser power was varied from 10 mW to 60 mW, scan speed was varied from 100 µm/s to 10 mm/s. Once assessed the best dose, an optimization of gelation time was performed, varying the onset printing time after dispending the photoresist: 10 min, 20 min, 30 min, 40 min and 50 min. Additionally, a time frame for

printing prior to resist degradation was defined by cyclically printing of a cube with fixed LP and SS and observing degradation of printed structure while printing.

Additionally, diphenyl(2,4,6-trimethylbenzoyl)phosphine oxide nanoparticles (TPO NPs) were used as photoinitiator due to better light absorption at target wavelength of 390nm (Figure 2.11).

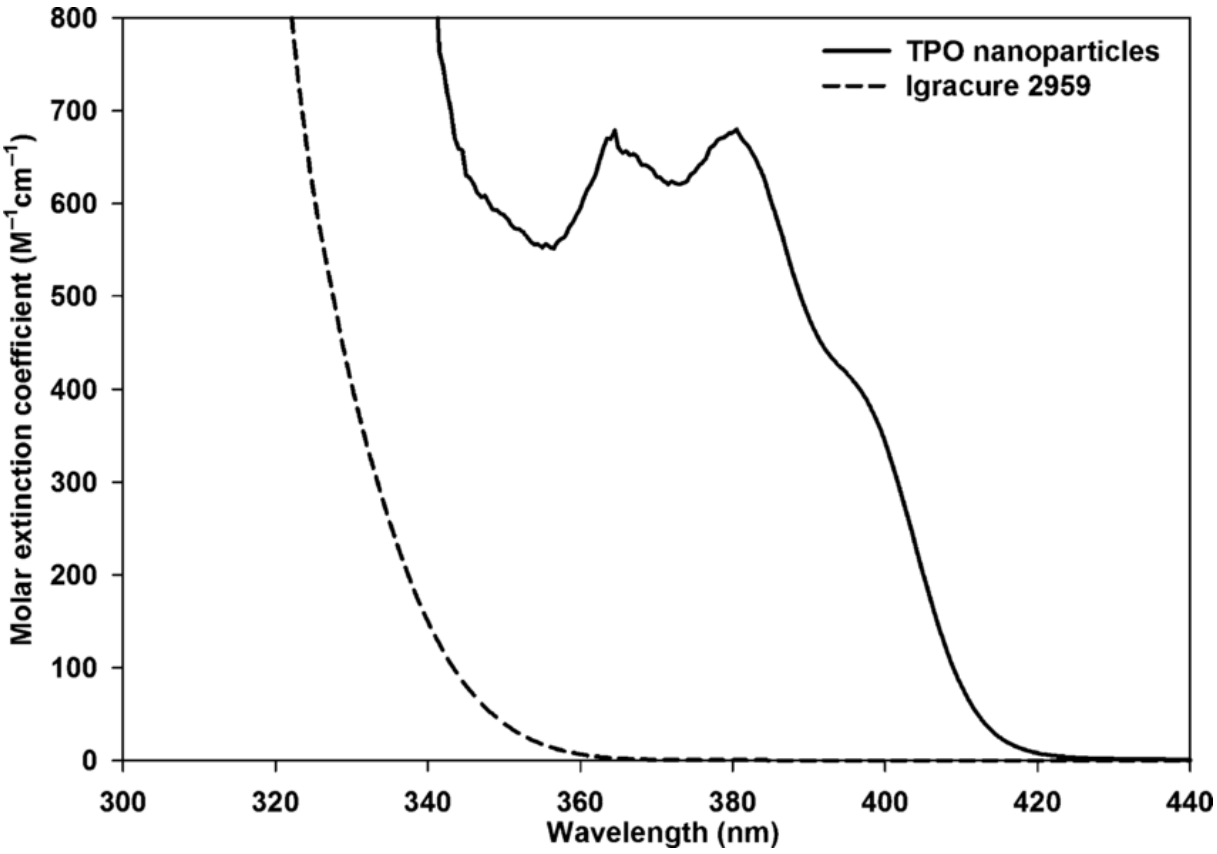

Figure 2.11 Molar extintion coefficient of Irgacure 2959 (dashed line) and TPO NPs (continuous line). Adapted from [293].

TPO NPs were dispersed into water at room temperature at 1%w/v concentration. The solution was heated up to 45°C prior to dissolve 10% w/v GelMA. Finally 0.3%w/v PEDOT:PSS was added to the blend while vigorously stirring. To study the effect of PEDOT:PSS on 2PP a pristine blend without PEDOT:PSS was also tested.

2.3 Biological Tests

2.3.1 Sterilization of substrates for cell culture

All substrates (glass coverslips and hydrogels) were sterilized prior to cell culturing by immersion in 70%v/v EtOH for 30 minutes followed by UV-C exposure for 1 hour.

2.3.2 Poly-L-Lysine coating of glass substrates

After cleaning as in 2.2.6 and sterilization as in 2.3.1, glass coverslips were coated with Poly-L-Lysine (PLL) by immersion into 500 µL of a 1:100 PLL solution in Hank's balanced salt solution (HBSS). After 1h at RT substrates were rinsed with HBSS three times. Finally, PLL coated substrates were stored in sterile conditions at 4°C up to two weeks.

2.3.3 Live\Dead assay

Live\Dead assay was performed employing HT22 cells (ATCC, Italy), an immortalized mouse hippocampal cell line. Cells were cultured on bare glass coverslip (1 cm in diameter), PLL coated glass coverslips (1 cm in diameter), GelMA 10%w/v hydrogel (1 cm diameter, 1 mm thickness) and GelMA\PEDOT:PSS 3%wt hydrogels (1 cm diameter, 1 mm thickness). Hydrogel precursors were prepared as explained in 2.1.3 and 2.2.1 using HT-22 cell medium (Dulbecco's Modified Eagle Medium/Nutrient Mixture F-12 + Glutamax (DMEM/F-12)(1:1), supplemented with 10%v/v Fetal bovine serum (FBS), 1%v/v penicillium streptomyces (PS)) as solvent and developer. All substrates were sterilized as explained in 2.3.1. HT-22 cells were seeded onto substrates, placed into a 24-multiwell, containing 1 mL of medium, at 25000 cells/cm^2 and maintained at 37°C, 5% CO_2. After two days, cells were incubated for 10 min at 37°C, 5% CO_2 with 1 mL of a 1 µg/mL Ethidium homodimer (EtHD) and 1 µg/mL Calcein acetoxymetyl (Calcein-AM) DPBS solution. After incubation samples were transferred into a 3 cm petri dish filled with 3 mL of DPBS and imaged with ZEISS Apotome 2 equipped with 20× immersion objective. Viable cells ratio was calculated as described in Equation 2.4:

Equation 2.4

$$Viable\ cells\ (\%) = \frac{live\ cells}{live\ cells + dead\ cells} * 100$$

2.3.4 MTT Assay

(3-(4,5-Dimethylthiazol-2-yl)-2,5-diphenyltetrazolium bromide) (MTT) assay is a method to quantitatively assess the proliferation rate of cells. The assay is based on the extracellular reduction of MTT by reduced nicotinamide adenine dinucleotide (NADH) produced in the mitochondria via trans-plasma membrane electron transport and an electron mediator. Reduction of MTT produces a water-insoluble formazan which concentration is proportional to the number of alive cells. MTT assay was performed on HT22 cells. Cells were cultured on untreated polypropylene 96-well plate, PLL coated polypropylene 96-well plate, GelMA 10%w/v hydrogel (0.5 cm diameter, 1 mm thickness) and GelMA\PEDOT:PSS 3%wt hydrogels (0.5 cm diameter, 1 mm thickness). Hydrogel precursors were

prepared as explained in 2.1.3 and 2.2.1 using HT-22 cell medium (Dulbecco's Modified Eagle Medium/Nutrient Mixture F-12 + Glutamax (DMEM/F-12)(1:1), supplemented with 10%v/v Fetal bovine serum (FBS), 1%v/v penicillium streptomyces (PS)) as solvent and developer. All substrates were sterilized as explained in 2.3.1. HT-22 cells were seeded onto substrates, placed into a 96-multiwell, containing 250 mL of medium, at 5000 cells/cm^2 and maintained at 37°C, 5% CO_2. After 24h and 48h of culture, the medium was discarded and replaced with 50 µL of MTT reagent (MTT Assay Kit (Cell Proliferation), Abcam) and 100 µL of clear DMEM/F12 (DMEM/F-12, no phenol red, Thermo Fisher). After 3h of incubation at 37°C, 5% CO_2, 150 µL of MTT developer (MTT Assay Kit (Cell Proliferation), Abcam) were added to each well in order to solubilize insoluble formazan. After 1h of development at 37°C, 5% CO_2, 150 µL of supernatant were transferred into a 96-multiwell and the absorbance was assessed by measuring optical density at 590 nm. Proliferation ratio was evaluated accordingly to Equation 2.5:

Equation 2.5

$$Proliferation\ ratio\ (\%) = \frac{Abs_{48h} - Abs_{24h}}{Abs_{24h}} * 100$$

Since gelatin can act as active site for redox reaction and PEDOT:PSS is blue in color additional, blank samples were used to normalize absorbance respectively for GelMA and GP3.

3 Results and discussion

3.1 GelMA synthesis and characterization

Gelatin, derived from collagen, inherently supports cell adhesion, proliferation, and differentiation due to the presence of cell-binding motifs. Methacrylation retains these beneficial properties while providing the additional functionality of crosslinking.

The synthesis of GelMA involves the modification of gelatin with methacrylate and methacrylamide groups. Methacrylate groups are reactive under UV light, especially when a photoinitiator is present (Figure 3.1). This allows for the controlled polymerization of GelMA into hydrogels, enabling precise control over the hydrogel's mechanical properties and degradation rates. The degree of methacryloylation can be varied to adjust the hydrogel's mechanical strength, porosity, and degradation rate.

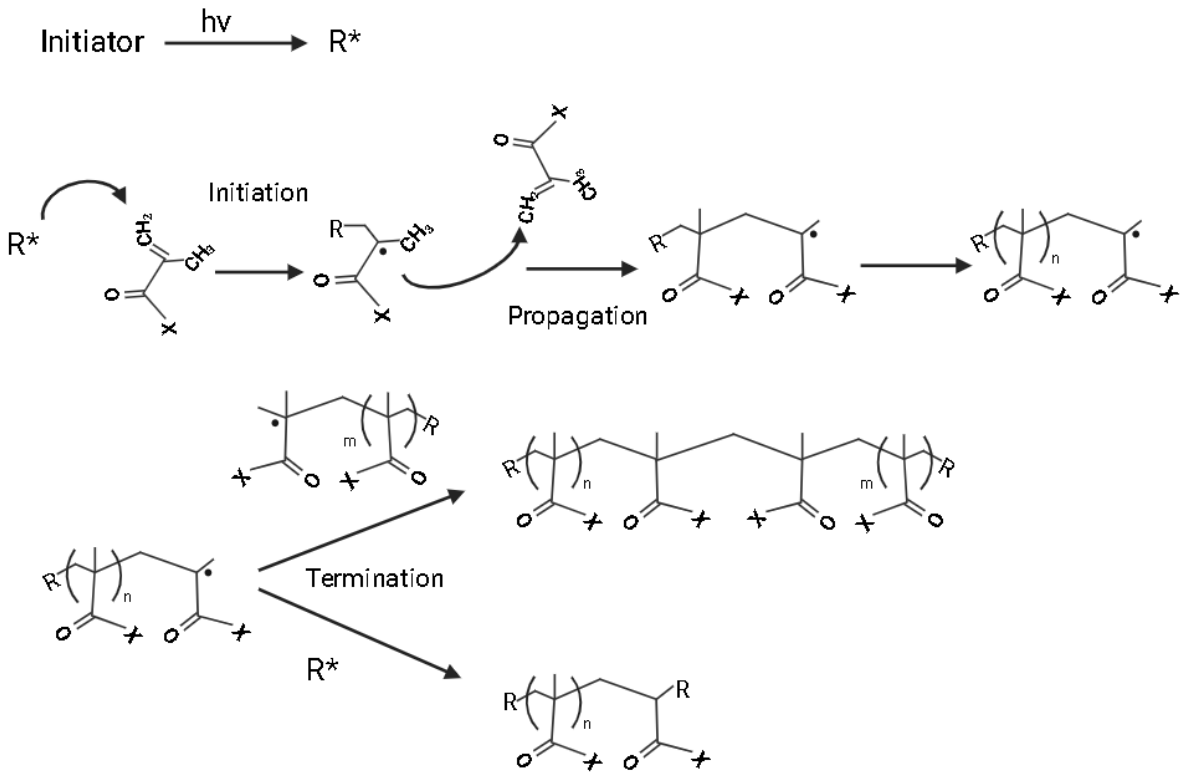

Figure 3.1 Photo activated free radical polymerization of methacrylates.

The degree of methacryloylation (DoM) quantifies the extent of this modification and is a critical parameter that influences the physical, chemical, and biological properties of the synthesized GelMA.

^{1}H-NMR analyses allowed to successfully calculate the Degree of methacryloylation of the three synthesized GelMAs, reporting varying DoM values for GelMA synthesized with different concentrations of methacrylic anhydride (i.e., with 0.06mg/$g_{gelatin}$, 0.12mg/$g_{gelatin}$ and 0.6mg/$g_{gelatin}$), demonstrating that the amount of methacrylic anhydride directly impacts the degree of modification.

Moreover, comparing ^{1}H-NMR spectra of gelatin and GelMA, the appearance of new peaks in GelMA compared to the gelatin control is indicative of successful methacrylation (Figure 3.2***Error! Reference source not found.***): chemical shifts between 5.75–5.9 and 5.5-5.65 ppm can be ascribed to acrylic protons (CH_2=C(CH_3)CONH) of methacrylamide groups, while the signal at 1.4 ppm corresponds to the methyl protons (CH_2=C(CH_3)CO-) of methacryloyl groups. Lysine methylene signal ($NH_2CH_2CH_2CH_2CH_2$-) at 3.0 ppm decreased in GelMA samples compared to gelatin control because of the reaction of its lateral chain with methacrylic anhydride. The degree of methacryloylation of the three synthesized polymers resulted to be 40% and 60% and 80%, according to the amount of methacrylic anhydride added during the synthesis.

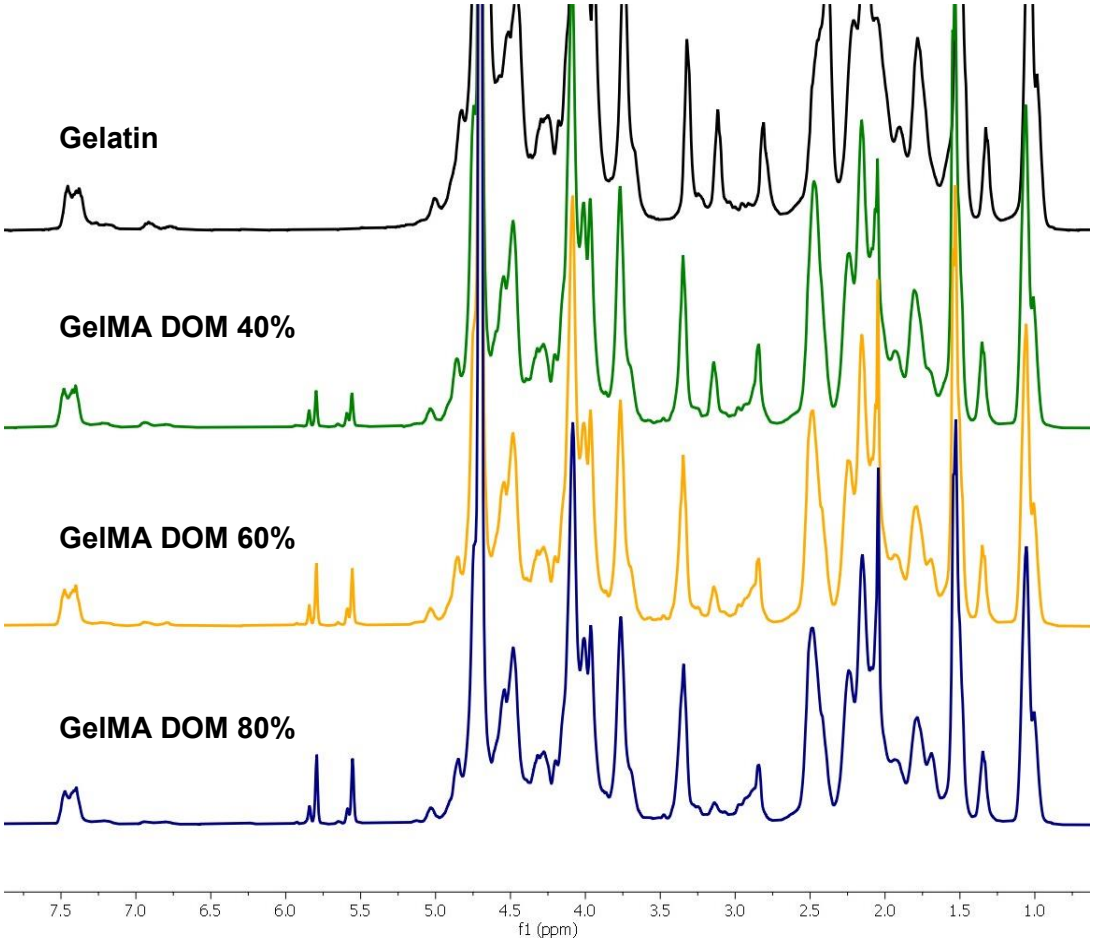

Figure 3.2 ^{1}H-NMR spectra of Gelatin and GelMA with increasing DOM, respectively from top to bottom

3.1.1 GelMA\PEDOT:PSS blends

Obtained blends changed in colour after addition of PEDOT:PSS. Intensity change is related to PEDOT:PSS concentration: from a light blue colour for GelMA:PEDOT:PSS 1%wt (GP1) to a dark blue colour for GelMA\PEDOT:PSS 5%wt (GP5). The correlation between color intensity and PEDOT:PSS concentration suggests that the PEDOT:PSS particles are well-dispersed within the GelMA matrix at lower concentrations, but as the concentration increases, the aggregation of PEDOT:PSS particles could lead to more pronounced color changes.

An increase in viscosity was observed during the preparation, after addition of increasing amount of PEDOT:PSS, highlighting the enhanced polymer-polymer interactions within the blend, affecting its rheological properties. For this reason, in order to easily handling the blend with higher amount of PEDOT:PSS, the temperature of blend was increased up to 55°C. Pipette tips were preheated into a 50°C water bath. These measures aim to reduce the blend's viscosity temporarily and prevent the gel from adhering to surfaces, ensuring more uniform and manageable preparations.

Precipitation of PEDOT:PSS occurred several times during preparation, especially for GelMA\PEDOT:PSS 3%wt (GP3) and 5%wt blends. This could be related to a decreased water content [197], [198], a long exposure to high temperature, which could lead to form PEDOT:PSS aggregates [197], and electrostatic interaction between negative PSS^- and Arginine's guanidinium group that has a positive charge [197]. Therefore, blends with a higher concentration of PEDOT:PSS were not possible to obtain. However, after optimizing mixing time, stable dispersions were possible to obtain in small volumes (<3mL).

To overcome the limitations imposed by PEDOT:PSS precipitation and ensure the preparation of higher concentration blends, several strategies could be explored. Enhancing the compatibility between GelMA and PEDOT:PSS through chemical modification or the use of compatibilizers could minimize phase separation and improve dispersion stability. Additionally, adjusting the pH of the blend or incorporating additives that counteract the electrostatic interactions leading to aggregation might prevent precipitation. Implementing controlled cooling protocols to gradually reduce the temperature after blending could also mitigate the risks of PEDOT:PSS aggregation and precipitation.

3.1.2 Tube inverting test

The tube inverting test is a straightforward experimental method that qualitatively assesses the phase transition of hydrogels from a liquid (SOL) to a solid (GEL) state and vice versa. In this work a point of interest was the influence of PEDOT:PSS concentration on gelation and melting time.

In Table 2 SOL indicates that the blend is in sol phase and thus flow of the blends was observed, GEL indicates that the bland is in gel phase and no flow was observed. When the wording (SOL or GEL) is accompanied by a minute mark, the latter indicates the time the blend took to reach that state.

The results highlighted in Table 2, illustrating the influence of increasing PEDOT:PSS concentration on the gelation and melting times of hydrogel blends, underscore the complex interplay between polymer concentration, water content, and polymer-polymer interactions. A decrease in gelation time with higher PEDOT:PSS concentration suggests that the presence of more conductive polymer networks within the hydrogel matrix facilitates a quicker transition to the gel phase. This can be attributed to the physical interaction of PEDOT:PSS, which promotes a more rigid network structure in a shorter time frame.

On the other hand, the observed increase in melting time with higher PEDOT:PSS concentrations points towards a more stable gel phase under thermal stress. This stability can be ascribed to the reduced water content and the specific interactions between the polystyrene sulfonate (PSS^-) components of PEDOT:PSS and GelMA. The PSS^- components are likely to form hydrogen bonds or electrostatic interactions with GelMA, contributing to a more robust gel network that is less prone to dissolution at elevated temperatures. It is also noteworthy that all formulations transitioned to the sol state at 37°C and returned to the gel state below 20°C, indicating a reversible thermoresponsive behavior. However, the distinct behavior of GelMA and GP1, which revert to the sol state after extended periods at 20°C, versus GP3 and GP5 maintaining the gel phase, highlights the role of formulation specifics in dictating the stability and reversibility of the gel phase. This could be related to the concentration of GelMA or the specific ratios of PEDOT:PSS to GelMA in the blends, suggesting a threshold concentration or ratio is necessary to maintain the gel phase under certain conditions.

Table 2 Gelation and melting times of GelMA, GP1, GP3 and GP5.

	37°C	**20°C**	**4°C**	**37°C**	**4°C**	**20°C**
GELMA	SOL	GEL 6’	GEL	SOL 4’	GEL 2’	SOL 20’
GELMA\PEDOT:PSS 1% Wt	SOL	GEL 6’	GEL	SOL 4’	GEL 2’	SOL 20’
GELMA\PEDOT:PSS 3% Wt	SOL	GEL 4’	GEL	SOL 6’	GEL 2’	GEL
GELMA\PEDOT:PSS 5% Wt	SOL	GEL 4’	GEL	SOL6’	GEL 2’	GEL

3.1.3 Photorheology

The photoactivated cross-linking process of hydrogels, with/without PEDOT:PSS, was investigated through photo-rheology. The photo-gelation process was monitored by recording the variations in the storage modulus (G') as a function of time.

Initial study was carried out on the pristine formulation. As shown in Figure 3.3, after an initial stabilization time with unchanged G', G' increased immediately after irradiation, finally reaching a plateau value, suggesting successful photopolymerization for all tested formulations.

The formulations containing PEDOT:PSS showed a photo-gelation kinetic comparable to that of the other doped formulations, but with a higher starting G'. This can be attributed to the intrinsic properties of PEDOT:PSS, which, being a conductive polymer, likely enhances the physical entanglements and electrostatic interactions within the hydrogel matrix. The presence of PEDOT:PSS facilitates a more robust pre-cross-linked structure, owing to the interaction between its sulfonic acid groups and the cationic sites on the polymer chains of the hydrogel. This pre-cross-linked network acts as a scaffold that contributes to a higher G' at the onset of photo-gelation [197], [291]. Moreover, the comparable photo-gelation kinetics between PEDOT:PSS-containing formulations and other doped formulations suggest that the incorporation of PEDOT:PSS does not hinder the photopolymerization efficiency.

Furthermore, the role of molecular interactions in the cross-linking process warrants a deeper investigation. The specific interactions between the anionic sulfonic groups of PEDOT:PSS and the cationic amino acids on the gelatin backbone highlight the importance of ionic interactions in modulating the gelation kinetics and the mechanical properties of the resultant hydrogel. Further studies could explore the quantification of these molecular interactions using spectroscopic techniques, such as Fourier Transform Infrared Spectroscopy (FTIR) or Nuclear Magnetic Resonance (NMR), to elucidate the specific bonding mechanisms at play. Additionally, investigating the effects of varying PEDOT:PSS concentrations on the gelation kinetics and the final hydrogel properties would provide insights into optimizing the formulation for specific applications.

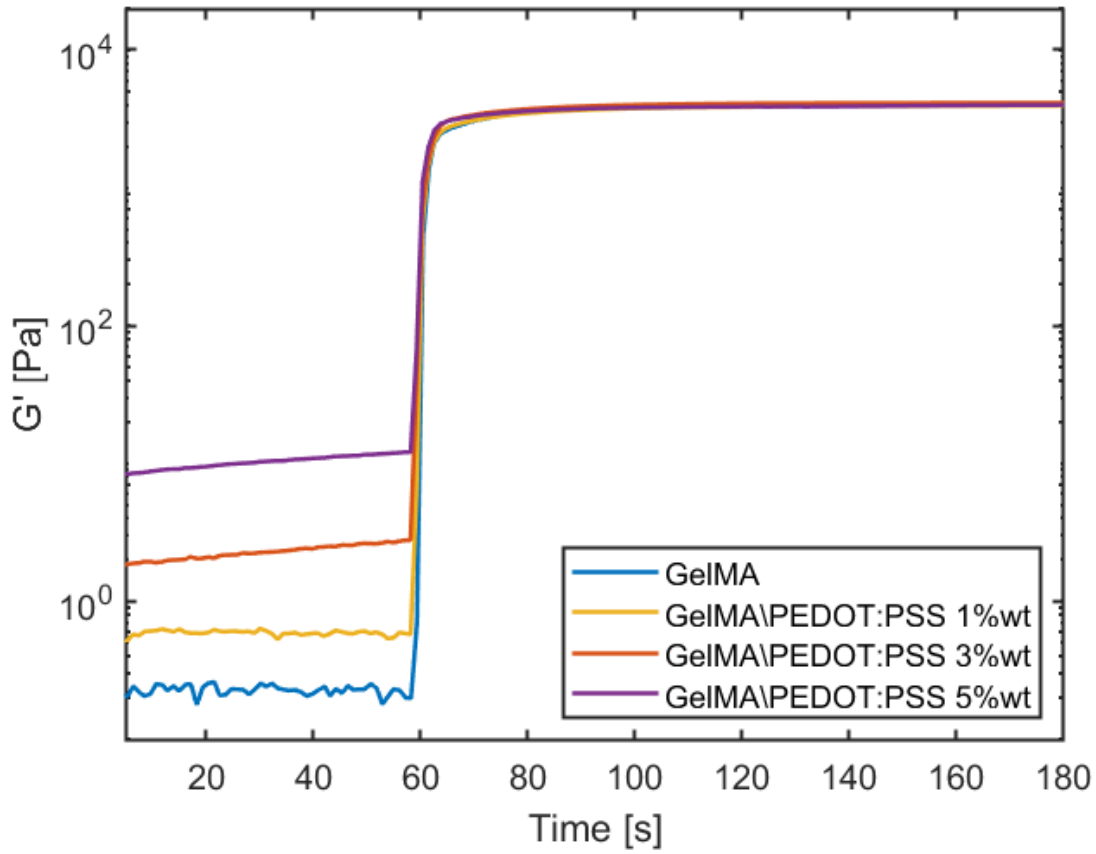

Figure 3.3 Photoplymerization kinetics of hydrogels.

3.2 GelMA and GelMA\PEDOT:PSS hydrogels characterization

3.2.1 Water Uptake

Water uptake percentage of GelMA and GelMA\PEDOT:PSS hydrogels was monitored as a function of time by incubating previously dried samples in DPBS (pH 7.4, 37°C). The observed increase in water uptake for composite hydrogels, as compared to pure GelMA hydrogels, highlights the impact of incorporating PEDOT:PSS particles on the hydrogel's physical and chemical properties. The variations in water uptake between the different hydrogel formulations (GP1, GP3, and GP5) suggest that the concentration and distribution of PEDOT:PSS within the GelMA matrix play a crucial role in modulating the hydrogel's behavior.

Water uptake can significantly affect the hydrogel's volume, mechanical properties, molecular diffusion capabilities, and electrical properties, which are critical factors for biomedical applications, including tissue engineering, drug delivery, and biosensors and ultimately to the interaction of hydrogels with living cells.

In this study, the water uptake was found to increase from 686 ± 20 % for pure GelMA hydrogels to 736 ± 40 % for GP1, 799 ± 53 % for GP3 and 717 ± 23 % for GP5 respectively after 24 h in DPBS (Figure 3.4 a). All hydrogels reached their maximum after 4h of incubation (Figure 3.4 b), after that water uptake slightly changed.

The reduced degree of crosslinking in the composite hydrogels containing PEDOT:PSS is a pivotal factor that likely contributes to their increased water uptake. This phenomenon could be attributed to several factors: the incorporation of PEDOT:PSS particles may affect the transparency of the hydrogel matrix, reducing the penetration of light that is necessary for the photopolymerization process. This reduced light penetration could lead to a less extensive crosslinking network within the hydrogel, thereby increasing its porosity and water uptake capacity; the interaction between the radical initiators used in the polymerization process and the conjugated polymer chains of PEDOT:PSS could lead to premature termination of growing polymer chains or the formation of less effective crosslinks. This cross-reactivity could diminish the overall crosslinking density, making the hydrogel more susceptible to water absorption; PEDOT:PSS is known for its conductive properties, which arise from its unique ionic composition. The presence of these charged species within the hydrogel matrix could promote water uptake through electrostatic interactions, further enhancing the hydrogel's ability to swell.

However a reduced swelling of GP5 in respect to GP3 was observed.

The observed water uptake characteristics of GelMA/PEDOT:PSS hydrogels underline the complex interplay between material composition, structural properties, and functional outcomes. Future studies could explore the optimization of PEDOT:PSS concentration and distribution within the hydrogel matrix

to balance mechanical strength, electrical conductivity, and biocompatibility, paving the way for innovative biomedical devices and therapies.

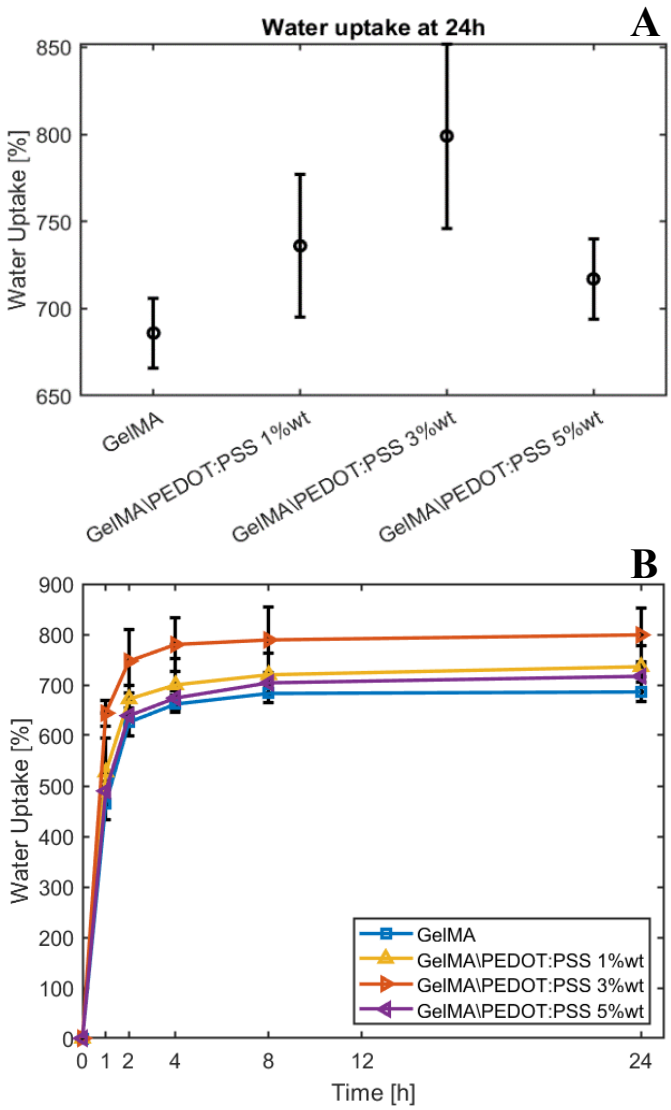

Figure 3.4 (a) Water uptake at 24h. (b) Water uptake after 1h, 2h, 4h, 8h and 24h.

3.2.2 Electro polymerization of PEDOT:PSS inside GelMA hydrogels

Electro polymerization of PEDOT:PSS is a common electrochemical synthesis method usually used to obtain a thin layer of polymer on a conductive substrate. The deposition of the organic layer enhances electrical coupling of inorganic material with biological environment. In a recently published study [276] electro polymerization of PEDOT:PSS in patterned GelMA is claimed. Results reported how impedance of electrode-PEDOT:PSS-GelMA system is reduced in comparison to bare electrode. To this aim electro polymerization of PEDOT:PSS inside GelMA network conducted as explained in section 2.2.3. Polymerization of PEDOT:PSS was achieved only at the interface between ITO electrode and GelMA hydrogel. This result can be due to the low electrical field inside the protein network, not enough to obtain polymerization of EDOT. Therefore, polymerization occurred only at the interface, where the electrical field is higher. In former study, by comparing the impedance curves of the electrode, electrode-PEDOT:PSS, electrode-GelMA, and electrode-PEDOT:PSS-GelMA systems, it can be seen that the presence of gelatine increases the impedance and the deposition of PEDOT:PSS reduces it. Considering the impedance of the electrode-PEDOT:PSS-GelMA system, the reduction of the impedance with respect to the bare electrode, and the increase with respect to the electrode-PEDOT:PSS system does not justify the fact that a deposition of PEDOT:PSS occurred within the polymer network, but only that GelMA increases it . It is reasonable to say that distribution of the electrical field inside hydrogels prepared in this study was not enough to trigger polymerization. Further investigation of this behaviour is needed to confirm this conclusion. For example, a comparison between impedance of GelMA on bare ITO electrodes and GelMA on PEDOT:PSS coated ITO electrodes.

3.2.3 Oxidative polymerization of PEDOT:PSS inside GelMA hydrogels

Oxidative polymerization is a type of polymerization process in which monomers undergo polymerization through the involvement of oxidative agents. This process typically involves the initiation of polymerization through the introduction of oxidizing agents, which facilitate the formation of polymer chains from monomer units. The oxidizing agents provide the necessary energy to initiate and propagate the polymerization reaction. The process begins with the initiation step, where an oxidizing agent, or a combination of oxidizing agents, reacts with the monomer molecules to generate radicals or other reactive species. The radicals formed in the initiation step react with monomers causing them to undergo polymerization by adding to the monomer units. This step leads to the elongation of the polymer chain. The polymerization reaction eventually reaches termination, where the polymer chains stop growing. Termination can occur through various mechanisms, such as the recombination of radicals or the reaction between radicals and certain species in the reaction mixture.

In this work, oxidative polymerization within GelMA hydrogels failed. Probably low diffusion of oxidizing agents within GelMA network did not permit polymerization to occur. However, not even polymerization on surface was observed. Degradation of monomers during UV exposure may occur.

3.2.4 Impedance spectroscopy: a comparison between two-electrodes set-up and three-electrodes set-up

GelMA and GelMA\PEDOT:PSS hydrogels have been characterized via Impedance spectroscopy as described in Chapter 2.2.5. Impedance Spectroscopy (IS) is a powerful technique used to investigate the electrical properties of materials by applying an alternating current (AC) and measuring the resultant voltage response. In the context of GelMA and GelMA/PEDOT:PSS hydrogels, IS helps in understanding how these materials conduct electricity, which is crucial for designing bioelectronic devices that interface with biological tissues.

The choice between a two-electrodes and a three-electrodes setup in IS experiments influences the interpretation of the hydrogel's electrical behavior: the Two-Electrodes Setup simulates a capacitive system where the hydrogel acts as a dielectric material between two electrode armors. It is particularly useful for assessing the bulk properties of the hydrogel, revealing how the material itself contributes to electrical impedance. The observed impedance values in this setup provide insights into the hydrogel's intrinsic electrical properties, unaffected by external electrolytic environments; the Three-Electrodes Setup introduces an electrolyte, allowing for the examination of the hydrogel-electrolyte interface. It simulates conditions closer to biological environments, where electrolytes are abundant. The presence of an electrolyte significantly reduces the system's impedance, highlighting the interface's role and the effects of electrolyte uptake by the hydrogels.

A difference of one order of magnitude between the two set-up is visible comparing Figure 3.5 and Figure 3.6. This is caused by presence of an electrolyte, that as demonstrated in section 3.2.1, is up taken by hydrogels in the three electrodes set-up and is concurring to the reduction of the impedance of the system. A clearer distinction of PEDOT:PSS concentration influence is more visible in absence of an electrolyte during measurement (Figure 3.5). But since this material will eventually interface with biological environment, which is rich in electrolytes, the three electrodes method might represent more faithfully what is happening at the interface. Considering these factors, a configuration with two electrodes may be better suited for illustrating the bulk properties of the material, while a setup with three electrodes may be more appropriate for examining interfacing properties.

The possibility to tune the electroconductive properties of GelMA/PEDOT:PSS hydrogels by PEDOT:PSS content was thoroughly studied. Since gelatin is a non-conductive material, these results show that presence of PEDOT:PSS reduces the impedance of the system (Figure 3.5) demonstrating a clear contribution of electronic transport introduced by PEDOT:PSS dispersion in the network. As shown in Figure 3.5 and Figure 3.6, all hydrogels exhibited higher impedance at lower frequencies and lower impedance at higher frequencies resembling a resistive and capacitive effect respectively.

At 1Hz, which is the characteristic heartbeat frequency of an adult human in resting conditions, and 1kHz, hydrogels containing PEDOT:PSS possessed lower impedance than pristine hydrogels (Figure

3.5, **Error! Reference source not found.**(a),(b),(d)). In the case of two electrodes set up, hydrogels presented impedance of 140 ± 27 kΩ , 140 ± 9 kΩ, 120 ± 9 kΩ, 100 ± 16 kΩ at 1Hz for GelMA ,GP1, GP3 and GP5 respectively; at 1000Hz 3,1 ± 0.9 kΩ , 3,1 ± 0.2 kΩ, 2,3 ± 0.2 kΩ, 1,6 ± 0.2 kΩ. In the case of three electrodes set up, hydrogels presented impedance of 10,9 ± 0.1 kΩ , 10,8 ± 0.5 kΩ, 11,0 ± 0.4 kΩ, 12,0 ± 2,5 kΩ at 1Hz for GelMA ,GP1, GP3 and GP5 respectively indicating a not significant contribution of PEDOT:PSS; at 1000Hz 93 ± 12 Ω , 86 ± 4 Ω, 76 ± 4 Ω, 62 ± 1 Ω where the effect of PEDOT:PSS is more appreciable. Such behaviour at low frequencies is justified by the higher charge transport contribute of electrolyte.

The impedance spectroscopy characterization of GelMA and GelMA/PEDOT:PSS hydrogels underlines the importance of experimental setup and material composition in determining their electrical properties. The distinction between bulk and interface properties, underscored by the choice of a two-electrodes or three-electrodes setup, provides a comprehensive understanding of how these hydrogels behave in different environments. Furthermore, the significant role of PEDOT:PSS in enhancing conductivity offers promising avenues for developing advanced bioelectronic devices that seamlessly integrate with biological systems.

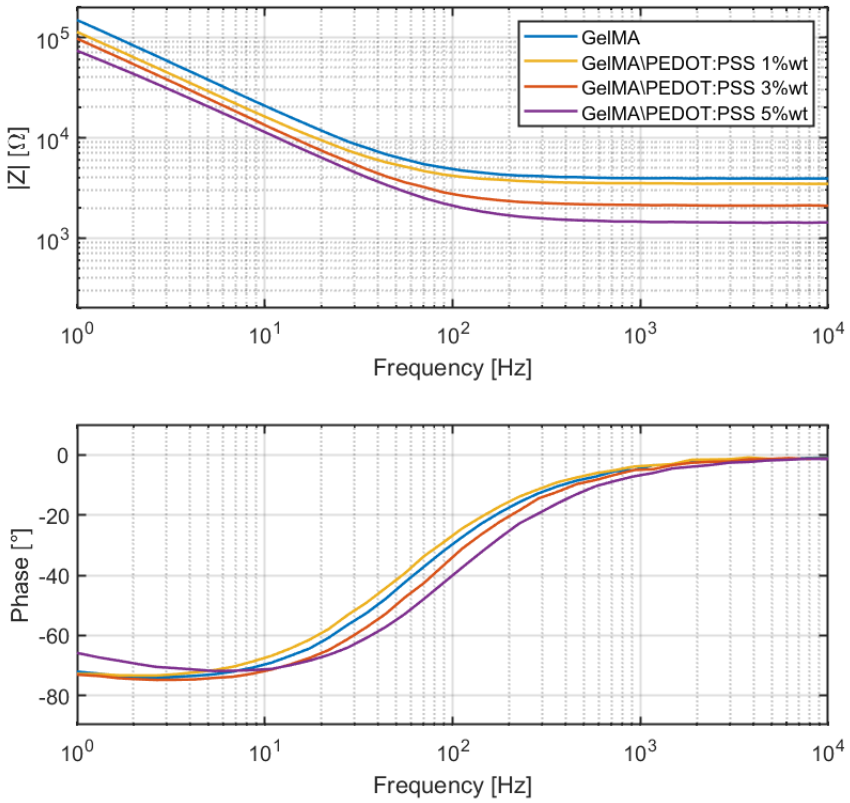

Figure 3.5 Impedance spectroscopy of GelMA and GelMA\PEDOT:PSS blends with PEDOT:PSS concentration from 1%wt to 5%wt measured in sandwich configuration.

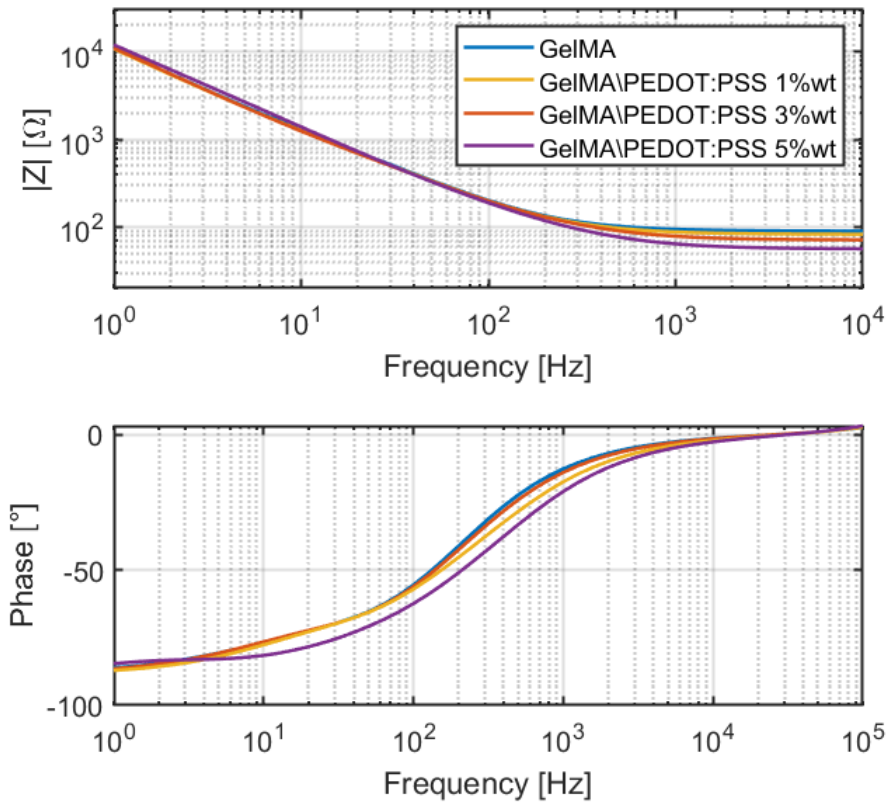

Figure 3.6 Impedance spectroscopy of GelMA and GelMA\PEDOT:PSS blends with PEDOT:PSS concentration from 1%wt to 5%wt measured in three-electrodes configuration.

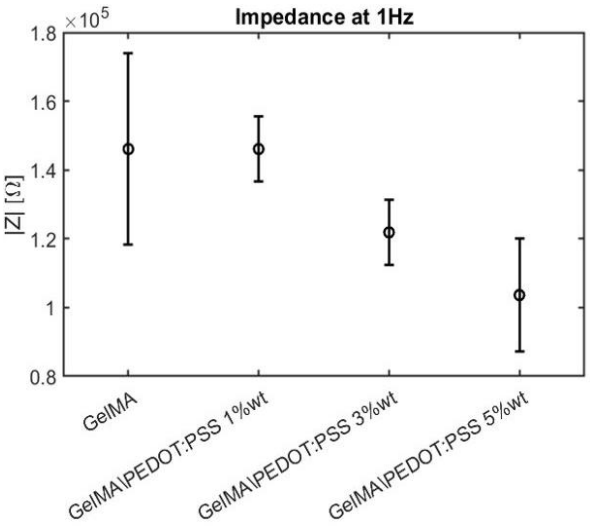

(a) Impedance measured at 1 Hz measured in sandwich configuration.

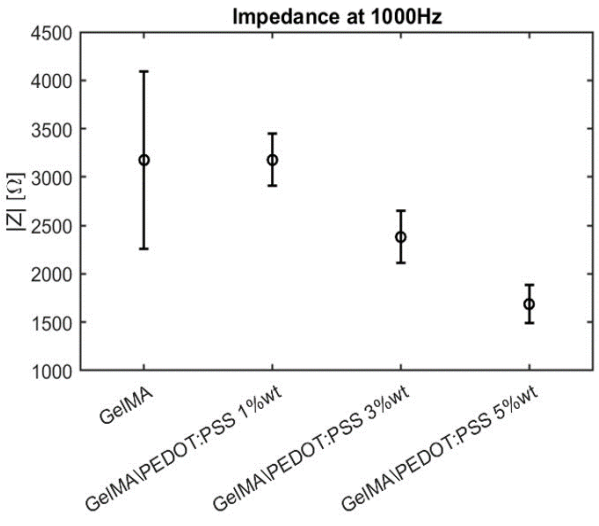

(b) Impedance measured at 1000 Hz measured in sandwich configuration.

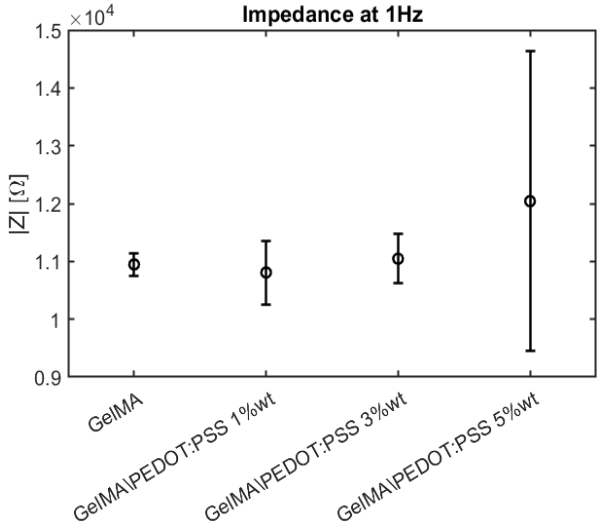

(c) Impedance measured at 1 Hz measured in three-electrodes configuration.

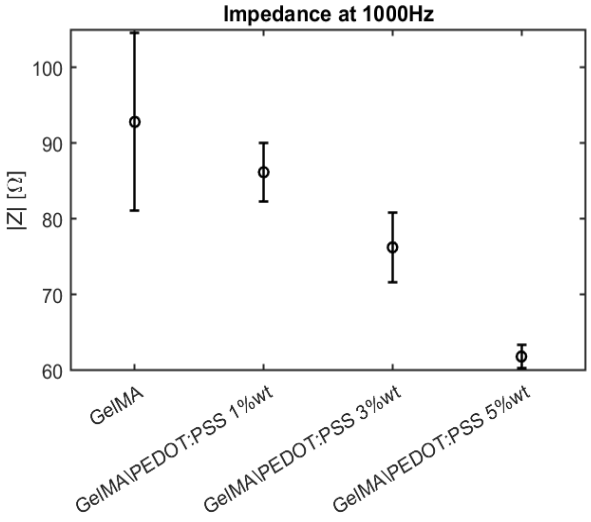

(d) Impedance measured at 1000 Hz measured in three-electrodes configuration.

Figure 3.7

3.2.5 Contact angle measurements

The use of contact angle measurements is a fundamental technique in surface science for assessing the wetting behavior of liquids on solid surfaces, which is indicative of surface hydrophilicity or hydrophobicity. Contact angle measurements have been carried out as described in Chapter 2.2.7. Figure 3.8 presents visual evidence of the wetting behavior for each case analyzed, serving as a qualitative assessment of the surface treatments. Figure 3.9 summarizes the quantitative data, showing the average contact angle for each treatment. In particular, after Oxygen Plasma treatment significantly increased the surface's hydrophilicity, to the point where measuring a contact angle was not feasible. Oxygen plasma treatment is known to introduce polar functional groups onto the surface, enhancing water absorption and reducing the contact angle, often making surfaces super-hydrophilic. In contrast, silanization increased the contact angle to 53±9°, indicating a reduction in hydrophilicity. This effect is attributed to the methacrylate groups exposed on the surface, which are less polar than the groups introduced by oxygen plasma treatment. The baseline measurement for the uncoated surface was 25±2°, indicating a relatively hydrophilic surface. Silanization treatment resulted to be crucial for the adhesion of gelatin structures on glass substrates both during patterning at mesoscale and macroscale. Future research may explore the long-term stability of these treatments, their effects on biocompatibility, and their application in complex, multi-material systems.

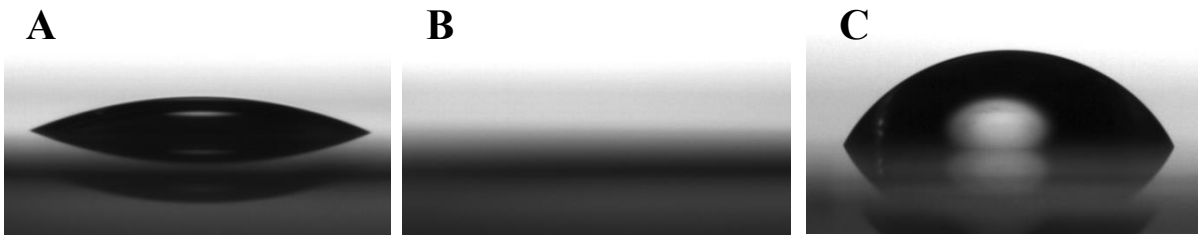

Figure 3.8 . Images from the contact angle measurements of water droplets on top of different surfaces:(a) bare glass, (b) oxygen plasma activated glass, (c) silanized glass.

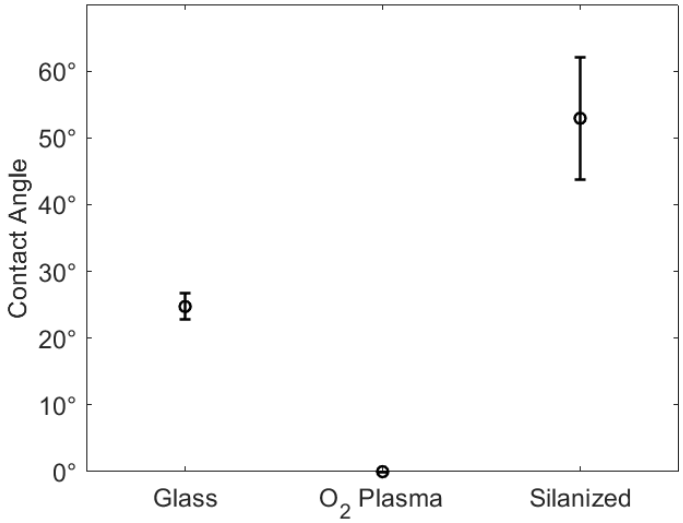

Figure 3.9 Results for the contact angle measurements for glass, oxygen plasma activated glass and silanized glass.

3.2.6 Fabrication of GelMA\PEDOT:PSS hydrogels at mesoscale

The fabrication of microscale circular structures as described in paragraph 2.2.9 involves a delicate balance of exposure time, protection from light, and careful development. Each step in the process, from the optimization of exposure to prevent overexposure and undesired diffusion, through the meticulous shielding of the resist from ambient light to avoid premature polymerization, to the precise timing of development to clear away unreacted material, is critical for achieving well-defined and precise microstructures. Circular structures with 500µm, 200µm and 100µm diameter were obtained (Figure 3.10). The optimization of the exposure time to 2 minutes played a pivotal role in this achievement. This careful calibration was necessary to avoid overexposure, which could compromise the precision of the patterned structures. Overexposure leads to undesirable effects due to the diffusion of light through the resist and the consequent propagation of polymerization beyond intended boundaries. Such diffusion blurs the edges of the structures, making them indistinct and compromising their definition. The light-sensitive nature of LAP necessitates stringent control over the exposure conditions. The resist used in this process is notably sensitive to visible light, to the extent that even brief unintended exposure to daylight can initiate polymerization. This underscores the critical need to cover and protect the resist from ambient light throughout the entire process. Failure to adequately shield the resist from daylight could result in premature and uncontrolled polymerization, adversely affecting the fidelity and integrity of the intended microstructures Following the exposure phase, development time emerges as a crucial step to ensure the removal of all unreacted resist, thereby revealing well-defined structures. The development process washes away the portions of the resist that did not undergo polymerization, a step essential for achieving the precise geometries and dimensions targeted in the fabrication process. The optimization of development time is therefore integral not only to the clarity and distinctness of the resulting structures but also to their overall quality and utility.

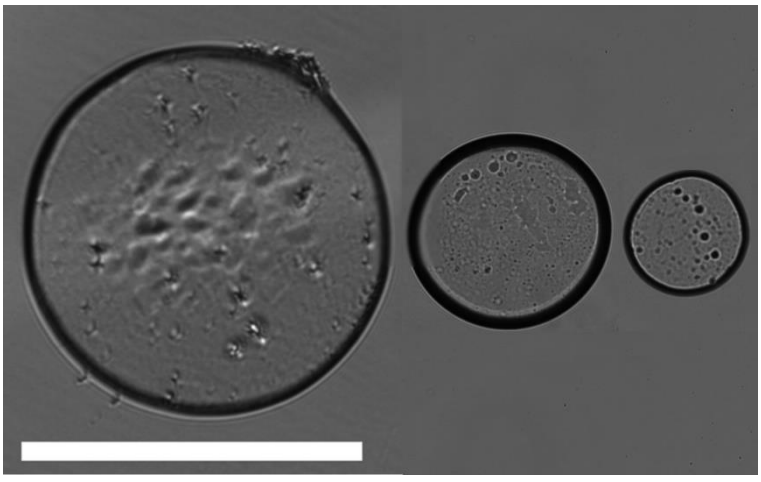

Figure 3.10 Mesoscale patterned GelMA structures. From left to right 500µm, 200µm and 100µm. Scale bar 500µm.

3.2.7 Two photon polymerization lithography

In the pursuit of optimizing polymerization conditions, an initial experimental setup was employed where the laser power (LP) was varied from 10 mW to 60 mW, alongside adjustments in scan speed (SS) from 1 mm/s to 10 mm/s. This range was selected to explore a broad spectrum of energy doses delivered to the material. Despite these variations, polymerization failed to occur. This outcome suggested that the energy dose, was insufficient for initiating polymerization within the tested parameters. To address the lack of polymerization, the parameter space was adjusted to target a higher energy density by reducing the scan speed range to 100 µm/s to 900 µm/s while keeping the laser power within a range of 30 mW to 60 mW. This adjustment was based on the hypothesis that a slower scan speed would allow more energy to be deposited into a given area, potentially overcoming the polymerization threshold. The results, as illustrated in Figure 3.11 (a), confirmed that polymerization occurred at combinations of higher laser power and lower scan speeds, delineating a high dose region conducive for the process. This region represents the optimal conditions where the energy delivered is sufficient to trigger polymerization without causing damage to the material. With the high dose region identified, a third set of experiments was designed to fine-tune the laser exposure process. By narrowing the range of laser power to 45 mW to 60 mW and scan speed to 100 µm/s to 500 µm/s, a more precise optimization was aimed at. The optimal dose was determined to be at a laser power of 50 mW and a scan speed of 200 µm/s. This specific combination was found to consistently yield stable polymerization, indicating a balanced energy input that promotes effective solidification without degrading the material.

Subsequent experiments further explored the impact of different concentrations of GelMA on the polymerization process. For resist based on GelMA 20%w/v the minimal gelation time was 30min at room temperature and the maximal gelation time was 45 min, after this time bubbling occurred as soon the laser started printing. Printing window was only 20min allowing to print only six cubes 10µm x 10µm x 10µm in dimensions. After this time the resist started to form bubbles during laser exposure compromising the printing quality. For resist based on GelMA 10%w/v the minimal gelation time was 50min at room temperature and the maximal gelation time was 120 min, after this time bubbling occurred as soon the laser started printing. The time frame for printing was only 10min allowing to print only three cubes 10µm x 10µm x 10µm in dimensions. After this time the resist started to form bubbles during laser exposure compromising the printing quality. An additional experiment investigated the effect of lowering the temperature by storing the GelMA resists at 4°C. This approach successfully reduced the gelation time for both concentrations of GelMA, albeit without extending the printing window for the 20%w/v solution. However, for the 10%w/v solution, the printable time frame increased to 45 minutes, suggesting that temperature control could be a viable strategy for managing the polymerization kinetics and extending the operational window for certain material formulations.

TPO NPs notably enhanced the efficiency of printing, particularly when combined with PEDOT:PSS. For the GelMA-TPO NPs photoresist, a lower laser power (LP) of 35mW is necessary for initiating polymerization, unlike the IG2959-based resist. This adaptation allowed for an increased scanning speed (SS) to 10 mm/s (Figure 3.13), facilitating the printing of more structures within a shorter timeframe. However, it is crucial to fine-tune the overall exposure dose to accurately fabricate microstructures swiftly. With the incorporation of PEDOT:PSS into the GelMA-TPO NPs photoresist, an even lower LP of 10mW suffices for polymerization, thereby minimizing heat production and extending the printing duration. Remarkably, it was feasible to boost the SS to 20 mm/s while still preserving the integrity of the structures (Figure 3.12). Existing studies suggest that PEDOT:PSS could enhance single photon free radical polymerization by absorbing UV light and generating free radicals. This process could potentially apply to two-photon polymerization, though no concrete evidence exists in literature to date. Further research is imperative to elucidate PEDOT:PSS's contribution to two-photon-induced free radical polymerization. It was notably achievable to pattern a PEDOT:PSS based resist, thereby enabling the controlled deposition of a conductive polymer in three dimensions within a biocompatible environment. Further research into the electrical characteristics of these structures is required to understand if PEDOT:PSS is stably immobilized and not damaged during exposure.

These experiments underscore the intricate balance between laser power, scan speed, and material properties in achieving successful polymerization two photon based polymerization. The optimal conditions identified offer a foundation for further exploration, particularly in adjusting material formulations and environmental conditions to enhance print quality and efficiency. Future research might delve into the underlying mechanisms of GelMA's response to laser sintering, exploring the role of molecular weight, crosslinking density, and other additives in modulating gelation dynamics and structural integrity post-printing.

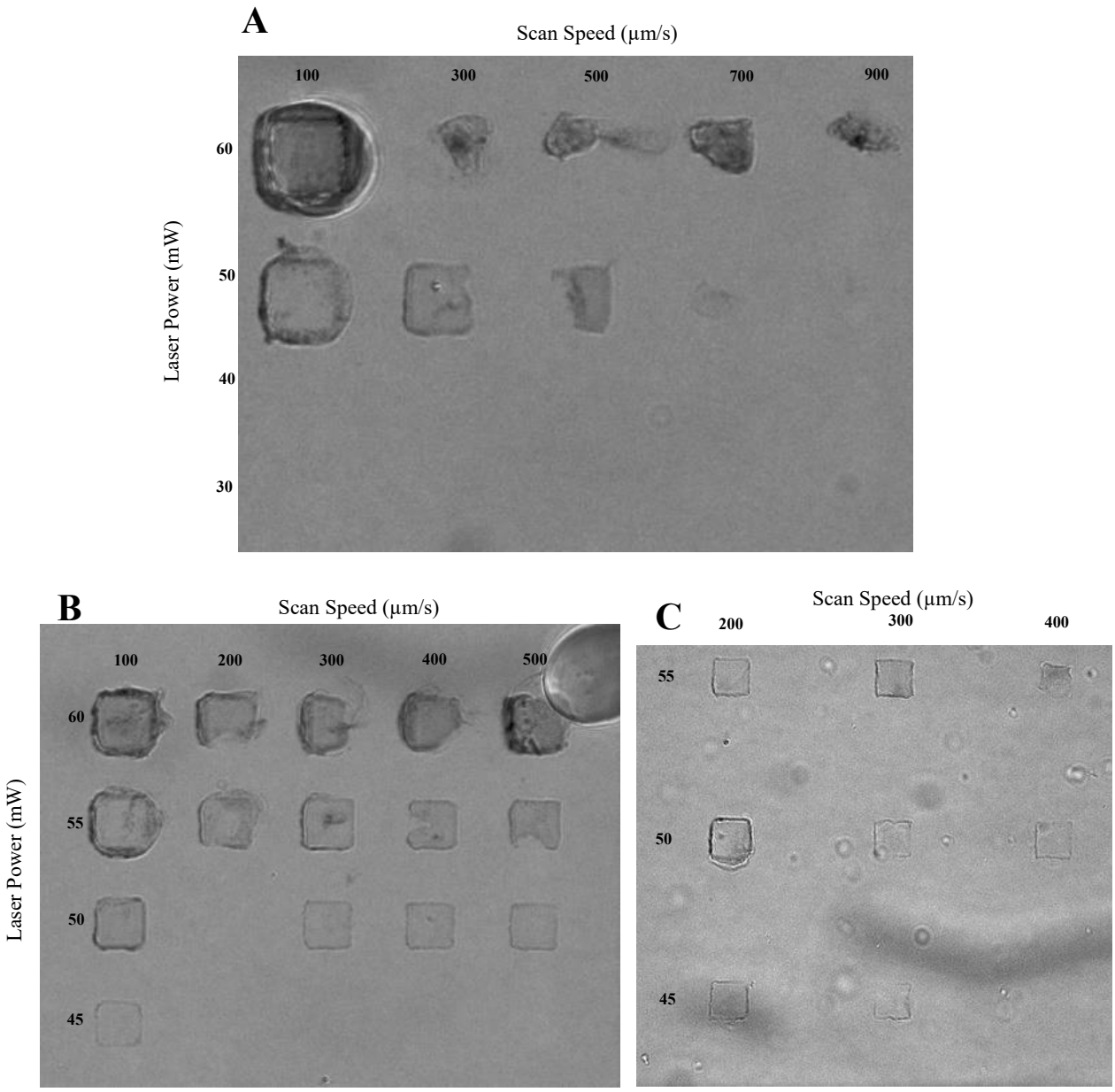

Figure 3.11 Dose test performed with GelMA 20%w/v. (a) LP 30mW to 60mW, SS 100µm/s to 900µm/s; (b) LP LP 45mW to 60mW, SS 100µm/s to 500µm/s; (c) LP 45mW to 55mW, SS 200µm/s to 400µm/s. Scale bars 10µm.

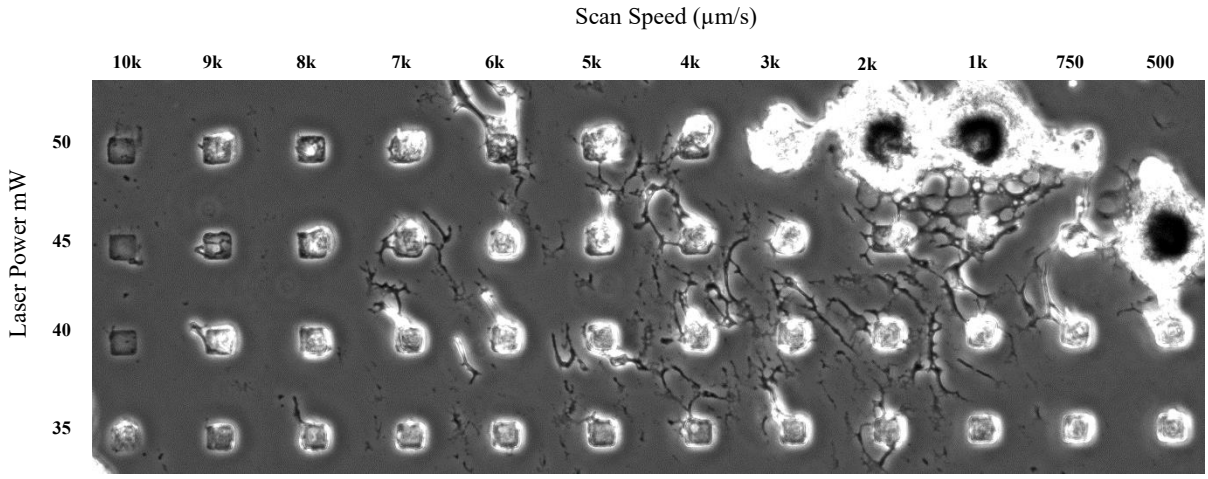

Figure 3.13 Dose test performed with GelMA 10%w/v, TPO NPs 1%w/v. LP 35mW to 50mW, SS 10mm/s to 500µm/s;

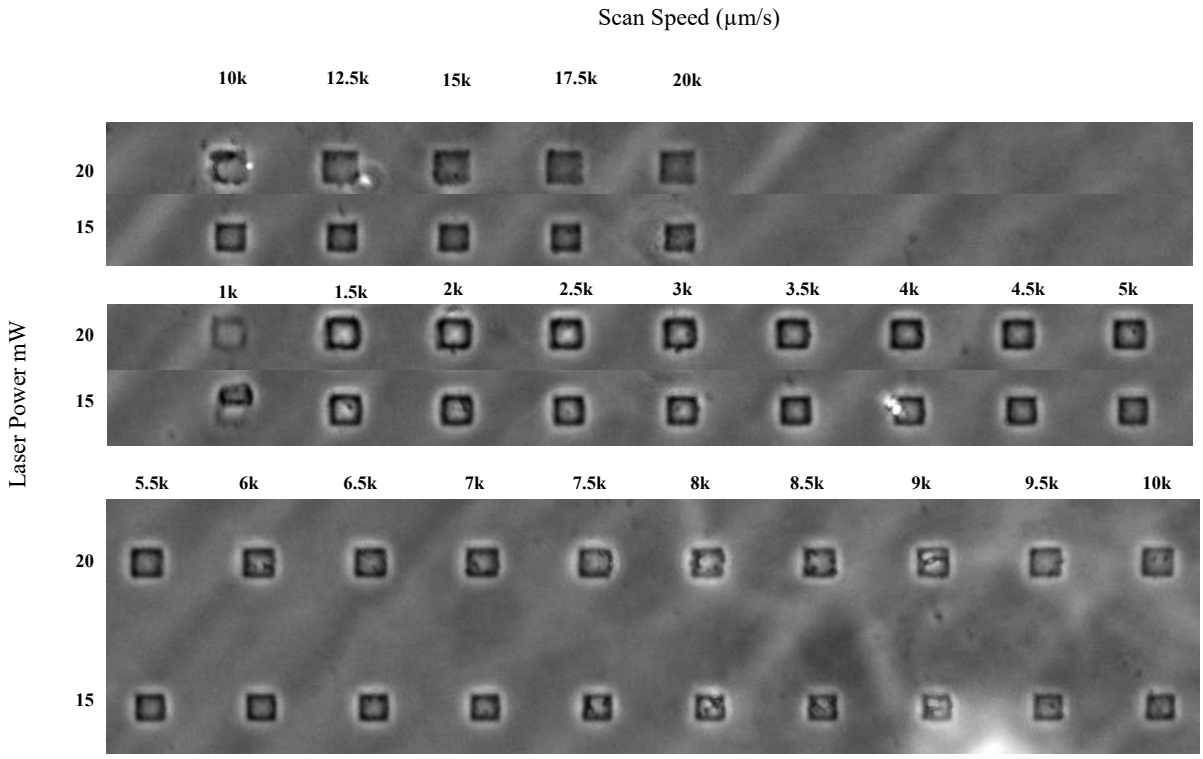

Figure 3.12 Dose test performed with GelMA 10%w/v, TPO NPs 1%w/v, PEDOT:PSS 0.3% w/v. LP 15mW to 20mW, SS 1mm/s to 20mm/s;

3.3 Biological Tests

3.3.1 Live/Dead assay

The live/dead assay refers back to a method detailed in Chapter 2.3.3. Live/dead assay involves staining cells with a combination of fluorescent dyes that differentiate live cells from dead ones. Live cells are stained with a green fluorescent dye (calcein AM) that indicates metabolic activity, while dead cells are stained with a red fluorescent dye (ethidium homodimer) that binds to nucleic acids in cells with compromised membrane integrity. This method allows for the direct observation and quantification of cell viability on different substrates, such as hydrogels with or without the addition of PEDOT:PSS, glass, and PLL (poly-L-lysine) coated glass.

Figure 3.14 shows an exemplary image for each case analyzed, while in Figure 3.15 the resulting average live/dead ratio is presented. In all four cases Live/Dead ratio was higher than 99% demonstrating high viability of cells seeded on hydrogels both in presence and absence of PEDOT:PSS. This indicates the hydrogel's effectiveness as a cell culture medium and suggests that the addition of PEDOT:PSS does not negatively impact cell viability.

Cells on glass and PLL-coated glass showed a more rounded morphology. This could indicate a less favorable environment for cell spreading, possibly due to the harder surface or lack of specific cell adhesion motifs. The presence of gelatin increased cell spreading and adhesion, attributed to gelatin's softer mechanical properties and the presence of the RGD sequence. RGD (arginine-glycine-aspartic acid) is a tripeptide that promotes cell adhesion by interacting with cell surface receptors (e.g., integrins). This finding underscores the importance of substrate composition and mechanical properties in regulating cell behavior.

The high viability observed across all substrates is promising for biomedical applications, suggesting that these materials can support cell growth and maintenance. However, the differences in cell morphology highlight how substrate properties can influence cell behavior, which is critical for applications where cell shape and function are closely linked. The softer mechanical properties of gelatin and the presence of cell adhesion motifs (RGD sequences) in promoting cell adhesion and spreading indicate a potential strategy for designing scaffolds that mimic the natural extracellular matrix, enhancing cell-material interactions.

Future research could explore the long-term effects of these substrates on cell proliferation, differentiation, and function. Additionally, investigating the interaction between electrical conductivity (in the case of PEDOT:PSS) and cell behavior could open new avenues for developing electrically active tissue engineering scaffolds.

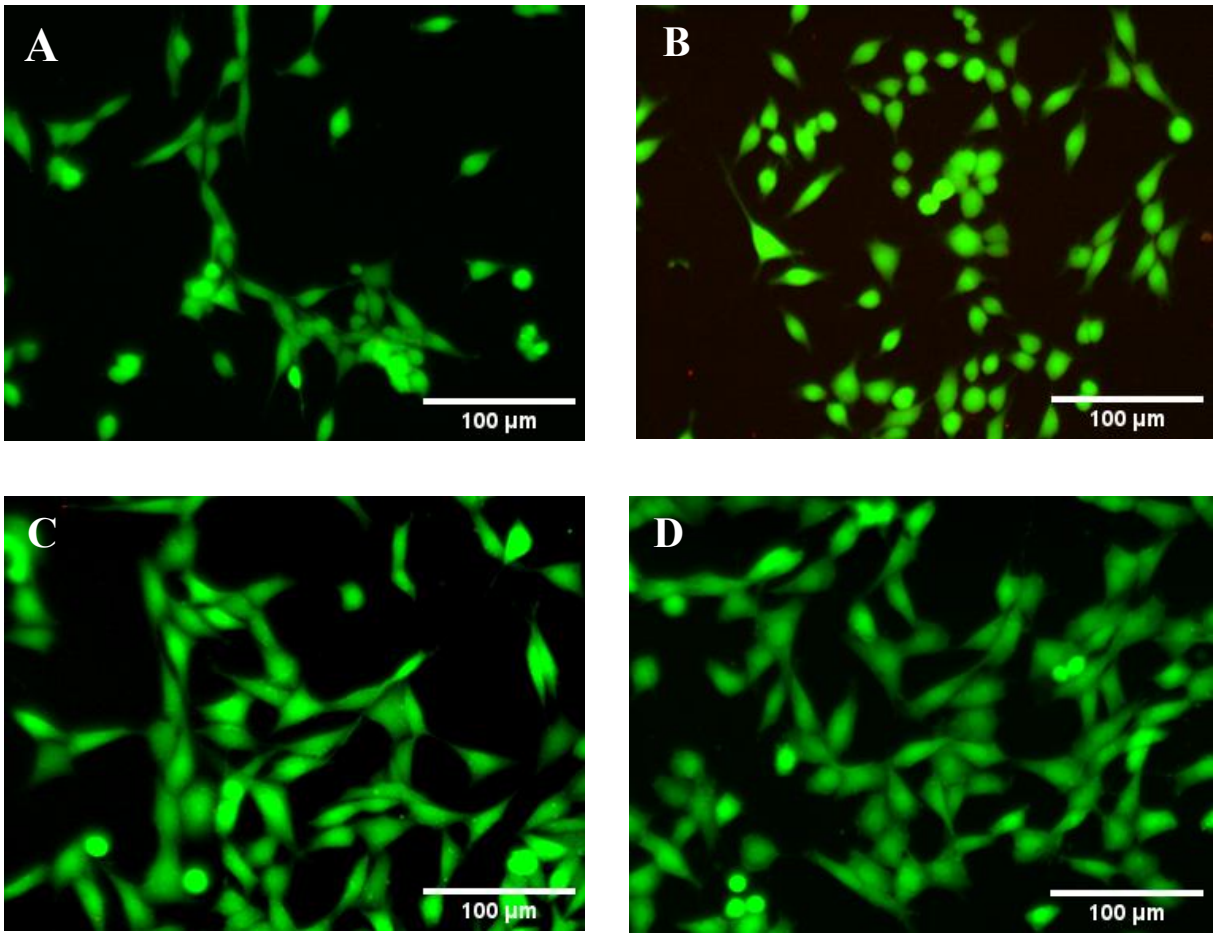

Figure 3.14 Live/Dead assay of HT-22 cells seeded on (a) bare glass, (b) PLL coated glass, (c) GelMA hydrogel and (d) GelMA\PEDOT:PSS hydrogel.

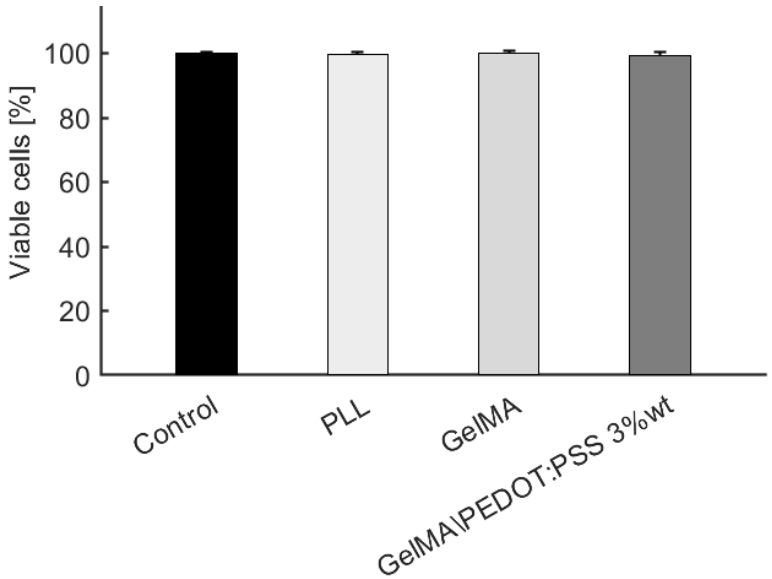

Figure 3.15 Results for the Live/Dead assay for glass, PLL, GelMA and GelMA\PEDOT:PSS 3%wt substrates.

3.3.2 MTT assay

Proliferation rate within 24h was assessed via MTT assay as explained in paragraph 2.3.4. The increase in cell number was obtained by assessing the number of cells after 24h and 48h of culturing on each substrate. Results are shown in Figure 3.16.

Key to this study is the contrast between cells cultured on glass, which serves as the control due to its high stiffness and lack of cell-anchoring moieties, and those grown on GelMA and GP3 substrates. GelMA and GP3 differ from glass in two critical aspects: they exhibit lower stiffness, and they present RGD (Arg-Gly-Asp) adhesion sequences to the cells. In addition GP3 substrate contains PEDOT:PSS.

The results indicated a notable increase in cell proliferation for cells plated on GelMA and GP3 compared to the control. This is attributable to the combination of reduced substrate stiffness and the presence of RGD sequences, which together create a more conducive environment for cell growth. Among the substrates tested, cells cultured on GP3 exhibited the highest proliferation rate. This suggests that the inclusion of PEDOT:PSS in GP3 not only contributes to the substrate's physical properties but also promotes cell proliferation, possibly through additional biochemical signaling or improved electrical conductivity, which could affect cellular behaviors.

Conversely, cells plated on PLL (Poly-L-Lysine) coated glass showed reduced proliferation. This observation might be linked to the presence of anchoring moieties (provided by PLL) on a stiff substrate (glass). While PLL enhances cell adhesion, the high stiffness of the glass substrate could negate the positive effect by providing a less favorable mechanical environment for cell growth. The findings underscore the complex interplay between mechanical and biochemical cues in regulating cell proliferation, highlighting the potential of engineering substrate properties to control cellular behaviors in vitro.

The study demonstrates that by fine-tuning the stiffness and chemical composition of substrates, it is possible to optimize cell growth and function, paving the way for the development of more effective biomaterials for various biomedical applications.

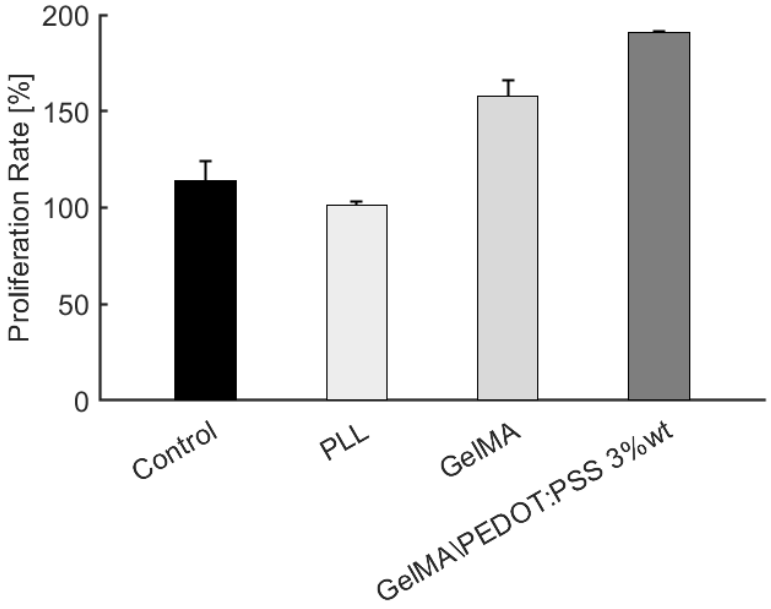

Figure 3.16 Results for the MTT assay for glass, PLL, GelMA and GelMA\PEDOT:PSS 3%wt substrates.

4 Conclusions

Cell-based in vitro models are increasingly utilized in tissue engineering, drug discovery, and toxicology. Bioelectronics, characterized by their bidirectional interfacing capabilities, enable continuous monitoring and precise control over biological processes, thereby expanding the applicability of in vitro systems in research and therapeutic interventions The integration of microfluidics technology further improves the reliability and functionality of in vitro models, aiming to minimize or even obviate the need for animal studies in various stages of drug development and toxicological assessments. This shift towards more ethical and efficient research methodologies is further supported by the advancements in tissue engineering and regenerative medicine, which exploit the beneficial effects of bioelectricity on cell and tissue function, including proliferation, differentiation, and overall tissue repair and regeneration.

The development of organic electronic materials, such as conductive polymers and hydrogels, addresses the limitations posed by traditional electronic materials in achieving intimate and biocompatible cell-electrode interfaces. These organic materials offer enhanced signal transduction capabilities within three-dimensional biological systems, due to their ability to more closely match the mechanical and electrical properties of biological tissues compared to conventional metal and silicon-based electrodes. The application of patterned 2.5D and 3D conductive scaffolds, inspired by the natural extracellular matrix architecture, provides superior spatial arrangements for electrical stimulation and sensing, thereby facilitating complex tissue engineering designs and applications, including neural stem cell differentiation and nerve regeneration.

The project's development of a water-based electro-conductive hydrogel represents a significant advancement in the creation of fully organic 3D electrodes for biomedical applications. Control over the degree of methacryloylation was obtained allowing to obtain hydrogels with different strength. Hydrogels were fabricated at different scale length using different approaches. For macroscale drop casting and UV irradiation was employed to obtain hydrogels up to 1cm in diameter and 1mm in thickness. At mesoscale, a custom mask aligner set up was employed to obtain hydrogels of 500µm,200µm and 100µm in diameter. Finally, two photon polymerization was used to obtain cubic hydrogels with 10µm side. The design is based on blend composed of modified gelatin and PEDOT:PSS. The conductivity of hydrogels was modulated by changing the ratio of PEDOT:PSS. HT-22 cells seeded on hydrogels showed high viability demonstrating cytocompatibility of materials.

This innovative approach not only underscores the potential of organic materials in developing flexible, soft, and conductive electrodes for sensing and stimulation in tissue engineering but also highlights the broader applicability of such materials in creating biomedical devices for *in vivo* applications.

The proposed approach offers a promising pathway for creating fully organic 3D electrodes for sensing and stimulating cells and tissues. Such electrodes could find applications in biomedical devices such as

implants, probes, and epidermal devices, where flexible, soft, and conductive materials are essential requirements. Substrates such as PDMS, polyurethane or PEG can be used as flexible and soft substrate to be implanted in the body, offering a promising alternative to rigid substrates. Looking forward, the continuous evolution of microfluidics and "*on-chip*" technologies necessitates the integration of sensing components to facilitate the standardization and validation of these advanced techniques. This integration could pave the way for the development of more sophisticated and miniaturized biomedical devices, capable of real-time monitoring and control of biological processes at the cellular and tissue levels. As these technologies mature, they promise to revolutionize the fields of drug discovery, toxicology, and tissue engineering, moving towards more personalized and precise medical interventions. The convergence of bioelectronics, microfluidics, and organic materials science opens new horizons for biomedical research and therapeutic applications, marking a significant step forward in our ability to understand, interact with, and manipulate biological systems at the molecular level.

Bibliography

[1] S. K. Doke e S. C. Dhawale, «Alternatives to animal testing: A review», *Saudi Pharm. J. SPJ Off. Publ. Saudi Pharm. Soc.*, vol. 23, fasc. 3, pp. 223–229, lug. 2015, doi: 10.1016/j.jsps.2013.11.002.

[2] S. Carrara e K. Iniewski, A c. di, *Handbook of Bioelectronics: Directly Interfacing Electronics and Biological Systems*. Cambridge: Cambridge University Press, 2015. doi: 10.1017/CBO9781139629539.

[3] A. Szent-Györgyi, «Bioelectronics: Intermolecular electron transfer may play a major role in biological regulation, defense, and cancer.», *Science*, vol. 161, fasc. 3845, pp. 988–990, set. 1968, doi: 10.1126/science.161.3845.988.

[4] J. O. Rivnay Róisín M. ;. Malliaras, George G., «The Rise of Organic Bioelectronics», *Chem. Mater.*, vol. 26, fasc. 1, pp. 679–685, 2013, doi: 10.1021/cm4022003.

[5] C. Pitsalidis *et al.*, «Organic Bioelectronics for In Vitro Systems», *Chem. Rev.*, vol. 122, fasc. 4, pp. 4700–4790, feb. 2022, doi: 10.1021/acs.chemrev.1c00539.

[6] G. Zhao *et al.*, «Rational design of electrically conductive biomaterials toward excitable tissues regeneration», *Prog. Polym. Sci.*, vol. 131, p. 101573, ago. 2022, doi: 10.1016/j.progpolymsci.2022.101573.

[7] J. G. H. Roth Michelle S. ;. Li, Thomas L. ;. Feig, Vivian R. ;. Jiang, Yuanwen; Cui, Bianxiao; Greely, Henry T. ;. Bao, Zhenan; Paşca, Sergiu P. ;. Heilshorn, Sarah C., «Advancing models of neural development with biomaterials.», *Nat. Rev. Neurosci.*, vol. 22, fasc. 10, pp. 593–615, 2021, doi: 10.1038/s41583-021-00496-y.

[8] G. L. ; D. Koons Mani; Mikos, Antonios G., «Materials design for bone-tissue engineering», *Nat. Rev. Mater.*, vol. 5, fasc. 8, pp. 584–603, 2020, doi: 10.1038/s41578-020-0204-2.

[9] M. Nikkhah e J. Rivnay, «Conductive and Electroactive Biomaterials and Bioelectronics», *Acta Biomater.*, vol. 139, pp. 1–3, feb. 2022, doi: 10.1016/j.actbio.2022.01.018.

[10] A. K. ; P. Jayaram Charalampos; Tan, Ellasia; Moysidou, Chrysanthi-Maria; De Volder, Michael; Kim, Ji-Seon; Owens, Róisín M., «3D Hybrid Scaffolds Based on PEDOT:PSS/MWCNT Composites.», *Front. Chem.*, vol. 7, fasc. NA, pp. 363-NA, 2019, doi: 10.3389/fchem.2019.00363.

[11] C.-M. P. Moysidou Charalampos; Al-Sharabi, Mohammed; Withers, Aimee M. ;. Zeitler, J. Axel; Owens, Róisín M., «3D Bioelectronic Model of the Human Intestine», *Adv. Biol.*, vol. 5, fasc. 2, pp. 2000306-NA, 2021, doi: 10.1002/adbi.202000306.

[12] S. Inal *et al.*, «Conducting Polymer Scaffolds for Hosting and Monitoring 3D Cell Culture», *Adv. Biosyst.*, vol. 1, fasc. 6, 2017, doi: 10.1002/adbi.201700052.

[13] D. Iandolo *et al.*, «Biomimetic and electroactive 3D scaffolds for human neural crest-derived stem cell expansion and osteogenic differentiation», *MRS Commun.*, vol. 10, fasc. 1, pp. 179–187, mar. 2020, doi: 10.1557/mrc.2020.10.

[14] C. F. Pitsalidis Magali; Iandolo, Donata; Tzounis, Lazaros; Inal, Sahika; Owens, Róisín M., «Transistor in a tube: A route to three-dimensional bioelectronics», *Sci. Adv.*, vol. 4, fasc. 10, pp. eaat4253-NA, 2018, doi: 10.1126/sciadv.aat4253.

[15] K. Li, Y. Jiang, Z. Yang, B. C. Heng, H. Tian, e Z. Ge, «Can Upregulation of Pluripotency Genes Enhance Stemness of Mesenchymal Stem Cells?», *Stem Cell Rev. Rep.*, vol. 17, fasc. 4, pp. 1505–1507, ago. 2021, doi: 10.1007/s12015-021-10154-6.

[16] «Electroactive Biomaterials and Systems for Cell Fate Determination and Tissue Regeneration: Design and Applications - Liu - 2021 - Advanced Materials - Wiley Online Library». Consultato: 14 ottobre 2023. [Online]. Disponibile su: https://onlinelibrary-wiley-com.ezproxy.biblio.polito.it/doi/full/10.1002/adma.202007429

[17] W. L. ; K. Stoppel David L. ;. Black, Lauren D., «Electrical and mechanical stimulation of cardiac cells and tissue constructs.», *Adv. Drug Deliv. Rev.*, vol. 96, fasc. NA, pp. 135–155, 2015, doi: 10.1016/j.addr.2015.07.009.

[18] «Electrical Stimuli in the Central Nervous System Microenvironment | Annual Review of Biomedical Engineering». Consultato: 14 ottobre 2023. [Online]. Disponibile su: https://www-annualreviews-org.ezproxy.biblio.polito.it/doi/10.1146/annurev-bioeng-121813-120655

[19] F. Vasquez-Sancho, A. Abdollahi, D. Damjanovic, e G. Catalan, «Flexoelectricity in Bones», *Adv. Mater.*, vol. 30, fasc. 21, p. 1801413, 2018, doi: 10.1002/adma.201801413.
[20] T. Dvir *et al.*, «Nanowired three-dimensional cardiac patches», *Nat. Nanotechnol.*, vol. 6, fasc. 11, Art. fasc. 11, nov. 2011, doi: 10.1038/nnano.2011.160.
[21] D. M. Mawad Catherine; Lauto, Antonio; Perbellini, Filippo; Nelson, Geoffrey W. ;. Tonkin, Joanne; Bello, Sean O. ;. Carrad, Damon J. ;. Micolich, Adam P. ;. Mahat, Mohd Muzamir; Furman, Jennifer; Payne, David J. ;. Lyon, Alexander R. ;. Gooding, J. Justin; Harding, Sian E. ;. Terracciano, Cesare M. ;. Stevens, Molly M., «A conducting polymer with enhanced electronic stability applied in cardiac models», *Sci. Adv.*, vol. 2, fasc. 11, pp. e1601007-NA, 2016, doi: 10.1126/sciadv.1601007.
[22] L. Z. Cui Jin; Zou, Jun; Yang, Xianrui; Guo, Hui; Tian, Huayu; Zhang, Peibiao; Wang, Yu; Zhang, Ning; Zhuang, Xiuli; Li, Zhong-Ming; Ding, Jianxun; Chen, Xuesi, «Electroactive composite scaffold with locally expressed osteoinductive factor for synergistic bone repair upon electrical stimulation.», *Biomaterials*, vol. 230, fasc. NA, pp. 119617-NA, 2019, doi: 10.1016/j.biomaterials.2019.119617.
[23] Y. W. Lu Yanan; Zhang, Jieyu; Hu, Xuefeng; Yang, Zeyu; Guo, Yi; Wang, Yunbing, «In-situ doping of a conductive hydrogel with low protein absorption and bacterial adhesion for electrical stimulation of chronic wounds», *Acta Biomater.*, vol. 89, fasc. NA, pp. 217–226, 2019, doi: 10.1016/j.actbio.2019.03.018.
[24] J. J. Park Jin; Kim, Byongyeon; Lee, Min Suk; Park, Sihyeon; Lim, Juhan; Yi, Jongdarm; Lee, Hwangjae; Yang, Hee Seok; Lee, Jae Young, «Electrically Conductive Hydrogel Nerve Guidance Conduits for Peripheral Nerve Regeneration», *Adv. Funct. Mater.*, vol. 30, fasc. 39, pp. 2003759-NA, 2020, doi: 10.1002/adfm.202003759.
[25] G. F. Zhao Yanjing; Xue, Li; Cui, Mengjie; Zhang, Qi; Xu, Feng; Peng, Niancai; Jiang, Zhuangde; Gao, Dengfeng; Zhang, Xiaohui, «Anisotropic conductive reduced graphene oxide/silk matrices promote post-infarction myocardial function by restoring electrical integrity.», *Acta Biomater.*, vol. 139, fasc. NA, pp. 190–203, 2021, doi: 10.1016/j.actbio.2021.03.073.
[26] R. E. Feiner Leeya; Fleischer, Sharon; Malki, Maayan; Gal, Idan; Shapira, Assaf; Shacham-Diamand, Yosi; Dvir, Tal, «Engineered hybrid cardiac patches with multifunctional electronics for online monitoring and regulation of tissue function», *Nat. Mater.*, vol. 15, fasc. 6, pp. 679–685, 2016, doi: 10.1038/nmat4590.
[27] B. L. Tian Jia; Dvir, Tal; Jin, Lihua; Tsui, Jonathan H. ;. Qing, Quan; Suo, Zhigang; Langer, Robert; Kohane, Daniel S. ;. Lieber, Charles M., «Macroporous nanowire nanoelectronic scaffolds for synthetic tissues», *Nat. Mater.*, vol. 11, fasc. 11, pp. 986–994, 2012, doi: 10.1038/nmat3404.
[28] Galvani, L. Galvani, e G. Aldini, *De viribus electricitatis in motu musculari: commentarius cum Joannis Aldini dissertatione et notis : accesserunt epistolae ad animalis electricitatis theoriam pertinentes*. Soc. Typogr., 1792.
[29] L. W. Poltawski Tim, «Bioelectricity and microcurrent therapy for tissue healing - a narrative review», *Phys. Ther. Rev.*, vol. 14, fasc. 2, pp. 104–114, 2009, doi: 10.1179/174328809x405973.
[30] B. Hille, «Ionic channels in excitable membranes. Current problems and biophysical approaches», *Biophys. J.*, vol. 22, fasc. 2, pp. 283–294, 1978, doi: 10.1016/s0006-3495(78)85489-7.
[31] Z. B. ; H. Friedenberg M. C; Heppenstall, R. B; Brighton, Carl T., «The cellular origin of bioelectric potentials in bone.», *Calcif. Tissue Res.*, vol. 13, fasc. 1, pp. 53–62, 1973, doi: 10.1007/bf02015396.
[32] I. S. FOULDS e A. T. BARKER, «Human skin battery potentials and their possible role in wound healing», *Br. J. Dermatol.*, vol. 109, fasc. 5, pp. 515–522, nov. 1983, doi: 10.1111/j.1365-2133.1983.tb07673.x.
[33] R. Nuccitelli, «Endogenous ionic currents and DC electric fields in multicellular animal tissues.», *Bioelectromagnetics*, vol. 13, fasc. S1, pp. 147–157, 1992, doi: 10.1002/bem.2250130714.

[34] M. S. ; H. Spach J. Francis; Dolber, Paul C. ;. Barr, Roger C., «Electrophysiological Effects of Remodeling Cardiac Gap Junctions and Cell Size Experimental and Model Studies of Normal Cardiac Growth», *Circ. Res.*, vol. 86, fasc. 3, pp. 302–311, 2000, doi: 10.1161/01.res.86.3.302.
[35] C. K. Thomas, J. J. Woods, e B. Bigland-Ritchie, «Impulse propagation and muscle activation in long maximal voluntary contractions», *J. Appl. Physiol.*, vol. 67, fasc. 5, pp. 1835–1842, nov. 1989, doi: 10.1152/jappl.1989.67.5.1835.
[36] A. L. HODGKIN e A. F. HUXLEY, «Propagation of electrical signals along giant nerve fibers.», *Proc. R. Soc. Lond. Ser. B Contain. Pap. Biol. Character R. Soc. G. B.*, vol. 140, fasc. 899, pp. 177–183, 1952.
[37] P. M. George *et al.*, «Electrical preconditioning of stem cells with a conductive polymer scaffold enhances stroke recovery», *Biomaterials*, vol. 142, pp. 31–40, ott. 2017, doi: 10.1016/j.biomaterials.2017.07.020.
[38] Z. G. Shi Huichang; Feng, Jiao; Ding, Beibei; Cao, Xiaodong; Kuga, Shigenori; Wang, Yingjun; Zhang, Lina; Cai, Jie, «In Situ Synthesis of Robust Conductive Cellulose/Polypyrrole Composite Aerogels and Their Potential Application in Nerve Regeneration», *Angew. Chem. Int. Ed Engl.*, vol. 53, fasc. 21, pp. 5380–5384, 2014, doi: 10.1002/anie.201402751.
[39] B. L. Zhu Shyh-Chyang; Zhao, Haichao; Lin, Hsing-An; Sekine, Jun; Nakao, Aiko; Chen, Chi; Yamashita, Yoshiro; Yu, Hsiao-hua, «Large enhancement in neurite outgrowth on a cell membrane-mimicking conducting polymer», *Nat. Commun.*, vol. 5, fasc. 1, pp. 4523–4531, 2014, doi: 10.1038/ncomms5523.
[40] A. M. ; Z. Rajnicek Zhiqiang; Moral-Vico, Javier; Cruz, Ana M. ;. McCaig, Colin D. ;. Casañ-Pastor, Nieves, «Controlling Nerve Growth with an Electric Field Induced Indirectly in Transparent Conductive Substrate Materials.», *Adv. Healthc. Mater.*, vol. 7, fasc. 17, pp. 1800473-NA, 2018, doi: 10.1002/adhm.201800473.
[41] E. Tomaskovic-Crook *et al.*, «Human Neural Tissues from Neural Stem Cells Using Conductive Biogel and Printed Polymer Microelectrode Arrays for 3D Electrical Stimulation», *Adv. Healthc. Mater.*, vol. 8, fasc. 15, p. 1900425, 2019, doi: 10.1002/adhm.201900425.
[42] W. Guo *et al.*, «Self-Powered Electrical Stimulation for Enhancing Neural Differentiation of Mesenchymal Stem Cells on Graphene–Poly(3,4-ethylenedioxythiophene) Hybrid Microfibers», *ACS Nano*, vol. 10, fasc. 5, pp. 5086–5095, mag. 2016, doi: 10.1021/acsnano.6b00200.
[43] I. E. Arioz Ozlem; Bakan, Gokhan; Dikecoglu, F. Begum; Topal, Ahmet; Urel, Mustafa; Dana, Aykutlu; Tekinay, Ayse B. ;. Guler, Mustafa O., «Biocompatible Electroactive Tetra(aniline)-Conjugated Peptide Nanofibers for Neural Differentiation», *ACS Appl. Mater. Interfaces*, vol. 10, fasc. 1, pp. 308–317, 2017, doi: 10.1021/acsami.7b16509.
[44] Z. A. Bagher Zhaleh; Alizadeh, Rafieh; Farhadi, Mohammad; Zarrintaj, Payam; Moroni, Lorenzo; Setayeshmehr, Mohsen; Komeili, Ali; Kamrava, S. Kamran, «Conductive hydrogel based on chitosan-aniline pentamer/gelatin/agarose significantly promoted motor neuron-like cells differentiation of human olfactory ecto-mesenchymal stem cells.», *Mater. Sci. Eng. C Mater. Biol. Appl.*, vol. 101, fasc. NA, pp. 243–253, 2019, doi: 10.1016/j.msec.2019.03.068.
[45] Y. Q. Sun Qi; Meng, Haoye; Zheng, Yudong; Peng, Jiang; Hu, Yaxin; Feng, Zhaoxuan; Sang, Xiao; Qiao, Kun; He, Wei; Chi, Xiaoqi; Zhao, Liang, «Enhanced Neurite Outgrowth on a Multiblock Conductive Nerve Scaffold with Self-Powered Electrical Stimulation.», *Adv. Healthc. Mater.*, vol. 8, fasc. 10, pp. 1900127-NA, 2019, doi: 10.1002/adhm.201900127.
[46] E. R. ; U. Aurand Sadaf; Medelin, Manuela; Scaini, Denis; Bosi, Susanna; Rosselli, Federica Bianca; Donato, Sandro; Tromba, Giuliana; Prato, Maurizio; Ballerini, Laura, «Nanostructures to Engineer 3D Neural-Interfaces: Directing Axonal Navigation toward Successful Bridging of Spinal Segments», *Adv. Funct. Mater.*, vol. 28, fasc. 12, pp. 1700550–1700561, 2017, doi: 10.1002/adfm.201700550.
[47] H. J. Qing Yuan; Li, Wenfang; Zhao, Guoxu; Yang, Qingzhen; Zhang, Xiaohui; Luo, Zhengtang; Lu, Tian Jian; Jin, Guorui; Xu, Feng, «Microfluidic Printing of Three-Dimensional Graphene Electroactive Microfibrous Scaffolds.», *ACS Appl. Mater. Interfaces*, vol. 12, fasc. 2, pp. 2049–2058, 2020, doi: 10.1021/acsami.9b17948.
[48] Y. Z. Qian Xiaotian; Han, Qixin; Chen, Wei; Li, Hui; Yuan, Weien, «An integrated multi-layer 3D-fabrication of PDA/RGD coated graphene loaded PCL nanoscaffold for peripheral nerve

restoration», *Nat. Commun.*, vol. 9, fasc. 1, pp. 323–323, 2018, doi: 10.1038/s41467-017-02598-7.

[49] S. J. L. Lee Hyo-Jung; Kim, Sung-Yeol; Seok, Ji Min; Lee, Junhee; Kim, Wan Doo; Kwon, Il Keun; Park, Shin-Young; Park, Su A., «In situ gold nanoparticle growth on polydopamine-coated 3D-printed scaffolds improves osteogenic differentiation for bone tissue engineering applications: in vitro and in vivo studies.», *Nanoscale*, vol. 10, fasc. 33, pp. 15447–15453, 2018, doi: 10.1039/c8nr04037k.

[50] U. S. S. Demir Reza; Calamak, Semih; Ozturk, Sukru; Gultekinoglu, Merve; Ulubayram, Kezban, «Gold nano-decorated aligned polyurethane nanofibers for enhancement of neurite outgrowth and elongation.», *J. Biomed. Mater. Res. A*, vol. 106, fasc. 6, pp. 1604–1613, 2018, doi: 10.1002/jbm.a.36365.

[51] Y. L. Zhao Yunyun; Ding, Supeng; Zhang, Kunyu; Mao, Hai-Quan; Yang, Yumin, «Application of conductive PPy/SF composite scaffold and electrical stimulation for neural tissue engineering», *Biomaterials*, vol. 255, fasc. NA, pp. 120164-NA, 2020, doi: 10.1016/j.biomaterials.2020.120164.

[52] J. Wang, H. Wang, X. Mo, e H. Wang, «Reduced Graphene Oxide-Encapsulated Microfiber Patterns Enable Controllable Formation of Neuronal-Like Networks», *Adv. Mater.*, vol. 32, fasc. 40, p. 2004555, 2020, doi: 10.1002/adma.202004555.

[53] J. Wang *et al.*, «In vitro and in vivo studies of electroactive reduced graphene oxide-modified nanofiber scaffolds for peripheral nerve regeneration», *Acta Biomater.*, vol. 84, pp. 98–113, gen. 2019, doi: 10.1016/j.actbio.2018.11.032.

[54] D. F. Xu Lin; Gao, Lingfeng; Xiong, Yan; Wang, Yanfeng; Ye, Qifa; Yu, Aixi; Dai, Honglian; Yin, Yixia; Cai, Jie; Zhang, Lina, «Micro-Nanostructured Polyaniline Assembled in Cellulose Matrix via Interfacial Polymerization for Applications in Nerve Regeneration», *ACS Appl. Mater. Interfaces*, vol. 8, fasc. 27, pp. 17090–17097, 2016, doi: 10.1021/acsami.6b03555.

[55] S. S. Das Manav; Saharia, Dhiren; Sarma, K. K. ;. Muir, Elizabeth M. ;. Bora, Utpal, «Electrospun silk-polyaniline conduits for functional nerve regeneration in rat sciatic nerve injury model», *Biomed. Mater. Bristol Engl.*, vol. 12, fasc. 4, pp. 045025–045025, 2017, doi: 10.1088/1748-605x/aa7802.

[56] A. E. ; S. Jakus Ethan B. ;. Rutz, Alexandra L. ;. Jordan, Sumanas W. ;. Hersam, Mark C. ;. Shah, Ramille N., «Three-dimensional printing of high-content graphene scaffolds for electronic and biomedical applications.», *ACS Nano*, vol. 9, fasc. 4, pp. 4636–4648, 2015, doi: 10.1021/acsnano.5b01179.

[57] M. N.-N. Salehi ; Ebrahimi-Barough, Somayeh; Nourani, Mohammdreza; Khojasteh, Arash; Hamidieh, Amir Ali; Amani, Amir; Farzamfar, Saeed; Ai, Jafar, «Sciatic nerve regeneration by transplantation of Schwann cells via erythropoietin controlled-releasing polylactic acid/multiwalled carbon nanotubes/gelatin nanofibrils neural guidance conduit», *J. Biomed. Mater. Res. B Appl. Biomater.*, vol. 106, fasc. 4, pp. 1463–1476, 2017, doi: 10.1002/jbm.b.33952.

[58] N. D.-A. Alegret Antonio; González-Domínguez, Jose M. ;. Arnaiz, Blanca; Cossío, Unai; Bosi, Susanna; Vázquez, Ester; Ramos-Cabrer, Pedro; Mecerreyes, David; Prato, Maurizio, «Three-Dimensional Conductive Scaffolds as Neural Prostheses Based on Carbon Nanotubes and Polypyrrole.», *ACS Appl. Mater. Interfaces*, vol. 10, fasc. 50, pp. 43904–43914, 2018, doi: 10.1021/acsami.8b16462.

[59] S. T. Vijayavenkataraman Siti; Zhang, Shuo; Lu, Wen Feng; Fuh, Jerry Y. H., «3D-Printed PCL/rGO Conductive Scaffolds for Peripheral Nerve Injury Repair.», *Artif. Organs*, vol. 43, fasc. 5, pp. 515–523, 2018, doi: 10.1111/aor.13360.

[60] C. Wu *et al.*, «Cell-Laden Electroconductive Hydrogel Simulating Nerve Matrix To Deliver Electrical Cues and Promote Neurogenesis», *ACS Appl. Mater. Interfaces*, vol. 11, fasc. 25, pp. 22152–22163, giu. 2019, doi: 10.1021/acsami.9b05520.

[61] L. W. Wang Yaobin; Hu, Tianli; X. ,. Peter; Guo, Baolin, «Aligned conductive core-shell biomimetic scaffolds based on nanofiber yarns/hydrogel for enhanced 3D neurite outgrowth alignment and elongation», *Acta Biomater.*, vol. 96, fasc. NA, pp. 175–187, 2019, doi: 10.1016/j.actbio.2019.06.035.

[62] X. Y. Li Wen; Xie, Hongjian; Wang, Jian; Zhang, Lei; Wang, Zheng; Wang, Lin, «CNT/Sericin Conductive Nerve Guidance Conduit Promotes Functional Recovery of Transected Peripheral Nerve Injury in a Rat Model.», *ACS Appl. Mater. Interfaces*, vol. 12, fasc. 33, pp. 36860–36872, 2020, doi: 10.1021/acsami.0c08457.

[63] M. S. Bicer Jonathan; Iandolo, Donata; Boateng, Samuel Y. ;. Cottrell, Graeme S. ;. Widera, Darius, «Electrical Stimulation of Adipose-Derived Stem Cells in 3D Nanofibrillar Cellulose Increases Their Osteogenic Potential», *Biomolecules*, vol. 10, fasc. 12, pp. 1696-NA, 2020, doi: 10.3390/biom10121696.

[64] K. Li, T. Ning, H. Wang, Y. Jiang, J. Zhang, e Z. Ge, «Nanosecond pulsed electric fields enhance mesenchymal stem cells differentiation via DNMT1-regulated OCT4/NANOG gene expression», *Stem Cell Res. Ther.*, vol. 11, fasc. 1, p. 308, lug. 2020, doi: 10.1186/s13287-020-01821-5.

[65] Y.-S. L. Hsiao Chung Chih; Hsieh, Hsin Jui; Tsai, Shih Min; Kuo, Chiung Wen; Chu, Chih-Wei; Chen, Peilin, «Manipulating location, polarity, and outgrowth length of neuron-like pheochromocytoma (PC-12) cells on patterned organic electrode arrays», *Lab. Chip*, vol. 11, fasc. 21, pp. 3674–3680, 2011, doi: 10.1039/c1lc20675c.

[66] X. L. Chen Chaoyuan; Huang, Zhongbing; Pu, Ximing; Shang, Lei; Yin, Guangfu; Xue, Chengjing, «Preparation of carboxylic graphene oxide-composited polypyrrole conduits and their effect on sciatic nerve repair under electrical stimulation.», *J. Biomed. Mater. Res. A*, vol. 107, fasc. 12, pp. 2784–2795, 2019, doi: 10.1002/jbm.a.36781.

[67] C. Liu *et al.*, «Fabrication of carboxylic graphene oxide-composited polypyrrole film for neurite growth under electrical stimulation», *Front. Mater. Sci.*, vol. 13, fasc. 3, pp. 258–267, set. 2019, doi: 10.1007/s11706-019-0467-y.

[68] J. Q. Zhang Kexin; Sun, Binbin; Fang, Jun; Zhang, Kuihua; EI-Hamshary, Hany; Al-Deyab, Salem S. ;. Mo, Xiumei, «The aligned core–sheath nanofibers with electrical conductivity for neural tissue engineering», *J. Mater. Chem. B*, vol. 2, fasc. 45, pp. 7945–7954, 2014, doi: 10.1039/c4tb01185f.

[69] W. Jing *et al.*, «Study of Electrical Stimulation with Different Electric-Field Intensities in the Regulation of the Differentiation of PC12 Cells», *ACS Chem. Neurosci.*, vol. 10, fasc. 1, pp. 348–357, gen. 2019, doi: 10.1021/acschemneuro.8b00286.

[70] A. J. I. Petty, R. L. Keate, B. Jiang, G. A. Ameer, e J. Rivnay, «Conducting Polymers for Tissue Regeneration in Vivo», *Chem. Mater.*, vol. 32, fasc. 10, pp. 4095–4115, mag. 2020, doi: 10.1021/acs.chemmater.0c00767.

[71] L. P. da Silva, S. C. Kundu, R. L. Reis, e V. M. Correlo, «Electric Phenomenon: A Disregarded Tool in Tissue Engineering and Regenerative Medicine», *Trends Biotechnol.*, vol. 38, fasc. 1, pp. 24–49, gen. 2020, doi: 10.1016/j.tibtech.2019.07.002.

[72] Y.-S. H. Hsiao Bo-Cheng; Yan, Hong-Xin; Kuo, Chiung-Wen; Chueh, Di-Yen; Yu, Hsiao-hua; Chen, Peilin, «Integrated 3D conducting polymer-based bioelectronics for capture and release of circulating tumor cells», *J. Mater. Chem. B*, vol. 3, fasc. 25, pp. 5103–5110, 2015, doi: 10.1039/c5tb00096c.

[73] S. Jeon, J.-M. Moon, E. S. Lee, Y. H. Kim, e Y. Cho, «An Electroactive Biotin-Doped Polypyrrole Substrate That Immobilizes and Releases EpCAM-Positive Cancer Cells», *Angew. Chem. Int. Ed.*, vol. 53, fasc. 18, pp. 4597–4602, 2014, doi: 10.1002/anie.201309998.

[74] T. Someya, Z. Bao, e G. G. Malliaras, «The rise of plastic bioelectronics», *Nature*, vol. 540, fasc. 7633, Art. fasc. 7633, dic. 2016, doi: 10.1038/nature21004.

[75] A. ; T. Evans Brianna C. ;. Wallace, Gordon G. ;. Millard, Rodney E. ;. O'Leary, Stephen; Clark, Graeme M. ;. Shepherd, Robert K. ;. Richardson, Rachael T., «Promoting neurite outgrowth from spiral ganglion neuron explants using polypyrrole/BDNF-coated electrodes.», *J. Biomed. Mater. Res. A*, vol. 91, fasc. 1, pp. 241–250, 2009, doi: 10.1002/jbm.a.32228.

[76] Q. Zhang, S. Beirne, K. Shu, D. Esrafilzadeh, X.-F. Huang, e G. G. Wallace, «Electrical Stimulation with a Conductive Polymer Promotes Neurite Outgrowth and Synaptogenesis in Primary Cortical Neurons in 3D», *Sci. Rep.*, vol. 8, fasc. 1, Art. fasc. 1, giu. 2018, doi: 10.1038/s41598-018-27784-5.

[77] K. H. Nagamine Takuya; Okamoto, Kohei; Abe, Yuina; Kaji, Hirokazu; Nishizawa, Matsuhiko, «Portable Micropatterns of Neuronal Cells Supported by Thin Hydrogel Films», *ACS Biomater. Sci. Eng.*, vol. 1, fasc. 5, pp. 329–334, 2015, doi: 10.1021/acsbiomaterials.5b00020.
[78] G. K. Rong Eric H. ;. Qiang, Yi; Di, Wenjun; Zhong, Yiding; Zhao, Xuanyi; Fang, Hui; Clark, Heather A., «Imaging Sodium Flux during Action Potentials in Neurons with Fluorescent Nanosensors and Transparent Microelectrodes», *ACS Sens.*, vol. 3, fasc. 12, pp. 2499–2505, 2018, doi: 10.1021/acssensors.8b00903.
[79] R. Kim e Y. Nam, «Polydopamine-doped conductive polymer microelectrodes for neural recording and stimulation», *J. Neurosci. Methods*, vol. 326, p. 108369, ott. 2019, doi: 10.1016/j.jneumeth.2019.108369.
[80] S. Ostrovsky *et al.*, «Conductive hybrid carbon nanotube (CNT)–polythiophene coatings for innovative auditory neuron-multi-electrode array interfacing», *RSC Adv.*, vol. 6, fasc. 48, pp. 41714–41723, apr. 2016, doi: 10.1039/C5RA27642J.
[81] Z. Aqrawe *et al.*, «The influence of macropores on PEDOT/PSS microelectrode coatings for neuronal recording and stimulation», *Sens. Actuators B Chem.*, vol. 281, pp. 549–560, feb. 2019, doi: 10.1016/j.snb.2018.10.099.
[82] E. G. R. ; Z. Fernandes Valtencir; de Queiroz, Alvaro Antonio Alencar, «Electrospinning of Hyperbranched Poly-L-Lysine/Polyaniline Nanofibers for Application in Cardiac Tissue Engineering», *J. Macromol. Sci. Part A*, vol. 47, fasc. 12, pp. 1203–1207, 2010, doi: 10.1080/10601325.2010.518847.
[83] D. P. Kai Molamma P. ;. Jin, Guorui; Ramakrishna, Seeram, «Biocompatibility evaluation of electrically conductive nanofibrous scaffolds for cardiac tissue engineering», *J. Mater. Chem. B*, vol. 1, fasc. 17, pp. 2305–2314, 2013, doi: 10.1039/c3tb00151b.
[84] K. V. Roshanbinfar Lena; Greber, Boris; Diecke, Sebastian; Boccaccini, Aldo R. ;. Scheibel, Thomas; Engel, Felix B., «Electroconductive biohybrid hydrogel for enhanced maturation and beating properties of engineered cardiac tissues», *Adv. Funct. Mater.*, vol. 28, fasc. 42, pp. 1803951-NA, 2018, doi: 10.1002/adfm.201803951.
[85] D. G. Khodagholy Jennifer N. ;. Thesen, Thomas; Doyle, Werner; Devinsky, Orrin; Malliaras, George G. ;. Buzsáki, György, «NeuroGrid: recording action potentials from the surface of the brain», *Nat. Neurosci.*, vol. 18, fasc. 2, pp. 310–315, 2014, doi: 10.1038/nn.3905.
[86] L. G. Xu Sarah R. ;. Ma, Yinji; Petrossians, Artin; Liu, Yuhao; Webb, R. Chad; Fan, Jonathan A. ;. Yang, Zijian; Xu, Renxiao; Whalen, John J. ;. Weiland, James D. ;. Huang, Yonggang; Efimov, Igor R. ;. Rogers, John A., «Materials and Fractal Designs for 3D Multifunctional Integumentary Membranes with Capabilities in Cardiac Electrotherapy», *Adv. Mater. Deerfield Beach Fla*, vol. 27, fasc. 10, pp. 1731–1737, 2015, doi: 10.1002/adma.201405017.
[87] X. B. Strakosas Manuelle; Owens, Róisín M., «The organic electrochemical transistor for biological applications», *J. Appl. Polym. Sci.*, vol. 132, fasc. 15, p. n/a-n/a, 2015, doi: 10.1002/app.41735.
[88] I. del Agua *et al.*, «Conducting Polymer Scaffolds Based on Poly(3,4-ethylenedioxythiophene) and Xanthan Gum for Live-Cell Monitoring», *ACS Omega*, vol. 3, fasc. 7, pp. 7424–7431, lug. 2018, doi: 10.1021/acsomega.8b00458.
[89] C. Hao, L. Ding, X. Zhang, e H. Ju, «Biocompatible Conductive Architecture of Carbon Nanofiber-Doped Chitosan Prepared with Controllable Electrodeposition for Cytosensing», *Anal. Chem.*, vol. 79, fasc. 12, pp. 4442–4447, giu. 2007, doi: 10.1021/ac062344z.
[90] F. Santoro *et al.*, «Revealing the Cell-Material Interface with Nanometer Resolution by Focused Ion Beam/Scanning Electron Microscopy», *ACS Nano*, vol. 11, fasc. 8, pp. 8320–8328, ago. 2017, doi: 10.1021/acsnano.7b03494.
[91] T.-H. Kim, K.-B. Lee, e J.-W. Choi, «3D graphene oxide-encapsulated gold nanoparticles to detect neural stem cell differentiation», *Biomaterials*, vol. 34, fasc. 34, pp. 8660–8670, nov. 2013, doi: 10.1016/j.biomaterials.2013.07.101.
[92] J. Li, J. Xie, L. Gao, e C. M. Li, «Au Nanoparticles–3D Graphene Hydrogel Nanocomposite To Boost Synergistically in Situ Detection Sensitivity toward Cell-Released Nitric Oxide», *ACS Appl. Mater. Interfaces*, vol. 7, fasc. 4, pp. 2726–2734, feb. 2015, doi: 10.1021/am5077777.
[93] H.-W. H. Zhang Xue-Bo; Qin, Yu; Jin, Zi-He; Zhang, Xin-Wei; Liu, Yan-Ling; Huang, Wei-Hua, «Conductive Polymer Coated Scaffold to Integrate 3D Cell Culture with Electrochemical

Sensing.», *Anal. Chem.*, vol. 91, fasc. 7, pp. 4838–4844, 2019, doi: 10.1021/acs.analchem.9b00478.
[94] S. K. Maji, S. Sreejith, A. K. Mandal, X. Ma, e Y. Zhao, «Immobilizing Gold Nanoparticles in Mesoporous Silica Covered Reduced Graphene Oxide: A Hybrid Material for Cancer Cell Detection through Hydrogen Peroxide Sensing», *ACS Appl. Mater. Interfaces*, vol. 6, fasc. 16, pp. 13648–13656, ago. 2014, doi: 10.1021/am503110s.
[95] M. H. Naveen, N. G. Gurudatt, H.-B. Noh, e Y.-B. Shim, «Dealloyed AuNi Dendrite Anchored on a Functionalized Conducting Polymer for Improved Catalytic Oxygen Reduction and Hydrogen Peroxide Sensing in Living Cells», *Adv. Funct. Mater.*, vol. 26, fasc. 10, pp. 1590–1601, 2016, doi: 10.1002/adfm.201504506.
[96] L. Amato *et al.*, «Pyrolysed 3D-Carbon Scaffolds Induce Spontaneous Differentiation of Human Neural Stem Cells and Facilitate Real-Time Dopamine Detection», *Adv. Funct. Mater.*, vol. 24, fasc. 44, pp. 7042–7052, 2014, doi: 10.1002/adfm.201400812.
[97] A. A. Aziz Muhammad; Azeem, Muhammad; Ashraf, Ghazala; Wang, Zhengyun; Xiao, Fei; Liu, Hongfang, «Self-stacking of exfoliated charged nanosheets of LDHs and graphene as biosensor with real-time tracking of dopamine from live cells», *Anal. Chim. Acta*, vol. 1047, fasc. NA, pp. 197–207, 2018, doi: 10.1016/j.aca.2018.10.008.
[98] M. Y. Emran *et al.*, «Broccoli-shaped biosensor hierarchy for electrochemical screening of noradrenaline in living cells», *Biosens. Bioelectron.*, vol. 100, pp. 122–131, feb. 2018, doi: 10.1016/j.bios.2017.08.050.
[99] S. Y. Yang *et al.*, «Detection of transmitter release from single living cells using conducting polymer microelectrodes», *Adv. Mater.*, vol. 23, fasc. 24, pp. H184–H188, 2011, doi: 10.1002/adma.201100035.
[100] M. M. Modena, K. Chawla, P. M. Misun, e A. Hierlemann, «Smart Cell Culture Systems: Integration of Sensors and Actuators into Microphysiological Systems», *ACS Chem. Biol.*, vol. 13, fasc. 7, pp. 1767–1784, lug. 2018, doi: 10.1021/acschembio.7b01029.
[101] J. Kieninger, A. Weltin, H. Flamm, e G. A. Urban, «Microsensor systems for cell metabolism – from 2D culture to organ-on-chip», *Lab. Chip*, vol. 18, fasc. 9, pp. 1274–1291, mag. 2018, doi: 10.1039/C7LC00942A.
[102] B. ; W. Alshammary Frank C. ;. Herrasti, Pilar; de León, C. Ponce, «Electrodeposited conductive polymers for controlled drug release: polypyrrole», *J. Solid State Electrochem.*, vol. 20, fasc. 4, pp. 839–859, 2015, doi: 10.1007/s10008-015-2982-9.
[103] D. T.-S. Svirskis Jadranka; Rodgers, Anthony; Garg, Sanjay, «Electrochemically controlled drug delivery based on intrinsically conducting polymers.», *J. Control. Release Off. J. Control. Release Soc.*, vol. 146, fasc. 1, pp. 6–15, 2010, doi: 10.1016/j.jconrel.2010.03.023.
[104] R. W. Feiner Lior; Gazit, Danielle; Kalish, Or; Mishal, Gal; Shapira, Assaf; Dvir, Tal, «A Stretchable and Flexible Cardiac Tissue-Electronics Hybrid Enabling Multiple Drug Release, Sensing, and Stimulation.», *Small Weinh. Bergstr. Ger.*, vol. 15, fasc. 14, pp. 1805526-NA, 2019, doi: 10.1002/smll.201805526.
[105] B. C. ; R. Thompson Rachael T. ;. Moulton, Simon E. ;. Evans, A. ;. O'Leary, Stephen; Clark, Graeme M. ;. Wallace, Gordon G., «Conducting polymers, dual neurotrophins and pulsed electrical stimulation - Dramatic effects on neurite outgrowth», *J. Control. Release Off. J. Control. Release Soc.*, vol. 141, fasc. 2, pp. 161–167, 2009, doi: 10.1016/j.jconrel.2009.09.016.
[106] L. Wu, J. Wang, N. Gao, J. Ren, A. Zhao, e X. Qu, «Electrically pulsatile responsive drug delivery platform for treatment of Alzheimer's disease», *Nano Res.*, vol. 8, fasc. 7, pp. 2400–2414, lug. 2015, doi: 10.1007/s12274-015-0750-x.
[107] C. C. Chen Xiao; Zhang, Heng; Zhang, Qi; Wang, Li; Li, Chenxi; Dai, Beibei; Yang, Jiazhi; Liu, Jian; Sun, Dongping, «Electrically-responsive core-shell hybrid microfibers for controlled drug release and cell culture.», *Acta Biomater.*, vol. 55, fasc. NA, pp. 434–442, 2017, doi: 10.1016/j.actbio.2017.04.005.
[108] C. Boehler *et al.*, «Actively controlled release of Dexamethasone from neural microelectrodes in a chronic in vivo study», *Biomaterials*, vol. 129, pp. 176–187, giu. 2017, doi: 10.1016/j.biomaterials.2017.03.019.

[109] S. E. C. Neumann Christian F. ;. Zare, Richard N., «Electrically controlled drug release using pH-sensitive polymer films.», *Nanoscale*, vol. 10, fasc. 21, pp. 10087–10093, 2018, doi: 10.1039/c8nr02602e.
[110] P. Mostafalu *et al.*, «A Textile Dressing for Temporal and Dosage Controlled Drug Delivery», *Adv. Funct. Mater.*, vol. 27, fasc. 41, 2017, doi: 10.1002/adfm.201702399.
[111] A. G. Johnna S. Temenoff, *Johnna S. Temenoff, Antonios G. Mikos Biomaterials The Intersection Of Biology And Materials Science (2008, Pearson) Libgen.lc*. 2008. Consultato: 16 febbraio 2024. [Online]. Disponibile su: http://archive.org/details/johnna-s.-temenoff-antonios-g.-mikos-biomaterials-the-intersection-of-biology-an
[112] B. D. Ratner, A c. di, *Biomaterials science: an introduction to materials in medicine*, Nachdr. San Diego London: Academic Press, 2002.
[113] K. A. Hosoyama Manuel; McTiernan, Christopher D. ;. Davis, Darryl R. ;. Variola, Fabio; Ruel, Marc; Liang, Wenbin; Suuronen, Erik J. ;. Alarcon, Emilio I., «Nanoengineered Electroconductive Collagen-Based Cardiac Patch for Infarcted Myocardium Repair», *ACS Appl. Mater. Interfaces*, vol. 10, fasc. 51, pp. 44668–44677, 2018, doi: 10.1021/acsami.8b18844.s002.
[114] J.-O. You, M. Rafat, G. J. C. Ye, e D. T. Auguste, «Nanoengineering the Heart: Conductive Scaffolds Enhance Connexin 43 Expression», *Nano Lett.*, vol. 11, fasc. 9, pp. 3643–3648, set. 2011, doi: 10.1021/nl201514a.
[115] K. Baranes, M. Shevach, O. Shefi, e T. Dvir, «Gold Nanoparticle-Decorated Scaffolds Promote Neuronal Differentiation and Maturation», *Nano Lett.*, vol. 16, fasc. 5, pp. 2916–2920, mag. 2016, doi: 10.1021/acs.nanolett.5b04033.
[116] Y. L. Zhao Zuhao; Li, Qiuju; Yang, Longfei; Liu, Hou; Yan, Ruyue; Xiao, Lizhi; Liu, He; Wang, Jingcheng; Yang, Bai; Lin, Quan, «Transparent Conductive Supramolecular Hydrogels with Stimuli-Responsive Properties for On-Demand Dissolvable Diabetic Foot Wound Dressings.», *Macromol. Rapid Commun.*, vol. 41, fasc. 24, pp. 2000441-NA, 2020, doi: 10.1002/marc.202000441.
[117] S. S. Lee Daisuke; Kim, Dongmin; Mori, Mami; Yokota, Tomoyuki; Lee, Hyunjae; Park, Sungjun; Fukuda, Kenjiro; Sekino, Masaki; Matsuura, Katsuhisa; Shimizu, Tatsuya; Someya, Takao, «Ultrasoft electronics to monitor dynamically pulsing cardiomyocytes», *Nat. Nanotechnol.*, vol. 14, fasc. 2, pp. 156–160, 2018, doi: 10.1038/s41565-018-0331-8.
[118] R. P. Carcione Sara; Iacob, Erica; Potrich, Cristina; Lunelli, Lorenzo; Vanzetti, Lia Emauela; Bartali, Ruben; Micheli, Victor; Pepponi, Giancarlo; Terranova, Maria Letizia; Tamburri, Emanuela, «Exploring a new approach for regenerative medicine: Ti-doped polycrystalline diamond layers as bioactive platforms for osteoblast-like cells growth», *Appl. Surf. Sci.*, vol. 540, fasc. 1, pp. 148334-NA, 2021, doi: 10.1016/j.apsusc.2020.148334.
[119] U. Aydemir Sezer, K. Ozturk, B. Aru, G. Yanıkkaya Demirel, S. Sezer, e M. R. Bozkurt, «Zero valent zinc nanoparticles promote neuroglial cell proliferation: A biodegradable and conductive filler candidate for nerve regeneration», *J. Mater. Sci. Mater. Med.*, vol. 28, fasc. 1, 2017, doi: 10.1007/s10856-016-5831-1.
[120] K. L. Mijnendonckx Natalie; Mahillon, Jacques; Silver, Simon; Van Houdt, Rob, «Antimicrobial silver: uses, toxicity and potential for resistance.», *Biometals Int. J. Role Met. Ions Biol. Biochem. Med.*, vol. 26, fasc. 4, pp. 609–621, 2013, doi: 10.1007/s10534-013-9645-z.
[121] S. H. Choi Sang Ihn; Jung, Dongjun; Hwang, Hye Jin; Lim, Chaehong; Bae, Soochan; Park, Ok Kyu; Tschabrunn, Cory M. ;. Lee, Min-Cheol; Bae, Sun Youn; Yu, Ji Woong; Ryu, Ji Ho; Lee, Sang Woo; Park, Kyungpyo; Kang, Peter M. ;. Lee, Won Bo; Nezafat, Reza; Hyeon, Taeghwan; Kim, Dae-Hyeong, «Highly conductive, stretchable and biocompatible Ag–Au core–sheath nanowire composite for wearable and implantable bioelectronics», *Nat. Nanotechnol.*, vol. 13, fasc. 11, pp. 1048–1056, 2018, doi: 10.1038/s41565-018-0226-8.
[122] Y. Zhao *et al.*, «Skin-Inspired Antibacterial Conductive Hydrogels for Epidermal Sensors and Diabetic Foot Wound Dressings», *Adv. Funct. Mater.*, vol. 29, fasc. 31, 2019, doi: 10.1002/adfm.201901474.
[123] Y. Z. Zhang Zhong; Yu, Mengliu; Hsu, Chinyun; Berthiaume, Emily A. ;. Pan, Hsin Chuan; Zhang, Xinli; Stieg, Adam Z. ;. Wu, Benjamin M. ;. Wang, Huiming; Ting, Kang; Soo, Chia,

«Using an Engineered Galvanic Redox System to Generate Positive Surface Potentials that Promote Osteogenic Functions», *ACS Appl. Mater. Interfaces*, vol. 10, fasc. 18, pp. 15449–15460, 2018, doi: 10.1021/acsami.8b02798.

[124] A. del B. Raslan Laura Saenz; Ciriza, Jesús; Pedraz, José Luis, «Graphene oxide and reduced graphene oxide-based scaffolds in regenerative medicine.», *Int. J. Pharm.*, vol. 580, fasc. NA, pp. 119226–119226, 2020, doi: 10.1016/j.ijpharm.2020.119226.

[125] Z. M. ; A. Wright Anne M. ;. Holt, Brian D. ;. Eckhart, Karoline E. ;. Sydlik, Stefanie A., «Functional Graphenic Materials, Graphene Oxide, and Graphene as Scaffolds for Bone Regeneration», *Regen. Eng. Transl. Med.*, vol. 5, fasc. 2, pp. 190–209, 2018, doi: 10.1007/s40883-018-0081-z.

[126] R. M. Kurapati Sourav P. ;. Martín, Cristina; Bepete, George; Vázquez, Ester; Pénicaud, Alain; Fadeel, Bengt; Bianco, Alberto, «Degradation of Single-Layer and Few-Layer Graphene by Neutrophil Myeloperoxidase», *Angew. Chem. Int. Ed Engl.*, vol. 57, fasc. 36, pp. 11722–11727, 2018, doi: 10.1002/anie.201806906.

[127] N. S. Annabi Su Ryon; Tamayol, Ali; Miscuglio, Mario; Bakooshli, Mohsen Afshar; Assmann, Alexander; Mostafalu, Pooria; Sun, Jeong-Yun; Mithieux, Suzanne M. ;. Cheung, Louis; Tang, Xiaowu Shirley; Weiss, Anthony S. ;. Khademhosseini, Ali, «Highly Elastic and Conductive Human-Based Protein Hybrid Hydrogels», *Adv. Mater. Deerfield Beach Fla*, vol. 28, fasc. 1, pp. 40–49, 2015, doi: 10.1002/adma.201503255.

[128] K. L. Zhang Jiashuai; Jin, Jing; Dong, Jian; Li, Lan; Xue, Bin; Wang, Wei; Jiang, Qing; Cao, Yi, «Injectable, anti-inflammatory and conductive hydrogels based on Graphene oxide and Diacerein-terminated four-armed polyethylene glycol for spinal cord injury repair», *Mater. Des.*, vol. 196, fasc. NA, pp. 109092-NA, 2020, doi: 10.1016/j.matdes.2020.109092.

[129] C. L. ; L. Weaver Jaclyn M. ;. Luo, Xiliang; Cui, Xinyan Tracy, «Electrically controlled drug delivery from graphene oxide nanocomposite films.», *ACS Nano*, vol. 8, fasc. 2, pp. 1834–1843, 2014, doi: 10.1021/nn406223e.

[130] Z. Fan *et al.*, «A Novel Wound Dressing Based on Ag/Graphene Polymer Hydrogel: Effectively Kill Bacteria and Accelerate Wound Healing», *Adv. Funct. Mater.*, vol. 24, fasc. 25, pp. 3933–3943, 2014, doi: 10.1002/adfm.201304202.

[131] H. Jo *et al.*, «Electrically conductive graphene/polyacrylamide hydrogels produced by mild chemical reduction for enhanced myoblast growth and differentiation», *Acta Biomater.*, vol. 48, pp. 100–109, gen. 2017, doi: 10.1016/j.actbio.2016.10.035.

[132] R. Ma *et al.*, «Nanocomposite sponges of sodium alginate/graphene oxide/polyvinyl alcohol as potential wound dressing: In vitro and in vivo evaluation», *Compos. Part B Eng.*, vol. 167, pp. 396–405, giu. 2019, doi: 10.1016/j.compositesb.2019.03.006.

[133] A. K. Vashist Ajeet; Vashist, Atul; Sagar, Vidya; Ghosal, Anujit; Gupta, Y. K. ;. Ahmad, Sharif; Nair, Madhavan, «Advances in Carbon Nanotubes-Hydrogel Hybrids in Nanomedicine for Therapeutics.», *Adv. Healthc. Mater.*, vol. 7, fasc. 9, pp. 1701213-NA, 2018, doi: 10.1002/adhm.201701213.

[134] S. Iijima, «Helical microtubules of graphitic carbon», *Nature*, vol. 354, fasc. 6348, pp. 56–58, 1991, doi: 10.1038/354056a0.

[135] S. R. M. Shin Bianca; Miccoli, Beatrice; Li, Yi-Chen; Mostafalu, Pooria; Seo, Jungmok; Mandla, Serena; Enrico, Alessandro; Antona, Silvia; Sabarish, Ram; Zheng, Ting; Pirrami, Lorenzo; Zhang, Kaizhen; Zhang, Yu Shrike; Wan, Kai-Tak; Demarchi, Danilo; Dokmeci, Mehmet R. ;. Khademhosseini, Ali, «Electrically Driven Microengineered Bioinspired Soft Robots.», *Adv. Mater. Deerfield Beach Fla*, vol. 30, fasc. 10, pp. 1704189-NA, 2018, doi: 10.1002/adma.201704189.

[136] D. Elgrabli *et al.*, «Carbon Nanotube Degradation in Macrophages: Live Nanoscale Monitoring and Understanding of Biological Pathway», *ACS Nano*, vol. 9, fasc. 10, pp. 10113–10124, ott. 2015, doi: 10.1021/acsnano.5b03708.

[137] A. Abarrategi *et al.*, «Multiwall carbon nanotube scaffolds for tissue engineering purposes», *Biomaterials*, vol. 29, fasc. 1, pp. 94–102, gen. 2008, doi: 10.1016/j.biomaterials.2007.09.021.

[138] Y. Z. Liang Xin; Hu, Tianli; Han, Yong; Guo, Baolin, «Mussel-inspired, antibacterial, conductive, antioxidant, injectable composite hydrogel wound dressing to promote the

regeneration of infected skin.», *J. Colloid Interface Sci.*, vol. 556, fasc. NA, pp. 514–528, 2019, doi: 10.1016/j.jcis.2019.08.083.
[139] H. N. Hu Yingchun; Mandal, Swadhin K. ;. Montana, Vedrana; Zhao, Bin; Haddon, Robert C. ;. Parpura, Vladimir, «Polyethyleneimine Functionalized Single-Walled Carbon Nanotubes as a Substrate for Neuronal Growth», *J. Phys. Chem. B*, vol. 109, fasc. 10, pp. 4285–4289, 2005, doi: 10.1021/jp0441137.
[140] S. R. Shin *et al.*, «A Bioactive Carbon Nanotube-Based Ink for Printing 2D and 3D Flexible Electronics», *Adv. Mater.*, vol. 28, fasc. 17, pp. 3280–3289, 2016, doi: 10.1002/adma.201506420.
[141] X. G. Liu Matthew N. ;. Park, Sungjo; Miller, A. Lee; Gaihre, Bipin; Li, Linli; Waletzki, Brian E. ;. Terzic, Andre; Yaszemski, Michael J. ;. Lu, Lichun, «3D-printed scaffolds with carbon nanotubes for bone tissue engineering: Fast and homogeneous one-step functionalization.», *Acta Biomater.*, vol. 111, fasc. NA, pp. 129–140, 2020, doi: 10.1016/j.actbio.2020.04.047.
[142] V. C. Martinelli Giada; Toma, Francesca M. ;. Long, Carlin S. ;. Caldwell, John H. ;. Zentilin, Lorena; Giacca, Mauro; Turco, Antonio; Prato, Maurizio; Ballerini, Laura; Mestroni, Luisa, «Carbon nanotubes instruct physiological growth and functionally mature syncytia: nongenetic engineering of cardiac myocytes.», *ACS Nano*, vol. 7, fasc. 7, pp. 5746–5756, 2013, doi: 10.1021/nn4002193.
[143] G. Z. Zhao Xu; Li, Bingcheng; Huang, Guoyou; Xu, Feng; Zhang, Xiaohui, «Solvent-Free Fabrication of Carbon Nanotube/Silk Fibroin Electrospun Matrices for Enhancing Cardiomyocyte Functionalities», *ACS Biomater. Sci. Eng.*, vol. 6, fasc. 3, pp. 1630–1640, 2020, doi: 10.1021/acsbiomaterials.9b01682.
[144] Y. L. Xia Shuang; Nie, Chuanxiong; Zhang, Jianguang; Zhou, Suqiong; Yang, Hua; Li, Mingjun; Li, Wenzhong; Cheng, Chong; Haag, Rainer, «A multivalent polyanion-dispersed carbon nanotube toward highly bioactive nanostructured fibrous stem cell scaffolds», *Appl. Mater. Today*, vol. 16, fasc. NA, pp. 518–528, 2019, doi: 10.1016/j.apmt.2019.07.006.
[145] S. Qian *et al.*, «Chemically revised conducting polymers with inflammation resistance for intimate bioelectronic electrocoupling», *Bioact. Mater.*, vol. 26, pp. 24–51, ago. 2023, doi: 10.1016/j.bioactmat.2023.02.010.
[146] T.-H. K. Le Yukyung; Yoon, Hyeonseok, «Electrical and Electrochemical Properties of Conducting Polymers», *Polymers*, vol. 9, fasc. 12, pp. 150-NA, 2017, doi: 10.3390/polym9040150.
[147] M. S. Vezie *et al.*, «Exploring the origin of high optical absorption in conjugated polymers», *Nat. Mater.*, vol. 15, fasc. 7, Art. fasc. 7, lug. 2016, doi: 10.1038/nmat4645.
[148] M. Jozefowicz, L. T. Yu, G. Belorgey, e R. Buvet, «Conductivité Electronique et Propriétés Chimiques de Polyanilines Oligomères», *J. Polym. Sci. Part C Polym. Symp.*, vol. 16, fasc. 5, pp. 2943–2954, 1967, doi: 10.1002/polc.5070160548.
[149] A. G. ; C. MacDiarmid J. C. ;. Richter, A. F. ;. Epstein, Arthur J., «Polyaniline: a new concept in conducting polymers», *Synth. Met.*, vol. 18, fasc. 1–3, pp. 285–290, 1987, doi: 10.1016/0379-6779(87)90893-9.
[150] M. C. Berggren Xavier; Fabiano, Simone; Jonsson, Magnus P. ;. Simon, Daniel; Stavrinidou, Eleni; Tybrandt, Klas; Zozoulenko, Igor, «Ion Electron-Coupled Functionality in Materials and Devices Based on Conjugated Polymers», *Adv. Mater. Deerfield Beach Fla*, vol. 31, fasc. 22, pp. 1805813-NA, 2019, doi: 10.1002/adma.201805813.
[151] A. H. Savva Rawad K. ;. Cendra, Camila; Surgailis, Jokubas; Hidalgo, Tania C. ;. Wustoni, Shofarul; Sheelamanthula, Rajendar; Chen, Xingxing; Kirkus, Mindaugas; Giovannitti, Alexander; Salleo, Alberto; McCulloch, Iain; Inal, Sahika, «Balancing Ionic and Electronic Conduction for High-Performance Organic Electrochemical Transistors», *Adv. Funct. Mater.*, vol. 30, fasc. 11, pp. 1907657-NA, 2020, doi: 10.1002/adfm.201907657.
[152] P. B. Leleux Jean-Michel; Rivnay, Jonathan; Bénar, Christian; Hervé, Thierry; Chauvel, Patrick; Malliaras, George G., «Conducting polymer electrodes for electroencephalography.», *Adv. Healthc. Mater.*, vol. 3, fasc. 4, pp. 490–493, 2013, doi: 10.1002/adhm.201300311.
[153] Z. Y. Huang Guangfu; Liao, Xiaoming; Gu, Jianwen, «Conducting polypyrrole in tissue engineering applications», *Front. Mater. Sci.*, vol. 8, fasc. 1, pp. 39–45, 2014, doi: 10.1007/s11706-014-0238-8.

[154] H. H. Xu Jeremy M. ;. Yan, Yuhua; Xu, Peihu; Zheng, Hua; Yin, Yixia; Li, Shipu; X. ,. Peter, «Conductive PPY/PDLLA conduit for peripheral nerve regeneration», *Biomaterials*, vol. 35, fasc. 1, pp. 225–235, 2013, doi: 10.1016/j.biomaterials.2013.10.002.
[155] Y. Y. He Genlan; Song, Chen; Li, Chuangkun; Xiong, Weirong; Yu, Lei; Qiu, Xiaozhong; Wang, Leyu, «Mussel-inspired conductive nanofibrous membranes repair myocardial infarction by enhancing cardiac function and revascularization», *Theranostics*, vol. 8, fasc. 18, pp. 5159–5177, 2018, doi: 10.7150/thno.27760.
[156] L. Z. Yan Bingxin; Liu, Xiaohong; Li, Xuan; Zeng, Chao; Shi, Haiyan; Xu, Xiaoxue; Lin, Tong; Dai, Liming; Liu, Yong, «Aligned Nanofibers from Polypyrrole/Graphene as Electrodes for Regeneration of Optic Nerve via Electrical Stimulation», *ACS Appl. Mater. Interfaces*, vol. 8, fasc. 11, pp. 6834–6840, 2016, doi: 10.1021/acsami.5b12843.
[157] M. S. Parchehbaf-Kashani Mohammadmajid; Talkhabi, Mahmood; Sayahpour, Forough Azam; Baharvand, Hossein; Pahlavan, Sara; Rajabi, Sarah, «Design and characterization of an electroconductive scaffold for cardiomyocytes based biomedical assays», *Mater. Sci. Eng. C Mater. Biol. Appl.*, vol. 109, fasc. NA, pp. 110603-NA, 2019, doi: 10.1016/j.msec.2019.110603.
[158] K. M. ; J. Sajesh Rangasamy; Nair, Shantikumar V. ;. Chennazhi, Krishna Prasad, «Biocompatible conducting chitosan/polypyrrole-alginate composite scaffold for bone tissue engineering.», *Int. J. Biol. Macromol.*, vol. 62, fasc. NA, pp. 465–471, 2013, doi: 10.1016/j.ijbiomac.2013.09.028.
[159] L. Zhou *et al.*, «Injectable muscle-adhesive antioxidant conductive photothermal bioactive nanomatrix for efficiently promoting full-thickness skeletal muscle regeneration», *Bioact. Mater.*, vol. 6, fasc. 6, pp. 1605–1617, giu. 2021, doi: 10.1016/j.bioactmat.2020.11.005.
[160] S. S. He Hui-Fang; Wu, Jun; Li, Shu-Hong; Weisel, Richard D. ;. Sung, Hsing-Wen; Jianding, Li; Li, Ren-Ke, «Preservation of conductive propagation after surgical repair of cardiac defects with a bio-engineered conductive patch.», *J. Heart Lung Transplant. Off. Publ. Int. Soc. Heart Transplant.*, vol. 37, fasc. 7, pp. 912–924, 2017, doi: 10.1016/j.healun.2017.12.011.
[161] S. He *et al.*, «The conductive function of biopolymer corrects myocardial scar conduction blockage and resynchronizes contraction to prevent heart failure», *Biomaterials*, vol. 258, p. 120285, nov. 2020, doi: 10.1016/j.biomaterials.2020.120285.
[162] A. C. Mihic Zhi; Wu, Jun; Vlacic, Goran; Miyagi, Yasuo; Li, Shu-Hong; Lu, Sun; Sung, Hsing-Wen; Weisel, Richard D. ;. Li, Ren-Ke, «A Conductive Polymer Hydrogel Supports Cell Electrical Signaling and Improves Cardiac Function After Implantation into Myocardial Infarct.», *Circulation*, vol. 132, fasc. 8, pp. 772–784, 2015, doi: 10.1161/circulationaha.114.014937.
[163] T. Wu *et al.*, «Coadministration of an Adhesive Conductive Hydrogel Patch and an Injectable Hydrogel to Treat Myocardial Infarction», *ACS Appl. Mater. Interfaces*, vol. 12, fasc. 2, pp. 2039–2048, gen. 2020, doi: 10.1021/acsami.9b17907.
[164] L. Wang *et al.*, «Mussel-Inspired Conductive Cryogel as Cardiac Tissue Patch to Repair Myocardial Infarction by Migration of Conductive Nanoparticles», *Adv. Funct. Mater.*, vol. 26, fasc. 24, pp. 4293–4305, 2016, doi: 10.1002/adfm.201505372.
[165] T. H. Qazi, R. Rai, e A. R. Boccaccini, «Tissue engineering of electrically responsive tissues using polyaniline based polymers: A review», *Biomaterials*, vol. 35, fasc. 33, pp. 9068–9086, nov. 2014, doi: 10.1016/j.biomaterials.2014.07.020.
[166] «Impulse propagation and muscle activation in long maximal voluntary contractions | Journal of Applied Physiology». Consultato: 14 ottobre 2023. [Online]. Disponibile su: https://journals-physiology-org.ezproxy.biblio.polito.it/doi/abs/10.1152/jappl.1989.67.5.1835
[167] J. He, Y. Liang, M. Shi, e B. Guo, «Anti-oxidant electroactive and antibacterial nanofibrous wound dressings based on poly(ε-caprolactone)/quaternized chitosan-graft-polyaniline for full-thickness skin wound healing», *Chem. Eng. J.*, vol. 385, p. 123464, apr. 2020, doi: 10.1016/j.cej.2019.123464.
[168] B. Guo, J. Qu, X. Zhao, e M. Zhang, «Degradable conductive self-healing hydrogels based on dextran-graft-tetraaniline and N-carboxyethyl chitosan as injectable carriers for myoblast cell therapy and muscle regeneration», *Acta Biomater.*, vol. 84, pp. 180–193, gen. 2019, doi: 10.1016/j.actbio.2018.12.008.

[169] G. Thrivikraman, G. Madras, e B. Basu, «Intermittent electrical stimuli for guidance of human mesenchymal stem cell lineage commitment towards neural-like cells on electroconductive substrates», *Biomaterials*, vol. 35, fasc. 24, pp. 6219–6235, ago. 2014, doi: 10.1016/j.biomaterials.2014.04.018.
[170] M. Kapnisi *et al.*, «Auxetic Cardiac Patches with Tunable Mechanical and Conductive Properties toward Treating Myocardial Infarction», *Adv. Funct. Mater.*, vol. 28, fasc. 21, 2018, doi: 10.1002/adfm.201800618.
[171] B. K. S. Shrestha Sita; Baral, Ek Raj; Lee, Ji Yeon; Kim, Beom-Su; Park, Chan Hee; Kim, Cheol Sang, «π-Conjugated polyaniline-assisted flexible titania nanotubes with controlled surface morphology as regenerative medicine in nerve cell growth», *Chem. Eng. J.*, vol. 360, fasc. NA, pp. 701–713, 2019, doi: 10.1016/j.cej.2018.12.027.
[172] L. W. Wang Yaobin; Hu, Tianli; Guo, Baolin; X. ,. Peter, «Electrospun conductive nanofibrous scaffolds for engineering cardiac tissue and 3D bioactuators.», *Acta Biomater.*, vol. 59, fasc. NA, pp. 68–81, 2017, doi: 10.1016/j.actbio.2017.06.036.
[173] P. G. Chakraborty Tom; Adadi, Nofar; Yadid, Moran; Brosh, Tamar; Adler-Abramovich, Lihi; Dvir, Tal; Gazit, Ehud, «A Self-Healing, All-Organic, Conducting, Composite Peptide Hydrogel as Pressure Sensor and Electrogenic Cell Soft Substrate.», *ACS Nano*, vol. 13, fasc. 1, pp. 163–175, 2018, doi: 10.1021/acsnano.8b05067.
[174] A. J. Fraczek-Szczypta Danuta; Ciepiela, Filip; Grzonka, Justyna, «Graphene oxide-conductive polymer nanocomposite coatings obtained by the EPD method as substrates for neurite outgrowth», *Diam. Relat. Mater.*, vol. 102, fasc. NA, pp. 107663-NA, 2020, doi: 10.1016/j.diamond.2019.107663.
[175] S. Shrestha, B. K. Shrestha, O. K. Joong, C. H. Park, e C. S. Kim, «Para-substituted sulfonic acid-doped protonated emeraldine salt nanobuds: a potent neural interface targeting PC12 cell interactions and promotes neuronal cell differentiation», *Biomater. Sci.*, vol. 9, fasc. 5, pp. 1691–1704, mar. 2021, doi: 10.1039/D0BM01034K.
[176] L. V. ; L. Kayser Darren J., «Stretchable Conductive Polymers and Composites Based on PEDOT and PEDOT:PSS.», *Adv. Mater. Deerfield Beach Fla*, vol. 31, fasc. 10, pp. 1806133-NA, 2019, doi: 10.1002/adma.201806133.
[177] D. Mantione, I. Del Agua, A. Sanchez-Sanchez, e D. Mecerreyes, «Poly(3,4-ethylenedioxythiophene) (PEDOT) Derivatives: Innovative Conductive Polymers for Bioelectronics», *Polymers*, vol. 9, fasc. 8, Art. fasc. 8, ago. 2017, doi: 10.3390/polym9080354.
[178] X. Y. Gu Chunlei; Liu, Ying; Hsing, I.-Ming, «16-Channel Organic Electrochemical Transistor Array for In Vitro Conduction Mapping of Cardiac Action Potential.», *Adv. Healthc. Mater.*, vol. 5, fasc. 18, pp. 2345–2351, 2016, doi: 10.1002/adhm.201600189.
[179] Y. L. Liu Jia; Chen, Shucheng; Lei, Ting; Kim, Yeongin; Niu, Simiao; Wang, Huiliang; Wang, Xiao; Foudeh, Amir M. ;. Tok, Jeffrey B. H. ;. Bao, Zhenan, «Soft and elastic hydrogel-based microelectronics for localized low-voltage neuromodulation», *Nat. Biomed. Eng.*, vol. 3, fasc. 1, pp. 58–68, 2019, doi: 10.1038/s41551-018-0335-6.
[180] H. Y. P. Gong Junggeon; Kim, Wondo; Kim, Jongbaeg; Lee, Jae Young; Koh, Won Gun, «A Novel Conductive and Micropatterned PEG-Based Hydrogel Enabling the Topographical and Electrical Stimulation of Myoblasts.», *ACS Appl. Mater. Interfaces*, vol. 11, fasc. 51, pp. 47695–47706, 2019, doi: 10.1021/acsami.9b16005.
[181] Z. Jia *et al.*, «Bioinspired Conductive Silk Microfiber Integrated Bioelectronic for Diagnosis and Wound Healing in Diabetes», *Adv. Funct. Mater.*, vol. 31, fasc. 19, 2021, doi: 10.1002/adfm.202010461.
[182] C. Tondera *et al.*, «Highly Conductive, Stretchable, and Cell-Adhesive Hydrogel by Nanoclay Doping», *Small*, vol. 15, fasc. 27, p. 1901406, 2019, doi: 10.1002/smll.201901406.
[183] A. M. D. ; B. Wan Daniel J. ;. Gumus, Abdurrahman; Fischbach, Claudia; Malliaras, George G., «Electrical control of cell density gradients on a conducting polymer surface», *Chem. Commun. Camb. Engl.*, vol. NA, fasc. 35, pp. 5278–5280, 2009, doi: 10.1039/b911130a.
[184] P. Jolly, A. Miodek, D. K. Yang, L. C. Chen, M. Lloyd, e P. Estrela, «Electro-engineered polymeric films for the development of sensitive aptasensors for prostate cancer marker detection», *ACS Sens.*, vol. 1, fasc. 11, pp. 1308–1314, nov. 2016, doi: 10.1021/acssensors.6b00443.

[185] L. S. S. Kumar, X. Wang, J. Hagen, R. Naik, I. Papautsky, e J. Heikenfeld, «Label free nano-aptasensor for interleukin-6 in protein-dilute bio fluids such as sweat», *Anal. Methods*, vol. 8, fasc. 17, pp. 3440–3444, apr. 2016, doi: 10.1039/C6AY00331A.
[186] M. G. Marzocchi Isacco; Calienni, Maria; Zironi, Isabella; Scavetta, Erika; Castellani, Gastone; Fraboni, Beatrice, «Physical and Electrochemical Properties of PEDOT:PSS as a Tool for Controlling Cell Growth.», *ACS Appl. Mater. Interfaces*, vol. 7, fasc. 32, pp. 17993–18003, 2015, doi: 10.1021/acsami.5b04768.
[187] S. G. Baek Rylie A. ;. Poole-Warren, Laura A., «The biological and electrical trade-offs related to the thickness of conducting polymers for neural applications», *Acta Biomater.*, vol. 10, fasc. 7, pp. 3048–3058, 2014, doi: 10.1016/j.actbio.2014.04.004.
[188] A. V. ; W. Volkov Kosala; Mitraka, Evangelia; Ail, Ujwala; Zhao, Dan; Tybrandt, Klas; Andreasen, Jens Wenzel; Berggren, Magnus; Crispin, Xavier; Zozoulenko, Igor, «Understanding the Capacitance of PEDOT:PSS», *Adv. Funct. Mater.*, vol. 27, fasc. 28, pp. 1700329-NA, 2017, doi: 10.1002/adfm.201700329.
[189] L. S. C. Pingree, B. A. MacLeod, e D. S. Ginger, «The Changing Face of PEDOT:PSS Films: Substrate, Bias, and Processing Effects on Vertical Charge Transport», *J. Phys. Chem. C*, vol. 112, fasc. 21, pp. 7922–7927, mag. 2008, doi: 10.1021/jp711838h.
[190] Y. C. Xu Meiying; Patsis, Panagiotis A. ;. Günther, Markus; Yang, Xuegeng; Eckert, Kerstin; Zhang, Yixin, «Reversibly Assembled Electroconductive Hydrogel via a Host-Guest Interaction for 3D Cell Culture.», *ACS Appl. Mater. Interfaces*, vol. 11, fasc. 8, pp. 7715–7724, 2019, doi: 10.1021/acsami.8b19482.
[191] B. Y. Yang Fanglian; Ye, Lei; Hao, Tong; Zhang, Yabin; Zhang, Lei; Dong, Dianyu; Fang, Wancai; Wang, Yan; Zhang, Xiaoyang; Wang, Changyong; Li, Junjie, «A conductive PEDOT/alginate porous scaffold as a platform to modulate the biological behaviors of brown adipose-derived stem cells», *Biomater. Sci.*, vol. 8, fasc. 11, pp. 3173–3185, 2020, doi: 10.1039/c9bm02012h.
[192] R. A. ; L. Green Nigel H. ;. Poole-Warren, Laura A., «Impact of co-incorporating laminin peptide dopants and neurotrophic growth factors on conducting polymer properties», *Acta Biomater.*, vol. 6, fasc. 1, pp. 63–71, 2009, doi: 10.1016/j.actbio.2009.06.030.
[193] A. Herland *et al.*, «Electrochemical Control of Growth Factor Presentation To Steer Neural Stem Cell Differentiation», *Angew. Chem. Int. Ed.*, vol. 50, fasc. 52, pp. 12529–12533, 2011, doi: 10.1002/anie.201103728.
[194] T. N. Teshima Hiroshi; Kasai, Nahoko; Sasaki, Satoshi; Tanaka, Aya; Tsukada, Shingo; Sumitomo, Koji, «Mobile Silk Fibroin Electrode for Manipulation and Electrical Stimulation of Adherent Cells», *Adv. Funct. Mater.*, vol. 26, fasc. 45, pp. 8185–8193, 2016, doi: 10.1002/adfm.201603302.
[195] S. G. Wang Shui; Wang, Jing; Liu, Hailong; Liu, Tianqing; Ma, Xuehu; Cui, Zhanfeng, «Fabrication and characterization of conductive poly (3,4-ethylenedioxythiophene) doped with hyaluronic acid/poly (l-lactic acid) composite film for biomedical application.», *J. Biosci. Bioeng.*, vol. 123, fasc. 1, pp. 116–125, 2016, doi: 10.1016/j.jbiosc.2016.07.010.
[196] E. A. ; G. Cuttaz Josef; Vallejo-Giraldo, Catalina; Aregueta-Robles, Ulises A. ;. Lovell, Nigel H. ;. Ghezzi, Diego; Green, Rylie A., «Conductive elastomer composites for fully polymeric, flexible bioelectronics», *Biomater. Sci.*, vol. 7, fasc. 4, pp. 1372–1385, 2019, doi: 10.1039/c8bm01235k.
[197] A. R. Spencer, A. Primbetova, A. N. Koppes, R. A. Koppes, H. Fenniri, e N. Annabi, «Electroconductive Gelatin Methacryloyl-PEDOT:PSS Composite Hydrogels: Design, Synthesis, and Properties», *ACS Biomater. Sci. Eng.*, vol. 4, fasc. 5, pp. 1558–1567, mag. 2018, doi: 10.1021/acsbiomaterials.8b00135.
[198] D. Testore, A. Zoso, G. Kortaberria, M. Sangermano, e V. Chiono, «Electroconductive Photo-Curable PEGDA-Gelatin/PEDOT:PSS Hydrogels for Prospective Cardiac Tissue Engineering Application», *Front. Bioeng. Biotechnol.*, vol. 10, p. 897575, 2022, doi: 10.3389/fbioe.2022.897575.
[199] D. N. Heo, S.-J. Lee, R. Timsina, X. Qiu, N. J. Castro, e L. G. Zhang, «Development of 3D printable conductive hydrogel with crystallized PEDOT:PSS for neural tissue engineering», *Mater. Sci. Eng. C*, vol. 99, pp. 582–590, giu. 2019, doi: 10.1016/j.msec.2019.02.008.

[200] S. Li, L. Wang, W. Zheng, G. Yang, e X. Jiang, «Rapid Fabrication of Self-Healing, Conductive, and Injectable Gel as Dressings for Healing Wounds in Stretchable Parts of the Body», *Adv. Funct. Mater.*, vol. 30, fasc. 31, 2020, doi: 10.1002/adfm.202002370.
[201] Q. Lei, J. He, e D. Li, «Electrohydrodynamic 3D printing of layer-specifically oriented, multiscale conductive scaffolds for cardiac tissue engineering», *Nanoscale*, vol. 11, fasc. 32, pp. 15195–15205, ago. 2019, doi: 10.1039/C9NR04989D.
[202] N.-C. Tsai, J.-W. She, J.-G. Wu, P. Chen, Y.-S. Hsiao, e J. Yu, «Poly(3,4-ethylenedioxythiophene) Polymer Composite Bioelectrodes with Designed Chemical and Topographical Cues to Manipulate the Behavior of PC12 Neuronal Cells», *Adv. Mater. Interfaces*, vol. 6, fasc. 5, 2019, doi: 10.1002/admi.201801576.
[203] A. Babaie *et al.*, «Synergistic effects of conductive PVA/PEDOT electrospun scaffolds and electrical stimulation for more effective neural tissue engineering», *Eur. Polym. J.*, vol. 140, p. 110051, nov. 2020, doi: 10.1016/j.eurpolymj.2020.110051.
[204] M. R. Yazdimamaghani Mehdi; Mozafari, Masoud; Vashaee, Daryoosh; Kotturi, Hari; Tayebi, Lobat, «Biomineralization and biocompatibility studies of bone conductive scaffolds containing poly(3,4-ethylenedioxythiophene):poly(4-styrene sulfonate) (PEDOT:PSS)», *J. Mater. Sci. Mater. Med.*, vol. 26, fasc. 12, pp. 274–274, 2015, doi: 10.1007/s10856-015-5599-8.
[205] A. Shahini *et al.*, «3D conductive nanocomposite scaffold for bone tissue engineering», *Int. J. Nanomedicine*, vol. 9, pp. 167–181, 2014, doi: 10.2147/IJN.S54668.
[206] Y.-S. L. Hsiao Yan Hao; Chen, Huan Lin; Chen, Peilin; Chen, Fang-Chung, «Organic Photovoltaics and Bioelectrodes Providing Electrical Stimulation for PC12 Cell Differentiation and Neurite Outgrowth.», *ACS Appl. Mater. Interfaces*, vol. 8, fasc. 14, pp. 9275–9284, 2016, doi: 10.1021/acsami.6b00916.
[207] Y.-S. L. Hsiao Chih-Ling; Liao, I.-Hsiang; Chen, Fang-Jung; Liu, Chun-Ting; Tseng, Hsueh-Sheng; Yu, Jiashing, «Facile Fabrication of Microwrinkled Poly(3,4-Ethylenedioxythiophene) Films that Promote Neural Differentiation under Electrical Stimulation», *ACS Appl. Bio Mater.*, vol. 4, fasc. 3, pp. 2354–2362, 2021, doi: 10.1021/acsabm.0c01204.
[208] X. Gu, S. Y. Yeung, A. Chadda, E. N. Y. Poon, K. R. Boheler, e I.-M. Hsing, «Organic Electrochemical Transistor Arrays for In Vitro Electrophysiology Monitoring of 2D and 3D Cardiac Tissues», *Adv. Biosyst.*, vol. 3, fasc. 2, p. e1800248, feb. 2019, doi: 10.1002/adbi.201800248.
[209] S. Zips *et al.*, «Fully Printed µ-Needle Electrode Array from Conductive Polymer Ink for Bioelectronic Applications», *ACS Appl. Mater. Interfaces*, vol. 11, fasc. 36, pp. 32778–32786, set. 2019, doi: 10.1021/acsami.9b11774.
[210] L. Du *et al.*, «Design of high conductive and piezoelectric poly (3,4-ethylenedioxythiophene)/chitosan nanofibers for enhancing cellular electrical stimulation», *J. Colloid Interface Sci.*, vol. 559, pp. 65–75, feb. 2020, doi: 10.1016/j.jcis.2019.10.003.
[211] Y. Z. Wang Yanping; Zhang, Zhongyang; Su, Yingchun; Wang, Zegao; Dong, Mingdong; Chen, Menglin, «An injectable high-conductive bimaterial scaffold for neural stimulation.», *Colloids Surf. B Biointerfaces*, vol. 195, fasc. NA, pp. 111210-NA, 2020, doi: 10.1016/j.colsurfb.2020.111210.
[212] X. D. Zhao Ruonan; Guo, Baolin; X. ,. Peter, «Dopamine-Incorporated Dual Bioactive Electroactive Shape Memory Polyurethane Elastomers with Physiological Shape Recovery Temperature, High Stretchability, and Enhanced C2C12 Myogenic Differentiation.», *ACS Appl. Mater. Interfaces*, vol. 9, fasc. 35, pp. 29595–29611, 2017, doi: 10.1021/acsami.7b10583.
[213] T. Hu *et al.*, «Micropatterned, electroactive, and biodegradable poly(glycerol sebacate)-aniline trimer elastomer for cardiac tissue engineering», *Chem. Eng. J.*, vol. 366, pp. 208–222, giu. 2019, doi: 10.1016/j.cej.2019.02.072.
[214] R. Dong, X. Zhao, B. Guo, e P. X. Ma, «Biocompatible Elastic Conductive Films Significantly Enhanced Myogenic Differentiation of Myoblast for Skeletal Muscle Regeneration», *Biomacromolecules*, vol. 18, fasc. 9, pp. 2808–2819, set. 2017, doi: 10.1021/acs.biomac.7b00749.
[215] I. D. Ozsoy Askin; Mimaroglu, Abdullah; Unal, Huseyin; Demir, Zafer, «The Influence of Micro- and Nano-Filler Content on the Mechanical Properties of Epoxy Composites», *Stroj. Vestn. - J. Mech. Eng.*, vol. 61, fasc. 11, pp. 601–609, 2015, doi: 10.5545/sv-jme.2015.2632.

[216] Z. L. Zhou Xifeng; Wu, Wei; Park, Sungjo; Miller, A. Lee; Terzic, Andre; Lu, Lichun, «Effective nerve cell modulation by electrical stimulation of carbon nanotube embedded conductive polymeric scaffolds.», *Biomater. Sci.*, vol. 6, fasc. 9, pp. 2375–2385, 2018, doi: 10.1039/c8bm00553b.
[217] R. V. Bellamkonda, «Peripheral nerve regeneration: An opinion on channels, scaffolds and anisotropy», *Biomaterials*, vol. 27, fasc. 19, pp. 3515–3518, lug. 2006, doi: 10.1016/j.biomaterials.2006.02.030.
[218] G. Zhao *et al.*, «Reduced graphene oxide functionalized nanofibrous silk fibroin matrices for engineering excitable tissues», *NPG Asia Mater.*, vol. 10, fasc. 10, Art. fasc. 10, ott. 2018, doi: 10.1038/s41427-018-0092-8.
[219] C. E. ; S. Schmidt Venkatram R. ;. Vacanti, Joseph P. ;. Langer, Robert, «STIMULATION OF NEURITE OUTGROWTH USING AN ELECTRICALLY CONDUCTING POLYMER», *Proc. Natl. Acad. Sci. U. S. A.*, vol. 94, fasc. 17, pp. 8948–8953, 1997, doi: 10.1073/pnas.94.17.8948.
[220] C. P. Gabriel A; Grant, E. H., «Electrical conductivity of tissue at frequencies below 1 MHz.», *Phys. Med. Biol.*, vol. 54, fasc. 16, pp. 4863–4878, 2009, doi: 10.1088/0031-9155/54/16/002.
[221] A. P. ; S. Mazzoleni Betty F. ;. Kahler, R. L., «Conductivity values of tissue culture medium from 20°C to 40°C», *Bioelectromagnetics*, vol. 7, fasc. 1, pp. 95–99, 1986, doi: 10.1002/bem.2250070111.
[222] S. Gribi, S. du Bois de Dunilac, D. Ghezzi, e S. P. Lacour, «A microfabricated nerve-on-a-chip platform for rapid assessment of neural conduction in explanted peripheral nerve fibers», *Nat. Commun.*, vol. 9, fasc. 1, 2018, doi: 10.1038/s41467-018-06895-7.
[223] A. J. Ryan *et al.*, «Electroconductive Biohybrid Collagen/Pristine Graphene Composite Biomaterials with Enhanced Biological Activity», *Adv. Mater.*, vol. 30, fasc. 15, p. 1706442, 2018, doi: 10.1002/adma.201706442.
[224] Y. G. Du Juan; Li, Yannan; X. ,. Peter; Lei, Bo, «Biomimetic elastomeric, conductive and biodegradable polycitrate-based nanocomposites for guiding myogenic differentiation and skeletal muscle regeneration.», *Biomaterials*, vol. 157, fasc. NA, pp. 40–50, 2017, doi: 10.1016/j.biomaterials.2017.12.005.
[225] H. Kai *et al.*, «Accelerated Wound Healing on Skin by Electrical Stimulation with a Bioelectric Plaster», *Adv. Healthc. Mater.*, vol. 6, fasc. 22, 2017, doi: 10.1002/adhm.201700465.
[226] H. T. M. ; S. Nguyen Shawn A. ;. Wei, Claudia; Chow, Jacqueline K. ;. Nguyen, Alvin; Coursen, Jeff; Luebben, Silvia; Chang, Emily; Ross, Robert; Schmidt, Christine E., «Electric field stimulation through a biodegradable polypyrrole-co-polycaprolactone substrate enhances neural cell growth.», *J. Biomed. Mater. Res. A*, vol. 102, fasc. 8, pp. 2554–2564, 2013, doi: 10.1002/jbm.a.34925.
[227] S. F. Peng Pei; Wu, Ping; Huang, Wei; Yang, Youwen; Guo, Wang; Gao, Chengde; Shuai, Cijun, «Graphene oxide as an interface phase between polyetheretherketone and hydroxyapatite for tissue engineering scaffolds.», *Sci. Rep.*, vol. 7, fasc. 1, pp. 46604–46604, 2017, doi: 10.1038/srep46604.
[228] K. T. Zhou George Anthony; Bernard, Claude C. A. ;. Nisbet, David R. ;. Finkelstein, David; Li, Dan; Forsythe, John S., «Method to impart electro- and biofunctionality to neural scaffolds using graphene-polyelectrolyte multilayers.», *ACS Appl. Mater. Interfaces*, vol. 4, fasc. 9, pp. 4524–4531, 2012, doi: 10.1021/am3007565.
[229] K. L. Elias, R. L. Price, e T. J. Webster, «Enhanced functions of osteoblasts on nanometer diameter carbon fibers», *Biomaterials*, vol. 23, fasc. 15, pp. 3279–3287, ago. 2002, doi: 10.1016/S0142-9612(02)00087-X.
[230] Y. L. Sun Xifeng; George, Matthew N. ;. Park, Sungjo; Gaihre, Bipin; Terzic, Andre; Lu, Lichun, «Enhanced nerve cell proliferation and differentiation on electrically conductive scaffolds embedded with graphene and carbon nanotubes.», *J. Biomed. Mater. Res. A*, vol. 109, fasc. 2, pp. 193–206, 2020, doi: 10.1002/jbm.a.37016.
[231] Q. Wang, M. Wu, X. Xu, C. Ding, J. Luo, e J. Li, «Direct Current Stimulation for Improved Osteogenesis of MC3T3 Cells Using Mineralized Conductive Polyaniline», *ACS Biomater. Sci. Eng.*, vol. 7, fasc. 3, pp. 852–861, mar. 2021, doi: 10.1021/acsbiomaterials.9b01821.

[232] K. L. Yang Jaehong; Lee, Jong Seung; Kim, Dayeong; Chang, Gyeong Eon; Seo, Jungmok; Cheong, Eunji; Lee, Taeyoon; Cho, Seung Woo, «Graphene Oxide Hierarchical Patterns for the Derivation of Electrophysiologically Functional Neuron-like Cells from Human Neural Stem Cells.», *ACS Appl. Mater. Interfaces*, vol. 8, fasc. 28, pp. 17763–17774, 2016, doi: 10.1021/acsami.6b01804.
[233] K. E. Eckhart, B. D. Holt, M. G. Laurencin, e S. A. Sydlik, «Covalent conjugation of bioactive peptides to graphene oxide for biomedical applications», *Biomater. Sci.*, vol. 7, fasc. 9, pp. 3876–3885, ago. 2019, doi: 10.1039/C9BM00867E.
[234] M. S. Tang Qin; Li, Ning; Jiang, Ziyun; Huang, Rong; Cheng, Guosheng, «Enhancement of electrical signaling in neural networks on graphene films», *Biomaterials*, vol. 34, fasc. 27, pp. 6402–6411, 2013, doi: 10.1016/j.biomaterials.2013.05.024.
[235] V. K. Kuzmenko Erdem; Pernevik, Elin; Enoksson, Peter; Gatenholm, Paul, «Tailor-made conductive inks from cellulose nanofibrils for 3D printing of neural guidelines.», *Carbohydr. Polym.*, vol. 189, fasc. NA, pp. 22–30, 2018, doi: 10.1016/j.carbpol.2018.01.097.
[236] A. R. ; M. Harris Paul J. ;. Kapsa, Robert M. I. ;. Clark, Graeme M. ;. Paolini, Antonio G. ;. Wallace, Gordon G., «Correlation of the impedance and effective electrode area of doped PEDOT modified electrodes for brain–machine interfaces», *The Analyst*, vol. 140, fasc. 9, pp. 3164–3174, 2015, doi: 10.1039/c4an02362e.
[237] I. Sahalianov, S. K. Singh, K. Tybrandt, M. Berggren, e I. Zozoulenko, «The intrinsic volumetric capacitance of conducting polymers: pseudo-capacitors or double-layer supercapacitors?», *RSC Adv.*, vol. 9, fasc. 72, pp. 42498–42508, dic. 2019, doi: 10.1039/C9RA10250G.
[238] A. A. Tamayol Mohsen; Annabi, Nasim; Paul, Arghya; Khademhosseini, Ali; Juncker, David, «Fiber-based tissue engineering: Progress, challenges, and opportunities», *Biotechnol. Adv.*, vol. 31, fasc. 5, pp. 669–687, 2012, doi: 10.1016/j.biotechadv.2012.11.007.
[239] I. H. Jun Hyung-Seop; Edwards, James R. ;. Jeon, Hojeong, «Electrospun Fibrous Scaffolds for Tissue Engineering: Viewpoints on Architecture and Fabrication.», *Int. J. Mol. Sci.*, vol. 19, fasc. 3, pp. 745-NA, 2018, doi: 10.3390/ijms19030745.
[240] Y. L. Ding Wei; Zhang, Feng; Liu, Zehua; Ezazi, Nazanin Zanjanizadeh; Liu, Dongfei; Santos, Hélder A., «Electrospun Fibrous Architectures for Drug Delivery, Tissue Engineering and Cancer Therapy», *Adv. Funct. Mater.*, vol. 29, fasc. 2, pp. 1802852-NA, 2018, doi: 10.1002/adfm.201802852.
[241] A. S. Timin *et al.*, «Multifunctional Scaffolds with Improved Antimicrobial Properties and Osteogenicity Based on Piezoelectric Electrospun Fibers Decorated with Bioactive Composite Microcapsules», *ACS Appl. Mater. Interfaces*, vol. 10, fasc. 41, pp. 34849–34868, ott. 2018, doi: 10.1021/acsami.8b09810.
[242] R. Feiner, S. Fleischer, A. Shapira, O. Kalish, e T. Dvir, «Multifunctional degradable electronic scaffolds for cardiac tissue engineering», *J. Controlled Release*, vol. 281, pp. 189–195, lug. 2018, doi: 10.1016/j.jconrel.2018.05.023.
[243] A. C.-P. Gelmi Artur; de Muinck, Ebo; Los, Marek; Rafat, Mehrdad; Jager, Edwin, «Direct Mechanical Stimulation of Stem Cells: A Beating Electromechanically Active Scaffold for Cardiac Tissue Engineering.», *Adv. Healthc. Mater.*, vol. 5, fasc. 12, pp. 1471–1480, 2016, doi: 10.1002/adhm.201600307.
[244] B. Sun *et al.*, «Polypyrrole-coated poly(L-lactic acid-co-ε-caprolactone)/silk fibroin nanofibrous membranes promoting neural cell proliferation and differentiation with electrical stimulation», *J. Mater. Chem. B*, vol. 4, fasc. 41, pp. 6670–6679, ott. 2016, doi: 10.1039/C6TB01710J.
[245] N. A. E. Aval Rahmatollah; Valiani, Ali; Kharaziha, Mahshid; Karimipour, Mohammad; Rahbarghazi, Reza, «Nano-featured poly (lactide-co-glycolide)-graphene microribbons as a promising substrate for nerve tissue engineering», *Compos. Part B Eng.*, vol. 173, fasc. NA, pp. 106863-NA, 2019, doi: 10.1016/j.compositesb.2019.05.074.
[246] Y. Z. Zhang Zhongyang; Wang, Yuting; Su, Yingchun; Chen, Menglin, «3D myotube guidance on hierarchically organized anisotropic and conductive fibers for skeletal muscle tissue engineering.», *Mater. Sci. Eng. C Mater. Biol. Appl.*, vol. 116, fasc. NA, pp. 111070-NA, 2020, doi: 10.1016/j.msec.2020.111070.

[247] X. Liu *et al.*, «Two-Dimensional Black Phosphorus and Graphene Oxide Nanosheets Synergistically Enhance Cell Proliferation and Osteogenesis on 3D Printed Scaffolds», *ACS Appl. Mater. Interfaces*, vol. 11, fasc. 26, pp. 23558–23572, lug. 2019, doi: 10.1021/acsami.9b04121.
[248] L. Li, M. Yu, P. X. Ma, e B. Guo, «Electroactive degradable copolymers enhancing osteogenic differentiation from bone marrow derived mesenchymal stem cells», *J. Mater. Chem. B*, vol. 4, fasc. 3, pp. 471–481, gen. 2016, doi: 10.1039/C5TB01899D.
[249] J. Pelto *et al.*, «Novel Polypyrrole-Coated Polylactide Scaffolds Enhance Adipose Stem Cell Proliferation and Early Osteogenic Differentiation», *Tissue Eng. Part A*, vol. 19, fasc. 7–8, pp. 882–892, apr. 2013, doi: 10.1089/ten.tea.2012.0111.
[250] L. Fan, C. Feng, W. Zhao, L. Qian, Y. Wang, e Y. Li, «Directional Neurite Outgrowth on Superaligned Carbon Nanotube Yarn Patterned Substrate», *Nano Lett.*, vol. 12, fasc. 7, pp. 3668–3673, lug. 2012, doi: 10.1021/nl301428w.
[251] Y.-J. W. Huang Hsi-Chin; Tai, Nyan-Hwa; Wang, Tzu-Wei, «Carbon Nanotube Rope with Electrical Stimulation Promotes the Differentiation and Maturity of Neural Stem Cells», *Small Weinh. Bergstr. Ger.*, vol. 8, fasc. 18, pp. 2869–2877, 2012, doi: 10.1002/smll.201200715.
[252] G. W. Ye Zubiao; Wen, Feng; Song, Xiaoping; Wang, Leyu; Li, Chuangkun; He, Yutong; Prakash, Sugandha; Qiu, Xiaozhong, «Mussel-inspired conductive Ti2C-cryogel promotes functional maturation of cardiomyocytes and enhances repair of myocardial infarction.», *Theranostics*, vol. 10, fasc. 5, pp. 2047–2066, 2020, doi: 10.7150/thno.38876.
[253] X. Zhao, B. Guo, H. Wu, Y. Liang, e P. X. Ma, «Injectable antibacterial conductive nanocomposite cryogels with rapid shape recovery for noncompressible hemorrhage and wound healing», *Nat. Commun.*, vol. 9, fasc. 1, 2018, doi: 10.1038/s41467-018-04998-9.
[254] F. F.-C. Velasco-Mallorquí Juan M. ;. Neves, Luisa; Ramón-Azcón, Javier, «New volumetric CNT-doped gelatin–cellulose scaffolds for skeletal muscle tissue engineering», *Nanoscale Adv.*, vol. 2, fasc. 7, pp. 2885–2896, 2020, doi: 10.1039/d0na00268b.
[255] J. Zhang, M. Li, E.-T. Kang, e K. G. Neoh, «Electrical stimulation of adipose-derived mesenchymal stem cells in conductive scaffolds and the roles of voltage-gated ion channels», *Acta Biomater.*, vol. 32, pp. 46–56, mar. 2016, doi: 10.1016/j.actbio.2015.12.024.
[256] Q. L. Yao Haixiao; Lin, Xin; Ma, Liwei; Zheng, Xiao; Liu, Yu; Huang, Pingping; Yu, Shanshan; Zhang, Wenjing; Lin, Mimi; Dai, Liming; Liu, Yong, «3D Interpenetrated Graphene Foam/58S Bioactive Glass Scaffolds for Electrical-Stimulation-Assisted Differentiation of Rabbit Mesenchymal Stem Cells to Enhance Bone Regeneration.», *J. Biomed. Nanotechnol.*, vol. 15, fasc. 3, pp. 602–611, 2019, doi: 10.1166/jbn.2019.2703.
[257] Y. L. Chen Yi; Liu, Jie; Yang, Jinrui; Jia, Naixin; Zhu, Chuhong; Zhang, Jiaping, «Optimizing microenvironment by integrating negative pressure and exogenous electric fields via a flexible porous conductive dressing to accelerate wound healing.», *Biomater. Sci.*, vol. 9, fasc. 1, pp. 238–251, 2021, doi: 10.1039/d0bm01172j.
[258] Y. Qian *et al.*, «3D Fabrication with Integration Molding of a Graphene Oxide/Polycaprolactone Nanoscaffold for Neurite Regeneration and Angiogenesis», *Adv. Sci.*, vol. 5, fasc. 4, 2018, doi: 10.1002/advs.201700499.
[259] Y.-W. K. Cho Da-Seul; Suhito, Intan Rosalina; Han, Dong Keun; Lee, Taek; Kim, Tae-Hyung, «Enhancing Neurogenesis of Neural Stem Cells Using Homogeneous Nanohole Pattern-Modified Conductive Platform.», *Int. J. Mol. Sci.*, vol. 21, fasc. 1, pp. 191-NA, 2019, doi: 10.3390/ijms21010191.
[260] K. Yue, G. Trujillo-de Santiago, M. M. Alvarez, A. Tamayol, N. Annabi, e A. Khademhosseini, «Synthesis, properties, and biomedical applications of gelatin methacryloyl (GelMA) hydrogels», *Biomaterials*, vol. 73, pp. 254–271, dic. 2015, doi: 10.1016/j.biomaterials.2015.08.045.
[261] T. Zhu *et al.*, «Recent advances in conductive hydrogels: classifications, properties, and applications», *Chem. Soc. Rev.*, vol. 52, fasc. 2, pp. 473–509, 2023, doi: 10.1039/D2CS00173J.
[262] C. H. Zhang Meng-Hsuan; Wu, Song-Yi; Li, Shu-Hong; Wu, Jun; Liu, Shi-Ming; Wei, Hao-Ji; Weisel, Richard D. ;. Sung, Hsing-Wen; Li, Ren-Ke, «A self-doping conductive polymer hydrogel that can restore electrical impulse propagation at myocardial infarct to prevent cardiac

arrhythmia and preserve ventricular function.», *Biomaterials*, vol. 231, fasc. NA, pp. 119672–119672, 2019, doi: 10.1016/j.biomaterials.2019.119672.
[263] J. Xue *et al.*, «An injectable conductive Gelatin-PANI hydrogel system serves as a promising carrier to deliver BMSCs for Parkinson's disease treatment», *Mater. Sci. Eng. C*, vol. 100, pp. 584–597, lug. 2019, doi: 10.1016/j.msec.2019.03.024.
[264] A. S. Navaei Harpinder; Christenson, Wayne; Sullivan, Ryan; Ros, Robert; Nikkhah, Mehdi, «Gold nanorod-incorporated gelatin-based conductive hydrogels for engineering cardiac tissue constructs.», *Acta Biomater.*, vol. 41, fasc. NA, pp. 133–146, 2016, doi: 10.1016/j.actbio.2016.05.027.
[265] K. Zhu *et al.*, «Gold Nanocomposite Bioink for Printing 3D Cardiac Constructs», *Adv. Funct. Mater.*, vol. 27, fasc. 12, 2017, doi: 10.1002/adfm.201605352.
[266] C. Xu *et al.*, «Black-Phosphorus-Incorporated Hydrogel as a Conductive and Biodegradable Platform for Enhancement of the Neural Differentiation of Mesenchymal Stem Cells», *Adv. Funct. Mater.*, vol. 30, fasc. 39, 2020, doi: 10.1002/adfm.202000177.
[267] J. Qu, X. Zhao, P. X. Ma, e B. Guo, «Injectable antibacterial conductive hydrogels with dual response to an electric field and pH for localized "smart" drug release», *Acta Biomater.*, vol. 72, pp. 55–69, mag. 2018, doi: 10.1016/j.actbio.2018.03.018.
[268] L. H. Mao Sanming; Gao, Yihua; Wang, Li; Zhao, Weiwei; Fu, Lina; Cheng, Haoyan; Xia, Lin; Xie, Shangxian; Ye, Weiliang; Shi, Zhijun; Yang, Guang, «Biodegradable and Electroactive Regenerated Bacterial Cellulose/MXene (Ti 3 C 2 T x) Composite Hydrogel as Wound Dressing for Accelerating Skin Wound Healing under Electrical Stimulation», *Adv. Healthc. Mater.*, vol. 9, fasc. 19, pp. 2000872-NA, 2020, doi: 10.1002/adhm.202000872.
[269] J. M. M. Lee Joo Yoon; Kim, Tae Hyun; Lee, Seung Won; Ahrberg, Christian D. ;. Chung, Bong Geun, «Conductive hydrogel/nanowire micropattern-based sensor for neural stem cell differentiation», *Sens. Actuators B Chem.*, vol. 258, fasc. NA, pp. 1042–1050, 2018, doi: 10.1016/j.snb.2017.11.151.
[270] Y. Kim *et al.*, «Integration of Graphene Electrodes with 3D Skeletal Muscle Tissue Models», *Adv. Healthc. Mater.*, vol. 9, fasc. 4, p. 1901137, 2020, doi: 10.1002/adhm.201901137.
[271] Y. W. Li Jiameng; Yang, Yongqiang; Shi, Jing; Zhang, Hongyu; Yao, Xiaohong; Chen, Weiyi; Zhang, Xiangyu, «A rose bengal/graphene oxide/PVA hybrid hydrogel with enhanced mechanical properties and light-triggered antibacterial activity for wound treatment», *Mater. Sci. Eng. C Mater. Biol. Appl.*, vol. 118, fasc. NA, pp. 111447–111447, 2020, doi: 10.1016/j.msec.2020.111447.
[272] D. Gan *et al.*, «Conductive and Tough Hydrogels Based on Biopolymer Molecular Templates for Controlling in Situ Formation of Polypyrrole Nanorods», *ACS Appl. Mater. Interfaces*, vol. 10, fasc. 42, pp. 36218–36228, ott. 2018, doi: 10.1021/acsami.8b10280.
[273] B. B. Peña Susanna; Aguado, Brian A. ;. Borin, Daniele; Farnsworth, Nikki L. ;. Dobrinskikh, Evgenia; Rowland, Teisha J. ;. Martinelli, Valentina; Jeong, Mark Y. ;. Taylor, Matthew R. G. ;. Long, Carlin S. ;. Shandas, Robin; Sbaizero, Orfeo; Prato, Maurizio; Anseth, Kristi S. ;. Park, Daewon; Mestroni, Luisa, «Injectable Carbon Nanotube-Functionalized Reverse Thermal Gel Promotes Cardiomyocytes Survival and Maturation.», *ACS Appl. Mater. Interfaces*, vol. 9, fasc. 37, pp. 31645–31656, 2017, doi: 10.1021/acsami.7b11438.
[274] S. Qian *et al.*, «Carbon nanotubes as electrophysiological building blocks for a bioactive cell scaffold through biological assembly to induce osteogenesis», *RSC Adv.*, vol. 9, fasc. 21, pp. 12001–12009, apr. 2019, doi: 10.1039/C9RA00370C.
[275] X. M. Liu A. Lee; Park, Sungjo; Waletzki, Brian E. ;. Zhou, Zifei; Terzic, Andre; Lu, Lichun, «Functionalized Carbon Nanotube and Graphene Oxide Embedded Electrically Conductive Hydrogel Synergistically Stimulates Nerve Cell Differentiation», *ACS Appl. Mater. Interfaces*, vol. 9, fasc. 17, pp. 14677–14690, 2017, doi: 10.1021/acsami.7b02072.
[276] M. Bansal *et al.*, «Patternable Gelatin Methacrylate/PEDOT/Polystyrene Sulfonate Microelectrode Coatings for Neuronal Recording», *ACS Biomater. Sci. Eng.*, vol. 8, fasc. 9, pp. 3933–3943, set. 2022, doi: 10.1021/acsbiomaterials.2c00231.
[277] O. Bettucci, G. M. Matrone, e F. Santoro, «Conductive Polymer-Based Bioelectronic Platforms toward Sustainable and Biointegrated Devices: A Journey from Skin to Brain across Human

Body Interfaces», *Adv. Mater. Technol.*, vol. 7, fasc. 2, p. 2100293, 2022, doi: 10.1002/admt.202100293.
[278] L. Brigo *et al.*, «3D high-resolution two-photon crosslinked hydrogel structures for biological studies», *Acta Biomater.*, vol. 55, pp. 373–384, giu. 2017, doi: 10.1016/j.actbio.2017.03.036.
[279] A. I. Ciuciu e P. J. Cywiński, «Two-photon polymerization of hydrogels – versatile solutions to fabricate well-defined 3D structures», *RSC Adv.*, vol. 4, fasc. 85, pp. 45504–45516, set. 2014, doi: 10.1039/C4RA06892K.
[280] P. Sanjuan-Alberte *et al.*, «Development of Conductive Gelatine-Methacrylate Inks for Two-Photon Polymerisation», *Polymers*, vol. 13, fasc. 7, p. 1038, gen. 2021, doi: 10.3390/polym13071038.
[281] D. Loessner *et al.*, «Functionalization, preparation and use of cell-laden gelatin methacryloyl–based hydrogels as modular tissue culture platforms», *Nat. Protoc.*, vol. 11, fasc. 4, Art. fasc. 4, apr. 2016, doi: 10.1038/nprot.2016.037.
[282] S. Lin, N. Sangaj, T. Razafiarison, C. Zhang, e S. Varghese, «Influence of Physical Properties of Biomaterials on Cellular Behavior», *Pharm. Res.*, vol. 28, fasc. 6, pp. 1422–1430, giu. 2011, doi: 10.1007/s11095-011-0378-9.
[283] C. Zhang *et al.*, «Exploration of the Effects of Substrate Stiffness on Biological Responses of Neural Cells and Their Mechanisms», *ACS Omega*, vol. 5, fasc. 48, pp. 31115–31125, nov. 2020, doi: 10.1021/acsomega.0c04279.
[284] A. Navaei, K. R. Eliato, R. Ros, R. Q. Migrino, B. C. Willis, e M. Nikkhah, «The influence of electrically conductive and non-conductive nanocomposite scaffolds on the maturation and excitability of engineered cardiac tissues», *Biomater. Sci.*, vol. 7, fasc. 2, pp. 585–595, gen. 2019, doi: 10.1039/C8BM01050A.
[285] X. Liu *et al.*, «3D Printing of Bioinspired Liquid Superrepellent Structures», *Adv. Mater.*, vol. 30, fasc. 22, p. 1800103, 2018, doi: 10.1002/adma.201800103.
[286] O. Dadras-Toussi, M. Khorrami, e M. R. Abidian, «Femtosecond Laser 3D-printing of Conductive Microelectronics for Potential Biomedical Applications», in *2021 43rd Annual International Conference of the IEEE Engineering in Medicine & Biology Society (EMBC)*, nov. 2021, pp. 1197–1200. doi: 10.1109/EMBC46164.2021.9630885.
[287] H. Wang *et al.*, «Two-Photon Polymerization Lithography for Optics and Photonics: Fundamentals, Materials, Technologies, and Applications», *Adv. Funct. Mater.*, vol. 33, fasc. 39, p. 2214211, 2023, doi: 10.1002/adfm.202214211.
[288] R. Infuehr *et al.*, «Functional polymers by two-photon 3D lithography», *Appl. Surf. Sci.*, vol. 254, fasc. 4, pp. 836–840, dic. 2007, doi: 10.1016/j.apsusc.2007.08.011.
[289] F. Perrucci *et al.*, «Optimization of a suspended two photon polymerized microfluidic filtration system», *Microelectron. Eng.*, vol. 195, pp. 95–100, ago. 2018, doi: 10.1016/j.mee.2018.04.001.
[290] S. Passinger, C. Reinhardt, e B. Chichkov, «2D and 3D photonic and plasmonic structures fabricated by two-photon-polymerization», in *Nanophotonics*, SPIE, apr. 2006, pp. 206–214. doi: 10.1117/12.660659.
[291] S. Lee, B. Ozlu, T. Eom, D. C. Martin, e B. S. Shim, «Electrically conducting polymers for bio-interfacing electronics: From neural and cardiac interfaces to bone and artificial tissue biomaterials», *Biosens. Bioelectron.*, vol. 170, p. 112620, dic. 2020, doi: 10.1016/j.bios.2020.112620.

A | Appendix A

In this section, a list of materials and chemicals employed in this thesis work is reported, with their catalogue and CAS number. The following chemicals has been used without any further purification.

Chemicals and Materials	Catalog Number	CAS Number	Vendor
2-Hydroxy-4′-(2-hydroxyethoxy)-2-methylpropiophenone	410896	106797-53-9	Sigma Aldrich
2-propanol p.a. 99,8%	1136,1	67-63-0	Chemsolute
2-propanone 99%	2614,25	67-64-1	Chemsolute
3-(Trimethoxysilyl)propyl methacrylate	440159	2530-85-0	Sigma Aldrich
3,4-Ethylenedioxythiophene (EDOT)	483028	126213-50-1	Sigma Aldrich
Alconox -- Hellmanex	Z742914		Sigma Aldrich
Clevios TM PH 1000		155090-83-8	Heraeus
Dialysis tubing, high retention seamless cellulose tubing, MWCO 12400, 99.99% retention	D0655		Sigma Aldrich
DPBS, no calcium, no magnesium	14190250		Thermo Fisher
Filter RC, 0.22 um, d 30 mm, non sterile	514-1241		VWR
Gelatin from bovine skin 225g Bloom, type B	G9382	9000-70-8	Sigma Aldrich
Glass coverslip 30mm	631-1347		VWR
Iron(iii) sulfate hydrate,plant cell culture tested, BioReagent	F0638	15244-10-7	Sigma Aldrich
ITO Glass Substrates - Unpatterned 25x25mm (100)	S2006B1		Ossila B.V.
Methacrylic anhydride	276682	760-93-0	Sigma Aldrich

Poly-(Sodium-4-styrenesulfonate) 70 000	243051	25704-18-1	Sigma-Aldrich
Sodium persulfate	216232	7775-27-1	Sigma Aldrich

Item	**Specification**	**Company**
Plasma oven	Plasmaanglege PICO	Diener electronic
Spin Coater	WS-650-23B Spin Coater	Laurell
Contact angle measurement tool	OCA 20	Dataphysics
Potentiostat	VSP-300	Biologic
Ultrasound Bath	HC – Series EMMI 40HC	EMAG
NMR spectrometer	Avance III™ HD 600 MHz	Bruker
High precision 3D printer	Photonic Professional GT2	Nanoscribe
3D printer	Mega X	Anycubic
Microplate reader	SpectraMax iD5	Molecular Devices
Optical slice microscope	Apotome2	Zeiss
UV lamp	E-Series	Spectroline
Rheometer	Discovery hybrid HR30	TA instruments

List of Figures

List of tables

List of abbreviations

3D, three-dimensional;

TMSPMA, 3-(trimethoxysilyl)propyl methacrylate;

AgNP, silver nanoparticle;

AgNW, silver nanowire;

APS, ammonium peroxydisulfate;

AuNP, gold nanoparticle;

AuNR, gold nanorod;

AuNW, gold nanowire;

Bio-IL, bio-ionic liquid;

BMP, bone morphogenetic protein;

BSA, bovine serum albumin;

CF, carbon fiber;

CNT, carbon nanotube;

CP, conducting polymer;

CVD, chemical vapor deposition;

DDS, drugs delivery system;

Dex, dexamethasone;

DNA, deoxyribonucleic acid;

ECM, extracellular matrix;

EDOT, 3, 4-ethylenedioxythiophene;

EpCAM, epithelial cell adhesion molecule;

GelMA, gelatin methacryloyl;

GNM, graphene nanomaterial;

GNP, graphene nanoplatelet;

GO, graphene oxide;

H_2O_2, hydrogel peroxide;

ITO, indium tin oxide;

LBL, layer-by-layer;

MeTro, methacryloyl-substituted tropoelastin;

MI, myocardial infarction;

MWCNT, multi-walled carbon nanotube;

MXene, Ti3C2Tx;

NSC, neural stem cell;

NO, nitric oxide;

OANi, oligoaniline;

OPF, oligo (polyethylene glycol fumarate);

P3HT, poly (3-hexylthiophene);

PAA, polyacrylic acid;

PAAm, polyacrylamide;

PAN, polyacrylonitrile;

PANi, polyaniline;

PCL, polycaprolactone;

PCLF, polycaprolactone fumarate;

PDA, polydopamine;

PDMS, polydimethylsiloxane;

PEDOT, poly (3, 4-ethylenedioxythiophene);

PEDOT:PSS, poly (3, 4-ethylenedioxythiophene) polystyrene sulfonate;

PEG, polyethylene glycol;

PEI, poly (ethyleneimine);

PGS, poly (glycerol-sebacate);

PLCL, poly (L-lactide-co-caprolactone);

PLGA, poly (lactic-co-glycolic acid);

PLA, poly lactic acid;

PLLA, poly (L-lactic acid);

PNIPAAm, poly (N-isopropylacrylamide-co-methacrylic acid) functionalized polyacrylamide;

PPy, polypyrrole;

PSSH, polystyrene sulfonic acid;

PSS polystyrene sulfonate;

pTS, para-toluene sulfonate;

PU, polyurethane;

PVA, polyvinyl alcohol;

PVDF, poly (vinylidene fluoride);

rGO, reduced graphene oxide;

SEM, scanning electron microscope;

SF, silk fibroin;

SiNW, silicon nanowire;

SWCNT, single-walled carbon nanotube;

TERM, tissue engineering and regenerative medicine;

UV, ultraviolet.

VEGF, vascular endothelial growth factor;